

**THE EFFECT OF TIN CONTENT IN ALUMINUM OXIDE FILM ON
THERMAL PERFORMANCE OF EVACUATED TUBE
COLLECTOR**



**A Thesis Submitted to the Graduate School of Naresuan University
In Partial Fulfillment of the Requirements
for the Doctor of Philosophy Degree in Renewable Energy**

June 2018

Copyright 2018 by Naresuan University


Thesis entitled “The Effect of Tin Content in Aluminum Oxide Film on Thermal Performance of Evacuated Tube Collector”

by Ms. Warisa Wamae

has been approved by the Graduate School as partial fulfillment of the requirements for the Doctor of Philosophy Degree in Renewable Energy of Naresuan University


Oral Defense Committee


..... Chair
(Assistance Professor Apiluck Eiad-ua, Ph.D.)


..... Advisor
(Assistance Professor Tawat Suriwong, Ph.D.)


..... Co – Advisor
(Thotsaphon Threrujirapapong, Ph.D.)


..... Internal Examiner
(Sukruedee Sukchai, Ph.D.)

Approved

.....
(Associate Professor Paisarn Muneesawang, Ph.D.)

Dean of the Graduate School

1 4 2 5 4 1 9

ACKNOWLEDGEMENT

I would like to thank and offer my sincere gratitude to my advisor, Assistant Professor Dr.Tawat Suriwong and co-advisors Dr.Thotsaphon Threrujirapapong. I greatly appreciated the guidance, support, and encouragement that were offered throughout the length of the study. I also would like to give special thanks to all thesis committee members, and deeply grateful for their helpful comments.

I would also like to thank you to Thailand's Office of the Higher Education Commission, who provides me the Ph.D. scholarship (Sandwich program) through the project of lecturer and personnel development for high education institutions in southern border provinces development area.

The support from other experts and staff members of School of Renewable Energy, Naresuan University is also appreciated. And I wish to give specially thank to my parents and all my family members for their understanding and motivation.

Finally, I would like to express my gratitude to all others for all supports to make me a complete this thesis but are not named in this acknowledgement.

Warisa Wamae

Title THE EFFECT OF TIN CONTENT IN ALUMINUM OXIDE FILM ON THERMAL PERFORMANCE OF EVACUATED TUBE COLLECTOR

Author Warisa Wamae

Advisor Assistant Professor Tawat Suriwong, Ph.D.

Co-Advisor Thotsaphon Threrujirapapong Ph.D.

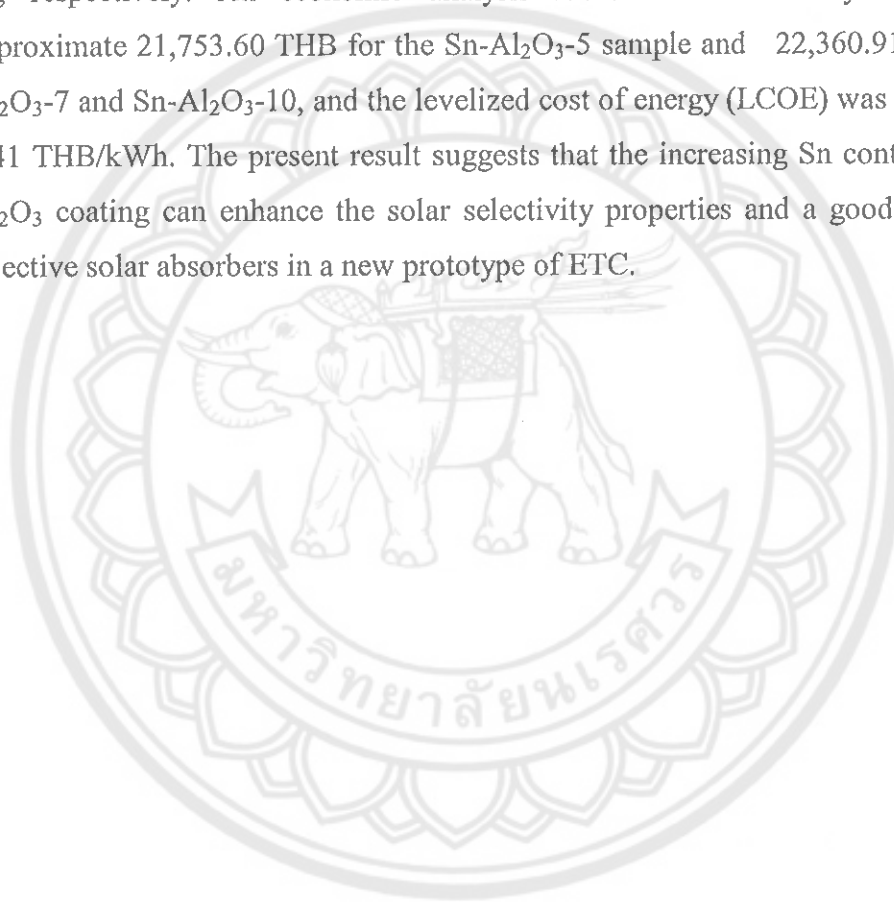
Academic Paper Thesis Ph.D. in Renewable Energy, Naresuan University, 2017

Keywords Evacuated tube collector, Selective solar absorber, Sn-Al₂O₃, Anodization, Solar absorptance, Thermal emittance, Thermal efficiency

ABSTRACT

The tin-pigmented aluminum oxide film (Sn-Al₂O₃) based solar selective absorber for a new prototype evacuated tube collector (ETC) was successfully prepared with 3 different contents of tin coated on aluminum fin by an anodization process. The Sn pigment was deposited into the pores of Al₂O₃ film for 5, 7 and 10 minutes, which coded as Sn-Al₂O₃-5, Sn-Al₂O₃-7 and Sn-Al₂O₃-10, respectively. The Sn-Al₂O₃ samples exhibited darker black color with increased coloring time. Aluminum and tin phases were detected at the coating surface. The Al₂O₃ films were formed and compacted as a barrier on the Al substrate. The compositions of the oxide film composed of tin (Sn), aluminum (Al) and oxygen (O) elements. The reflectance (R) of the coating was determined by Ultraviolet-visible-near infrared spectrophotometer in the wavelength interval of 300-2500 nm and the Fourier transform infrared spectrophotometer in the wavelength of infrared region (2500-25000 nm) to calculate the solar absorptance (α_{sol}) and thermal emittance (ϵ_{therm}) respectively. As a result, the α_{sol} were 0.89, 0.93 and 0.94 and the ϵ_{therm} were 0.23, 0.24 and 0.21 for the Sn-Al₂O₃-5, Sn-Al₂O₃-7 and Sn-Al₂O₃-10 respectively. In more detail, the solar selectivity ($\alpha_{sol}/\epsilon_{therm}$) was evaluated, and the results were 3.87, 3.88 and 4.48 for Sn-Al₂O₃-5, Sn-Al₂O₃-7 and Sn-Al₂O₃-10 respectively. The thermal conductivity of Sn-Al₂O₃ samples decreased with increasing Sn content. In order to investigate the thermal performance

of ETC using Sn-Al₂O₃ on an Al fin as a solar receiver, thermal efficiency (η) of the ETC was collected under steady-state conditions, as prescribed by ISO 9806-1 standard. The maximum thermal efficiency ($F_R (\tau\alpha)$) of the ETC under the nearly constant heat loss coefficient (U_L), was obviously increased with the increasing Sn content. The $F_R (\tau\alpha)$ was 0.42, 0.54, and 0.61, while the non-useful energy ($-F_R U_L$) was -9.62, -11.64 and -11.49 W/m².°C for the Sn-Al₂O₃-5, Sn-Al₂O₃-7 and Sn-Al₂O₃-10, respectively. An economic analysis identified the life cycle cost (LCC) approximate 21,753.60 THB for the Sn-Al₂O₃-5 sample and 22,360.91 THB for Sn-Al₂O₃-7 and Sn-Al₂O₃-10, and the levelized cost of energy (LCOE) was 2.05, 1.66 and 1.41 THB/kWh. The present result suggests that the increasing Sn content in the Sn-Al₂O₃ coating can enhance the solar selectivity properties and a good candidate for selective solar absorbers in a new prototype of ETC.

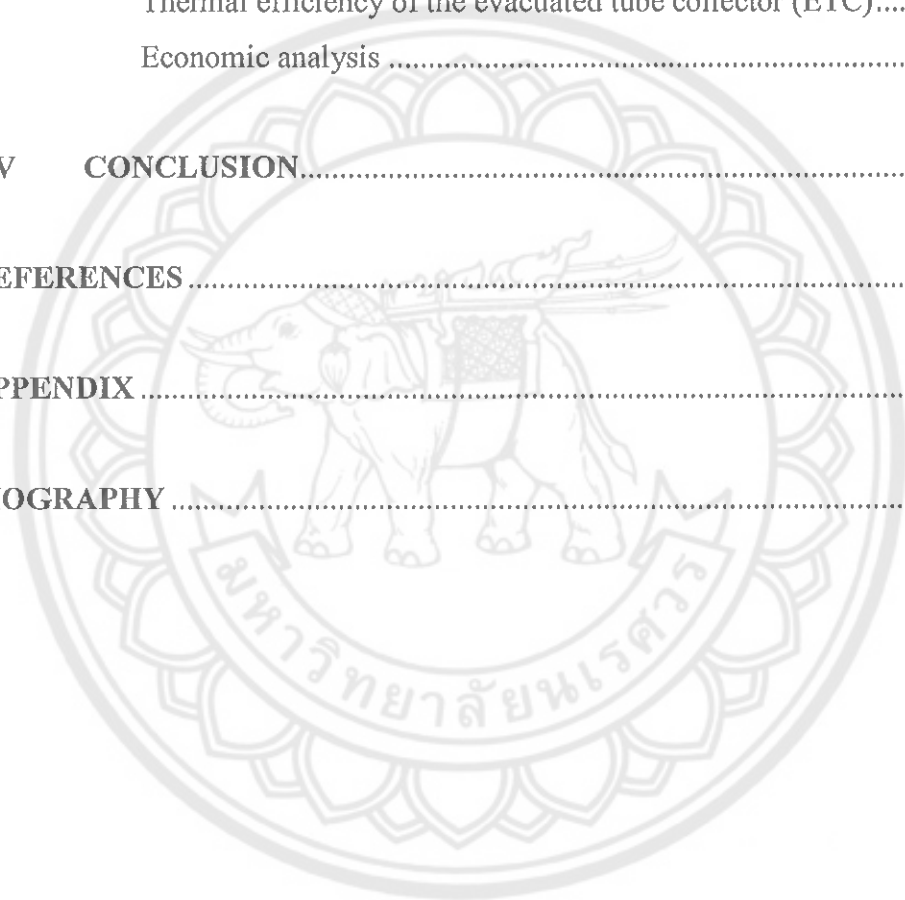


LIST OF CONTENTS

Chapter	Page
I INTRODUCTION.....	1
Rationale for the study and statement of the problem	1
Purposes of the study	3
Scopes of the study	4
Benefits of the study	4
II LITERATURE REVIEW.....	6
Solar collectors.....	6
Evacuated tube collector	6
Selective solar absorber	8
Aluminum coating	11
Anodized aluminum.....	12
Properties of anodized aluminum	16
Determination of anodized aluminum	17
Collector thermal performance	17
Absorptance and emittance	20
Thermal conductivity	20
Economic Analysis	21
Literature Review.....	22
III RESEARCH METHODOLOGY	28
Procedure and methodology	28
Preparation of anodized aluminum sheet	29
Characterization of Tin	29
Apparatus for characterization of anodized aluminum sheet.....	29
Sample preparation for analysis.....	40
Thermal efficiency	42
Economic analysis	43

LIST OF CONTENTS (CONT.)

Chapter	Page
IV RESULT AND DISCUSSION.....	44
Characterization of phase and morphology of the Sn-Al ₂ O ₃	45
Thermal efficiency of the evacuated tube collector (ETC).....	59
Economic analysis	61
V CONCLUSION.....	67
REFERENCES	70
APPENDIX	80
BIOGRAPHY	123

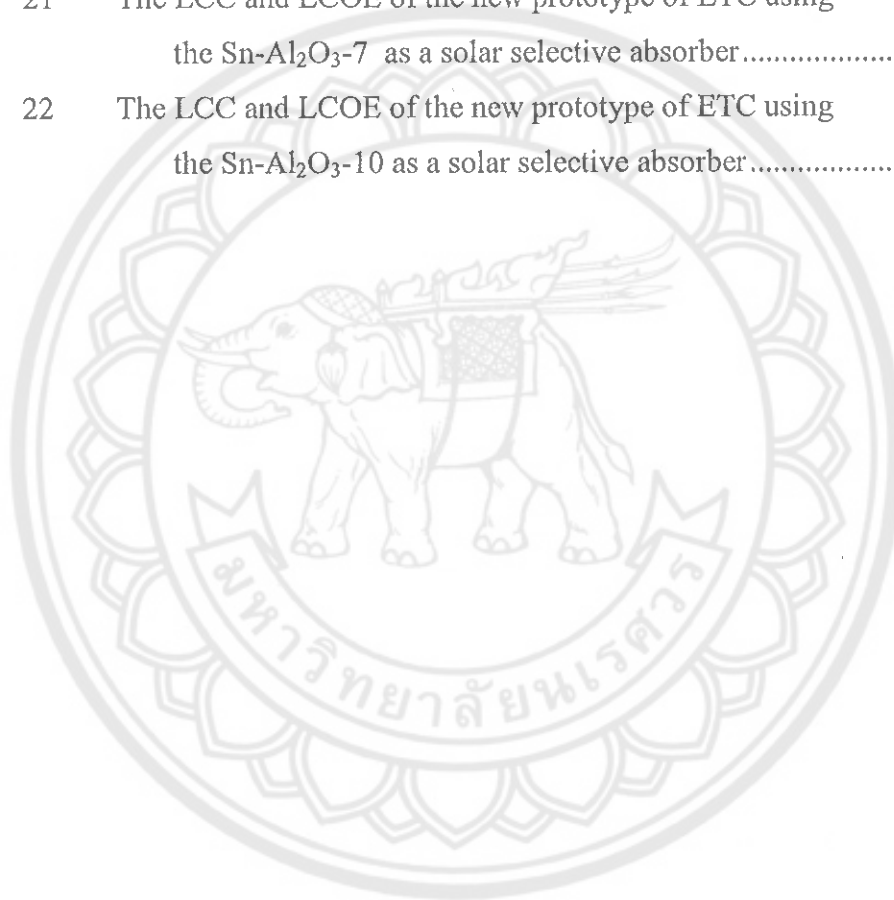


LIST OF TABLES

Table		Page
1	Solar energy collectors	7
2	Properties of selective coatings	21
3	Parameters for the thermal efficiency test	43
4	The solar absorptance (α_{sol}) and thermal emittance (ϵ_{therm}) of the Sn-Al ₂ O ₃ samples with different Sn contents compared with the previous studies	53
5	The solar selectivity ($\alpha_{sol}/\epsilon_{therm}$) of the Sn-Al ₂ O ₃	56
6	Summary of thermal performance parameters of the new ETC prototype using Sn-Al ₂ O ₃ as a selective solar absorber	60
7	The thermal efficiency of the ETC using Sn-Al ₂ O ₃ as solar selective absorber compared with previous studies	61
8	The investment costs and benefits of the project	62
9	The parameters for calculation	63
10	Parameters for calculation the annual energy of the ETC	63
11	The annual energy from the new prototypes of ETC with different Sn content coatings	64
12	The LCC and LCOE of the Sn-Al ₂ O ₃ solar absorbers	65
13	The calculation of the solar absorptance of the Sn-Al ₂ O ₃ -5	88
14	The calculation of the solar absorptance of the Sn-Al ₂ O ₃ -7	90
15	The calculation of the solar absorptance of the Sn-Al ₂ O ₃ -10	92
16	The thermal efficiency of ETC with the Sn-Al ₂ O ₃ -5 as solar selective absorber	94
17	The thermal efficiency of ETC with the Sn-Al ₂ O ₃ -7 as solar selective absorber	98
18	The thermal efficiency of ETC with the Sn-Al ₂ O ₃ -10 as solar selective absorber	103
19	The calculation of annual energy	108

LIST OF TABLES (CONT.)

Table		Page
20	The LCC and LCOE of the new prototype of ETC using the Sn-Al ₂ O ₃ -5 as a solar selective absorber	109
21	The LCC and LCOE of the new prototype of ETC using the Sn-Al ₂ O ₃ -7 as a solar selective absorber	110
22	The LCC and LCOE of the new prototype of ETC using the Sn-Al ₂ O ₃ -10 as a solar selective absorber	111



LIST OF FIGURES

Figure		Page
1	Cross-sectional images of the evacuated tube collector; (a, b) original coating and (c, d) Sn-Al ₂ O ₃ coating on Al fins	2
2	Evacuated tube collector and its components.....	8
3	Normalized spectral power density of a black body (BB) at 720 K and the solar spectrum (air mass 1.5, AM 1.5). The spectral absorptivity is shown for an ideal absorber at 720K.....	9
4	Flow chart of the anodization steps	13
5	Anodizing method of substrate in the acid electrolyte	14
6	Anodization procedure on the aluminum sheet	15
7	Cross section of anodic oxide layer on the aluminum surface	16
8	ETC performance curve	19
9	Open loop collector test system.....	19
10	Flow chart of procedure and methodology of the study.....	28
11	Bragg's law diagram	30
12	X-ray Diffractometer (XRD, PHILIPS X'Pert-MPD)	31
13	Internal component of Scanning Electron Microscope	33
14	Low Vacuum Scanning Electron Microscope equipped with an Energy Dispersive X-ray analyzer) LV-SEM-EDX, JSM-5910 JEOL).....	34
15	Light interaction with a solid.....	35
16	Ultraviolet-Visible-Near Infrared Spectrophotometer (UV-Vis-NIR Spectrophotometer, ShimadzuUV-3101PC)	36
17	Principle thermal diffusivity analysis by laser flash method	37
18	Laser Flash Analyzer (NETZSCH LFA 447 NanoFlash-A)	37
19	Schematic of a Michelson interferometer	39
20	Fourier Transform Infrared spectrometer (FTIR, Bruker Tensor 27) ...	39
21	The 1x1 square centimeter samples for phase and reflectance	41
22	The samples were mounted in Bakelite for morphologies	41

LIST OF FIGURES (CONT.)

Figure		Page
23	The 1.25x1.25 square centimeter samples for thermal diffusivity	41
24	The evacuated tube collector equipped with header and stand as a solar water heater system for thermal efficiency test	42
25	(a) Aluminum sheet and (b) Sn-Al ₂ O ₃ coating on Al fin with variation of coloring time	44
26	The XRD patterns of the Sn-Al ₂ O ₃ at different Sn contents	46
27	LV-SEM images of a-c) surface and d-f) sectional image of Sn-Al ₂ O ₃ -5, Sn-Al ₂ O ₃ -7 and Sn-Al ₂ O ₃ -10.....	47
28	SEM-EDX line scanning of (a) Sn-Al ₂ O ₃ -5, (b) Sn-Al ₂ O ₃ -7 and (c) Sn-Al ₂ O ₃ -10.....	48
29	SEM-EDX Mapping of the (a) Sn-Al ₂ O ₃ -5, (b) Sn-Al ₂ O ₃ -7 and (c) Sn- Al ₂ O ₃ -10.....	49
30	Elemental distributions of the (a) Sn-Al ₂ O ₃ -5, (b) Sn-Al ₂ O ₃ -7 and (c) Sn- Al ₂ O ₃ -10.....	50
31	Spectral reflectance (R) of the Sn-Al ₂ O ₃ solar absorber, compared with the sun spectrum at AM 1.5 in the wavelength range of 300 - 2500 nm	52
32	Reflectance of non-anodized Al and anodized Al at different Sn in the IR region.....	54
33	Thermal conductivity of anodized Al with different Sn contents	57
34	Heat flow in the thermal conductivity measurement on the Sn-Al ₂ O ₃ specimen.....	58
35	Solar radiation and heat transfer through the Sn-Al ₂ O ₃ specimen	58
36	Thermal performance curve of the new prototype ETC using (a) Sn-Al ₂ O ₃ -5, (b) Sn-Al ₂ O ₃ -7 and (c) Sn- Al ₂ O ₃ -10 as selective solar absorber	60
37	The LCC and LCOE of the new prototype of ETC using Sn-Al ₂ O ₃	66

CHAPTER I

INTRODUCTION

Rationale for the study and statement of the problem

Thailand is located in a tropical area that receives the energy from sun light approximately $18.2 \text{ MJ/m}^2\text{-day}$. The ratio of diffusion and total radiation is 0.42 and the remaining is the beam radiation. In consequence; this is a potential country for using solar energy as renewable energy, because it is clean, non-polluting and endless. Presently, various technologies are used for solar applications, both for electric production and heat production. In heat production, solar collectors are the main implement for proceeding; focusing solar concentrators (for high temperature production) and non-focusing solar collector (for low temperature production), are used in the country. In order that, non-focusing solar collector is extensively used, because of low cost and stable heat producing. Commercial flat type collectors are generally used, e.g. flat plate collector ($30 - 80 \text{ }^\circ\text{C}$) and evacuated tube collector, called ETC ($50 - 200 \text{ }^\circ\text{C}$) [1]. In this way, because of worthwhileness in higher generate temperature than flat plate collector, evacuated tube collector is the most one extensively collector for hot water producing. The performance of evacuated tube collector according to solar selective absorber that coating on the glass tube inside surface. The normal selective solar absorber coating, is coated on the surface of the inner glass tube as in Figure 1 (a, b), which is applied by high technology and complicated in the process, this causes high production costs. During applications, it has a drawback when it cracks or splits, because it needs to change by a new one, that caused an extra dissipation cost. A changing of solar absorber coating on aluminum (Al) fin and inserting method into the transparent evacuated tube were developed to be a new prototype of ETC as shown in Figure 1 (c, d), while the spectral properties, thermal efficiency and potential for energy production are the same as the ETC in commercial tubes [2].

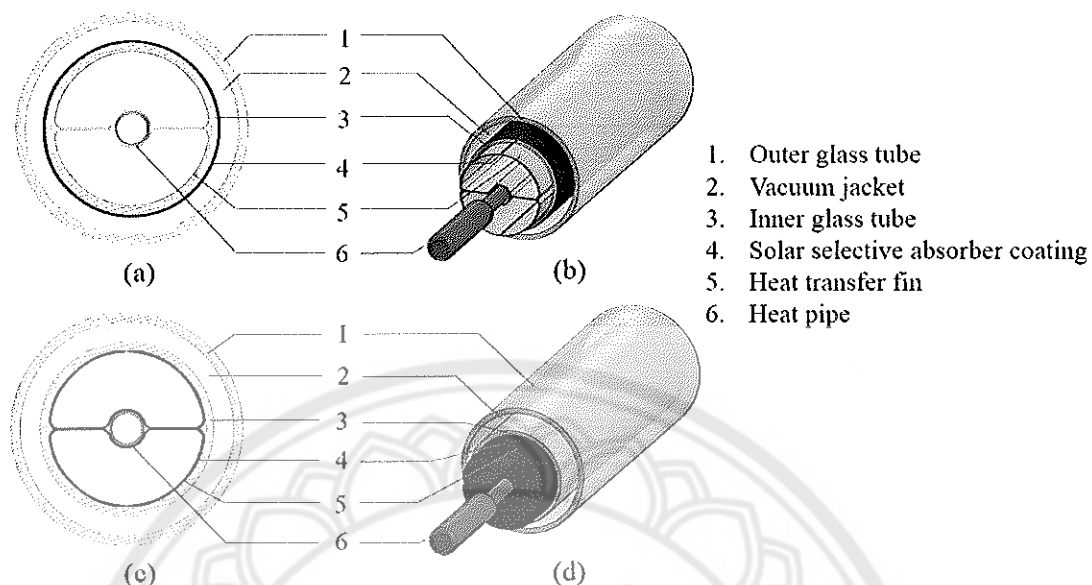


**Figure 1 Cross-sectional images of the evacuated tube collector;
(a, b) original coating and (c, d) Sn-Al₂O₃ coating on Al fins**

The selective spectral properties of a solar absorber can be enhanced by an appropriate choice of substrate and antireflection layers, which can also protect its surface [3]. There are many techniques for selective coating preparation, along with prevent degradation and corrosion of the surface, such as sputtering, evaporation, chemical vapor deposition (CVD), physical vapor deposition (PVD), spray pyrolysis, sol-gel/dip-coating, electroplating, painting, anodization and other methods [3]. The anodization is a simple technique in the aluminum coating industry that satisfies each of these factors to produce a high-performance aluminum finish, which can have an extremely long lifetime and offer significant economic advantages through maintenance and operating savings. Metal pigmented-Al₂O₃ solar absorbers prepared by the anodization process are one of the cermet solar absorber coatings. Cermet coatings consist of fine metal particles in a dielectric or ceramic matrix, which present a good candidate for solar absorber materials at high temperature, and have been successfully commercialized [3, 4]. The solar selectivity of the solar absorber materials can be optimized by variation of metals and ceramic constituent elements, thickness, concentration, shape, size, and orientation [3]. Several black metal pigments can be deposited to the pores of the film as a solar selective absorber. The thickness of

Al_2O_3 based cermet coatings was considered in the previous reports [5, 6, 7], which correlated with spectral selective properties. But the thicker of Al_2O_3 is affect the thermal emittance to be higher [5, 8]. Another way to improve the spectral selectivity of the solar selective absorber and high corrosion resistance, several pigments deposited in the aluminum oxide film have been studied, e.g., coatings of black Cu-Ni, black Ni-Co by electro-deposition [9, 10], Co- Al_2O_3 by anodization [11], Cu- CuAl_2O_4 hybrids deposited in anodic aluminum oxide (AAO) by electrochemical processes [12], carbon nano-particles embedded in SiO_2 , ZnO and NiO matrices by a sol-gel technique[13], W- Al_2O_3 cermet, Mo- Al_2O_3 , Pt- Al_2O_3 , Ag- Al_2O_3 nanocermet, and $\text{CrN}_x\text{O}_y/\text{SiO}_2$ coated with a sputtering technique [14, 15, 16, 17]. Content variation of the pigment or composite coating on the surface has an influence on the spectral properties [8], according to the theoretical properties of the solar absorbers. Tin (Sn) is one of the famous pigments which is able to be deposited into the Al_2O_3 film layer as the cermet (metal-dielectric composite) coating for applying as solar absorber materials in solar thermal applications [18, 19]. In addition, the tin pigmented- Al_2O_3 ($\text{Sn-Al}_2\text{O}_3$) coating prepared by the anodization process has been considered due to an eco-innovative production method for sustainable development. Presently, the applications of $\text{Sn-Al}_2\text{O}_3$ coating as a solar absorber in solar thermal devices with low and mid-operational temperature ranges have not been investigated. Recently, there is a little prior research on the influence of Sn content on phase, morphology, thermal conductivity, solar selectivity of Al_2O_3 based cermet coatings, including the heat transfer mechanism through the $\text{Sn-Al}_2\text{O}_3$ coatings, and the thermal efficiency of the new prototype of ETC using $\text{Sn-Al}_2\text{O}_3$ on Al fin applied as a selective solar absorber.

Purposes of the study

1. To investigate the influence of $\text{Sn-Al}_2\text{O}_3$ coatings with 3 different contents of Sn pigment by the anodization process as a solar selective absorber on the phase, morphology, chemical distributions, solar selective properties, together with the thermal conductivity and heat transfer mechanism through the $\text{Sn-Al}_2\text{O}_3$ coatings.

2. To investigate the thermal efficiencies and thermal performances of various Sn pigment contents in the Sn-Al₂O₃ coatings on the Al fin applied as a solar selective absorber for a new prototype of evacuated tube collector (ETC).

3. To evaluate the Life Cycle Cost (LCC) and Levelized Cost of Energy (LCOE) of the new prototype of ETC when using different Sn-Al₂O₃ coated on Al fin as selective solar absorbers.

Scopes of the study

1. Aluminum (Al) sheet of 9 cm wide × 160 cm long with a thickness of 0.02 cm was used as a substrate.

2. The aluminum oxide (Al₂O₃) film was formed on its surface by the anodization process and it was controlled to an identical thickness in all samples. Various Sn pigment contents were composed into the film as the Sn-Al₂O₃ selective solar absorbers according to the appropriate conditions from a previous study which can be produced by the factory.

3. The anodized Al was investigated the phase, morphologies, chemical distributions, solar selective properties and thermal conductivity by X-ray Diffraction (XRD), Scanning electron microscopy equipped with Energy dispersive X-ray spectroscopy (SEM-EDX), Ultraviolet-visible-near infrared spectroscopy (UV-Vis-NIR), Fourier transform infrared spectrophotometer (FTIR) and laser flash analyzer.

4. The Sn-Al₂O₃ selective solar absorber coated on the Al fin was assembled with a heat pipe and transparent double layer borosilicate evacuated tube as one set of solar receiver tubes. And thermal efficiency tested under steady-state conditions as prescribed by the ISO 9806-1 standard.

5. The economic analysis was evaluated by the Life Cycle Cost (LCC) and Levelized Cost of Energy (LCOE) of the collector.

Benefits of the study

1. The efficiency of various tin pigment contents applied based on the anodized aluminum oxide film as a solar selective absorber in evacuated tube collector (ETC) will be demonstrated for further development to increase the performance of the collector.

2. Leverage capability in local manufacturing for hot water producing materials, which can reduce the initial and maintenance costs of a solar collector system.



CHAPTER II

LITERATURE REVIEW

Solar collectors

Solar collector is a solar absorb device which transform solar energy to heat, and transfer the heat to a working fluid (usually water, air or oil), then the collected heat in the fluid is used directly or kept in a storage tank. The solar energy can produce either heat or electricity, dependging on the conversion device [8]. There are 2 types of solar collector; non-concentrating and concentrating. Non-concentrating collectors have the area intercepting the same as the absorber area, and the most common type of non-concentrating collectors are suitable for low- to mid-temperatures. While the concentrating collectors have a greater area intercepting the solar radiation, and usually move for high temperature applications [1].

The solar collectors are also distinguished by their motion; non-tracking systems and tracking systems (single-axis tracking and two-axis tracking). The comprehensive collectors are available in the market are shown in the Table 1.

Evacuated tube collector

The evacuated tube is benefit collector which can generate higher temperatures than flat plate collectors (50 - 200°C). The evacuated tube collector (ETC) consists of 2 layers of vacuum glass tubes. The vacuum acts as an insulator to reduce any heat loss to the surroundings either through convection or radiation. This makes the collector much more efficient than flat plate collectors. A solar absorber is coated onto inner glass tube surface. Liquid-vapor phase change materials are used to be the operating fluid inside the copper heat pipe. Aluminum or copper fin is attached to the heat pipe. The fin transfers heat to the heat pipe via conduction, and through to the fluid via convection to a “hotbulb” that indirectly heats the manifold within a header as shown in Figure 2. These heat pipes and glass tubes are connected to a storage tank to collect the produced hot water for using at night time or the next day [20].

Table 1 Solar energy collectors [1]

Motion	Collector type	Absorber type	Concentration ratio	Indication temperature range (°C)
Stationary	Flat-plate collector (FPC)	Flat	1	30-80
	Evacuated tube collector (ETC)	Flat	1	50-200
	Compound parabolic collector (CPC)	Tubular	1-5	60-240
	Compound parabolic collector (CPC)	Tubular	5-15	60-300
	Linear Fresnel reflector (LFR)	Tubular	10-40	60-250
Single-axis tracking	Cylindrical trough collector (CTC)	Tubular	15-50	60-300
	Parabolic trough collector (PTC)	Tubular	10-85	60-400
	Parabolic dish reflector (PDR)	Point	600-2000	100-1500
Two-axis tracking	Heliostat field collector (HFC)	Point	300-1500	150-2000

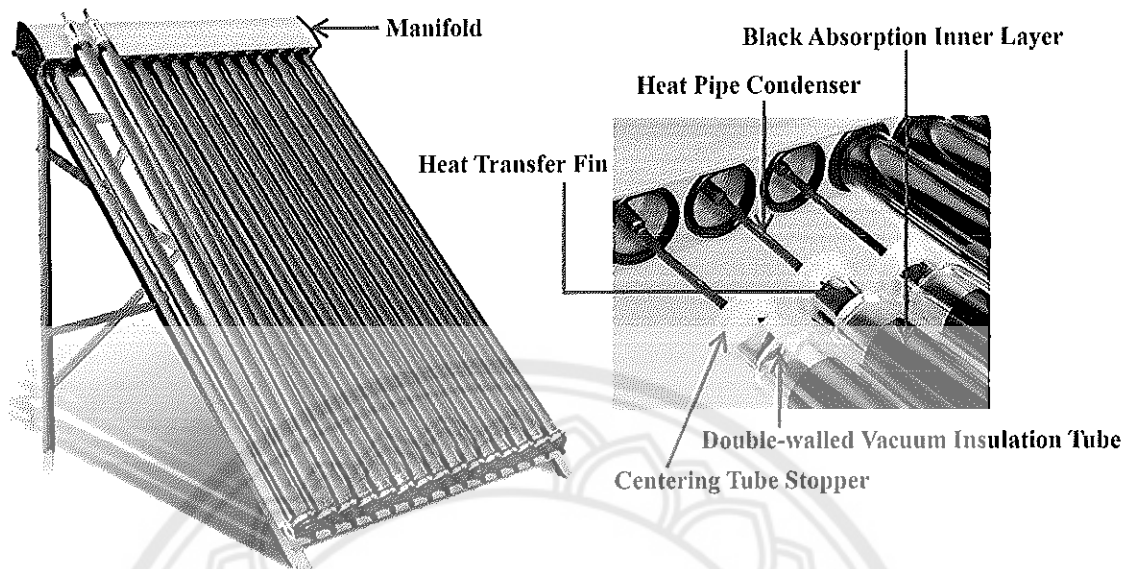


Figure 2 Evacuated tube collector and its components

The process in the evacuated tube is operated by fluid flowing through the absorber and it can be collected as heat by means of the heat pipe principle. There is a small amount of fluid sealed inside each evacuated tube and the energy transfer takes place in these steps:

1. The fluid is evaporated by solar radiation.
2. The vapor rises to the top, and when it meets a colder pipe, where a liquid flows through.
3. The vapor is condensed, transferring the latent heat to the liquid in the top pipe.
4. The condensed fluid in the tubes runs back to the bottom, where the process can start again.

Selective solar absorber

A Solar absorber function transforms solar radiation to heat, by using heat transfer fluid inside, yet the normal solar absorber surface reflectance is high and non-selective in wavelength. Development of selective solar absorber gains the advantage by increasing the solar absorptance efficiency, and decreasing the heat loss. The satisfying selective solar absorber materials ought to high absorptance or low

reflectance in the ultra violet – visible – near Infrared wavelength ranges (0.3 – 2.5 μm), and low emittance or high reflectance in the infrared region (2.5 – 25 μm) [8] as shown in Figure 3.

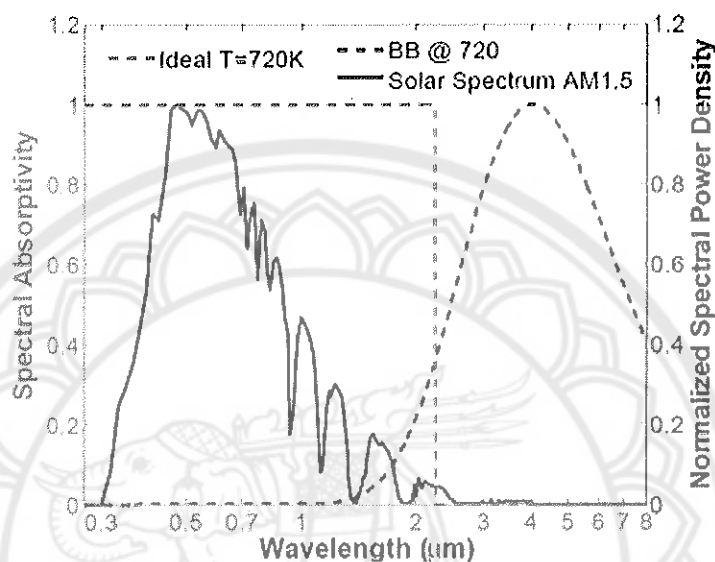


Figure 3 Normalized spectral power density of a black body (BB) at 720 K and the solar spectrum (air mass 1.5, AM1.5). The spectral absorptivity is shown for an ideal absorber at 720K [21]

Several types of selective solar absorber applied a absorber coating on the solar collector surface (usually deposited on metals or metallized substrates), although black paint is selected normally because of high absorptance, but it also has high thermal emissivity (Emittance, ε). General coating materials; black nickel (NiS-ZnS), black copper (Cu-Cu₂O:Cu), Black chrome (Cr-Cr₂O₃), stable nickel pigment (Ni)-pigment alumina (Al₂O₃) etc. [3].

The physical properties of selective solar absorber, solar absorptance and emittance consider the following; 1. High absorptance for solar spectrum range 0.2-2.5 μm and low emittance greater than 2.0 μm , 2) The region between high absorptance and low emittance of spectrum transition has to be as sharp as possible, 3) The coating must be stable under long term operation at high temperature, repeating thermal cycling, air exposure and radiations etc, 4) The coating must have a good fixing on the

substrate, 5) The coating should be appropriately to apply, 6) The coating must be economical [22, 23].

Table 2 Properties of selective coatings [24]

Coating	Substrate	Absorptivity	Emissivity	T _{max} (°C)	
Selective electroplate deposits, Type A					
Black Nickel on bright Ni	Fe, Cu	0.96	0.07	> 288	
Black Nickel	Zn/Al	0.96	0.07	> 288	
	Zn/Fe	0.94	0.09		
NiS/ZnS	Fe	0.90	Low		
	Al	0.94	0.15		
Black Chrome on bright Ni	Fe, Cu	0.95	0.09	427	
	Zn/Al	0.95	0.12	427	
	Any	0.96	0.10		
	Ni/Al	0.95	0.50		
	Cu	0.95	0.08	316	
				0.14	
		Zn/Fe	0.95	0.16	427
	Fe	0.91	0.07	427	
	Fe	0.94	0.20	150	
Selective electroplate deposits, Type B					
Black copper	Cu	0.85	0.10	316	
Natural oxide	Cu	0.75	0.33		
CuO	Cu	0.09	0.11		

Table 2 (cont.)

Coating	Substrate	Absorptivity	Emissivity	T _{max} (°C)
CuO	Al	0.93	0.11	
CuO/ZnO	Zn/Al	0.88	0.20	
KMnO ₄ treatment	Al	0.70	0.08	
CuO	Fe	0.90	0.16	427
Fe _x O _y	Fe	0.85	0.08	150
+Silicon	Fe	0.89	0.32	
Zn, Cr ₂ O or ZnO,	Zn/Fe	0.93	0.08	
Co ₂ O	Ni	0.92	0.08	

Types of absorbers were categorized to 1) intrinsic, 2) semiconductor-metal tandems, 3) multilayer absorber, 4) multi-dielectric composite coating, 5) textured surfaces and 6) selectively solar-transmitting coating on a blackbody-like absorber [23, 24]. Suitability of application of each type absorber is considered by temperature range of produced requirement and high efficiency in terms of high absorbance and low emittance. Property of selective coatings are shown in Table 2.

Aluminum coating

The aluminum coating is the process to add anticorrosive on the aluminum, by making thin films coating the aluminum surface, this can be prepared by various deposition methods, e.g., evaporation, sputtering, polymer coating by electrochemical technique [25] and also by an anodization method. The coatings of colored and black solar thermal absorber on aluminum surface were studied for the application of building integration such roofs, compared the chromaticity and optical properties by varying the film thickness, 3-layer stack. Co-sputtering Ti_xAl_yN samples. The results show the solar absorbance of such a single layer coating at 0.8 - 0.86 and the thermal emittance of 0.04 - 0.08, the solar absorbance of green color is 0.92 and emittance of 0.08 which is close to the valuable of the black solar absorbers in the common market if anti-reflection is added on the top layer [26].

Anodized aluminum

Anodizing is a decomposition protecting method of aluminum that causes stable oxide of aluminum (Al_2O_3) by electrolysis. The oxide of aluminum that was anodized is hardened with small porous that reserve the stain pigment, this is more durable from corrosion and an insulator. The steps of anodization are shown in Figure 4, starting with the cleaning of the sample to remove all surface dirty, as the pre-treatment, etching is the next step to remove a thin layer of aluminum by alkaline (Sodium hydroxide) and desmutting. Rinsing in an acidic solution to remove unwanted surface particles which are not removed by the etching process, and the passing the anodizing step by immersing the sample in the tank containing an electrolyte, acid solution (sulfuric, chromic, phosphoric or nitric). The direct current is passed through the sample to making anodized film, and coloring on anodic film by absorptive dyeing then, the final step is sealing the porous oxide coating to resist corrosion and stains. De-ionized water was used for rinsing in each step of the process, some using. The properties of produced thin films can be controlled by appropriate condition; chemical composition of the electrolyte and other parameters such as temperature and current density in case of an anodizing preparation process.

The main types of aluminum anodization method as;

Type I – Chromic acid anodization

Type II – Sulfuric acid anodization

Type III – Sulfuric acid hardcoat anodization

Other methods; following MIL-A-63576, AMS 2469, AMS 2470, AMS 2471, AMS 2472, AMS 2482, ASTM B580, ISO 10074 and BS 5599 [27].

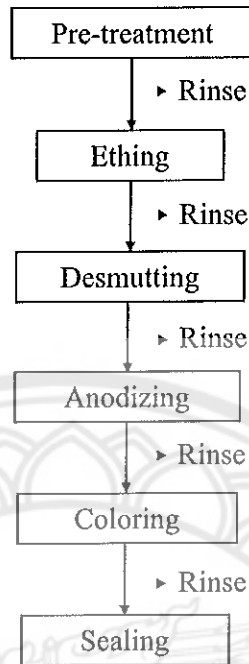
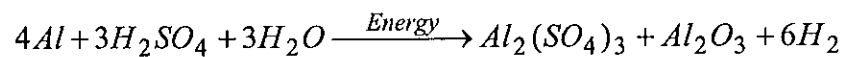
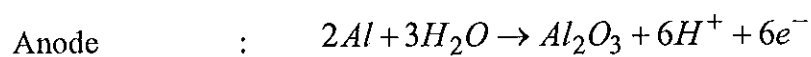


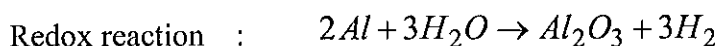
Figure 4 Flow chart of the anodization steps

Surface cleaning is necessary before anodizing. Direct current electricity is used in the anodize coating and the aluminum sheet is soaked in solution (Chromic acid, Sulfuric acid, Phosphoric acid, chemical organic acid etc.) as shown in Figure 5. The sulfuric acid (H_2SO_4) is the most commonly use as electrolyte, because it can make several film thickness, colorless film (for filling any pigments into the film). The reaction releases hydrogen atoms at the cathode then becomes to hydrogen gas. The oxygen ion from water splitting and hit the aluminum surface to build the aluminum oxide up, chemical reaction as follows [28];



The redox reaction is shown below;





When the current is flowing to the cells continuously, sulfuric acid begins to decompose. The negatively charged anions, i.e. hydroxide, sulfate move to the anode. The electrical charge in the circuit makes positively charged aluminum ions (Al^{3+}) to generate in the anode and form aluminum oxide at the surface. At the same time, the hydrogen ions move to the cathode, where they are reduced to hydrogen gas.

The factors that affect the thickness of aluminum oxide formation, depending on concentration of anodizing solution, temperature of anodizing solution and electric current. More thickness as a result of higher corrosion durable, the shape of the oxide film is hexagonal form, 5 – 150 μm thickness could be produced.

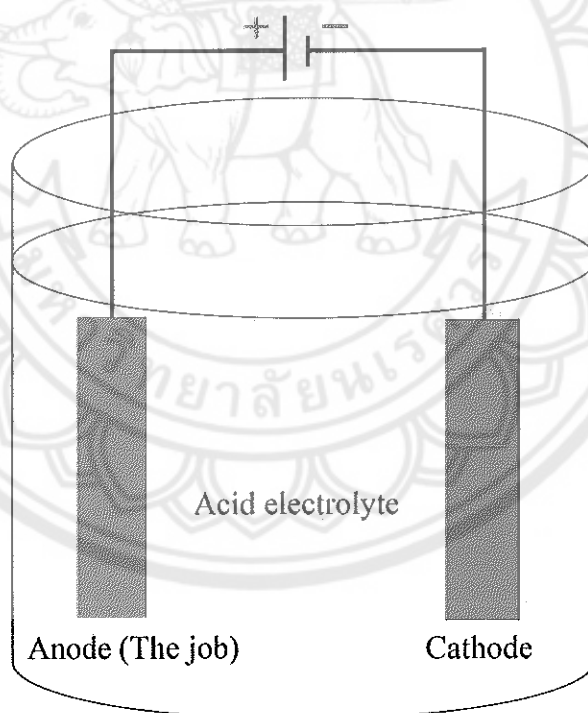


Figure 5 Anodizing method of substrate in the acid electrolyte

The anodization method goes through an electrolytic oxidation process to increase the oxide layer thickness on the aluminum surface by dipping the aluminum in the electrolytic solution and then passing the current through it. The aluminum

serves as the positive electrode and the hydrogen is formed by the reaction at the negative electrode. The oxygen from the composition of water is reacted with the aluminum surface causing the build-up of aluminum oxide film. The following 3 basic methods are shown in detail below.

1. Surface dyes or pigments

The anodized substrate is soaked in the bath containing organic or inorganic pigments. The colorant is absorbed into the pores of the film and subsequently sealed in. The color from organic dyes can change and become pale from environmental factors such as UV radiation. While the color from inorganic pigments is more durable from UV radiation convincing, but no acceptable for longer time in environmentally.

2. Integral color

The integral coloring process is like the electro-chemical method by soaking the aluminum substrate in special electrolyte, with carefully controlled electrical conditions and temperature for various time periods to produce a variety of colors. The colors are due to the coloring of the intermetallic particles that are spread throughout the depth of the anodic film.

3. Electrolytic Deposition

Coloring on the metal and metal oxide are electrolytic deposited at the base of the porous anodic film, and the film is sealed and locked within the clear anodic film.

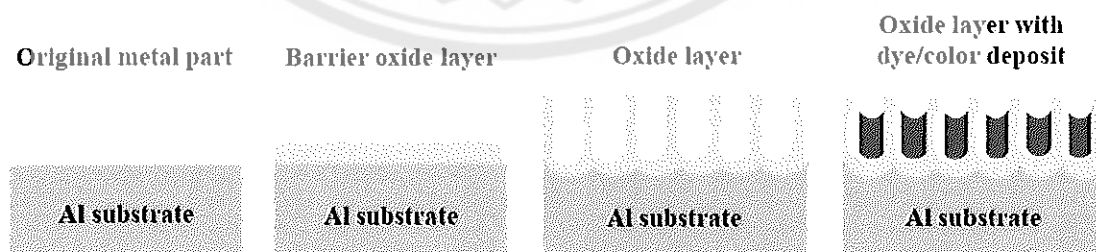


Figure 6 Anodization procedure on the aluminum sheet

The process of anodizing on the aluminum sheet along with dye or color deposit is shown in Figure 6, and the anodic film consists a small porous hexagonal

cylinder on the substrate surface as shown in Figure 7, that can absorb and are ready for the coloring process, absorptive dyeing and slither maintain, but it is not yet corrosion durable until sealing by some coating the pigments such as teflon, nickel acetate, cobalt acetate and sodium dichromate or potassium dichromate etc.

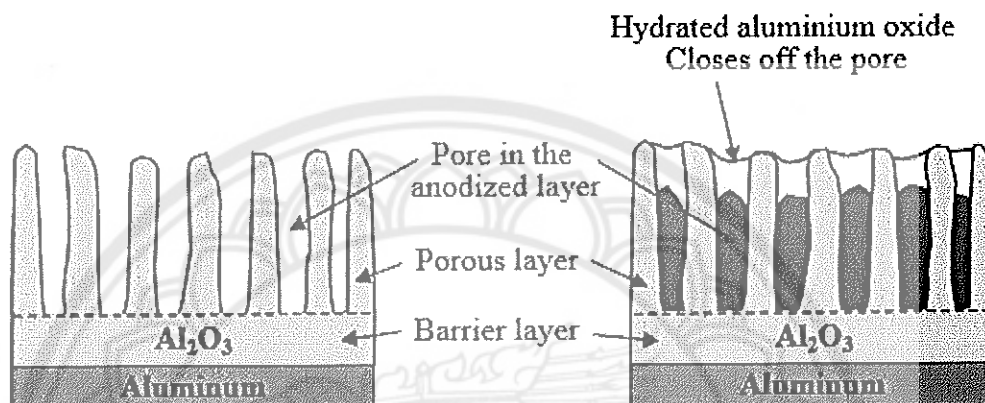


Figure 7 Cross section of anodic oxide layer on the aluminum surface

The relationship of reflectance and the deposited nickel and tin amount on the aluminum anodic oxide film on the surfaces was investigated by two distinct methods; energy dispersive X-ray fluorescence and specular reflectance measurement. Nickel borate and boric acid, tin sulfate and sulfuric acid were used during electrolytic coloring. In order to compare the surface density, the result shown that absorbance of nickel and tin electroplated aluminum specimens, as a function of the surface density that almost presented by linear relation, both of blank sample and also additives in coloring solutions. Nickel and tin had no significant difference properties. The absorbance of the electrolytic colored aluminum increases when the quantity of metal contained with the oxide layer increase until maximum absorbance value is reached [29].

Properties of anodized aluminum

The range of anodized aluminum has very good corrosion resistance, especially in the pH 4 – 9. Generally, the oxide layer is transparent and harder than glass and as hard as corundum but it depends on the anodizing process used. The

reflectivity of bright etched aluminum is high. The oxide layer is an electrical insulator. A sealed 15 μm oxide layer has a breakdown voltage of 500 – 600 V [30].

Determination of anodized aluminum

The physical and mechanical properties of aluminum oxide form (Al_2O_3) depending on the temperature of formation, which make it quite different thickness, structure, porosity, micro-hardness and resistant to change, while their chemical compositions almost remain unchanged. Determination method for characterized the anodized aluminum was presented by Oliver and Pharr approximation method [31]. The mechanical property of Al_2O_3 is determined by instrumented indentation techniques. The means of nano-indentation measurements is a method of determination of anodized aluminum material characteristics, that the indentation hardness and the indentation modulus are determined on the alumina film, SEM and EDX are used to analyze for performance to understand the structure changing, visualize the imprints and surrounding area of the aluminum layer [32].

Collector thermal performance

The collector performance test is operated with steady radiant energy falling on the collector surface under steady-state conditions [1], that can obtain and maintain the temperature to the fluid outlet, according to the ISO 9806-1 standard which provide the basic information to determine the efficiency base on the gross area of collector aperture area as shown in the following equation.

$$\eta = \frac{\dot{m} c_p (T_o - T_i)}{A_a G_t} \quad (1)$$

Where

η = Collector efficiency

\dot{m} = Fluid flow rate (kg/s)

c_p = Specific heat capacity (J/kg·K)

T_o = Fluid temperature at the collector outlet ($^{\circ}\text{C}$)

T_i = Fluid temperature at the collector inlet ($^{\circ}\text{C}$)

A_a = The gross collector aperture area (m^2)

G_t = Global solar irradiance at the collector plane (W/m^2)

The useful energy gain of the collector is calculated from

$$Q_u = \dot{m}c_p(T_o - T_i) \quad (2)$$

Where

$$Q_u = \text{Useful energy (W)}$$

And the useful energy from a solar collector at steady state is given by

$$Q_u = A_a F_R [G_t (\tau\alpha)_n - U_L (T_i - T_a)] \quad (3)$$

Where

F_R = heat removal factor

τ = Transmittance

α = Solar absorptance

U_L = overall heat loss coefficient ($\text{W}/\text{m}^2 \cdot ^\circ\text{C}$)

T_a = Ambient air temperature ($^\circ\text{C}$)

The thermal efficiency is taken by dividing Q_u by the energy input ($A_a G_t$), as shown in this equation.

$$\eta = F_R (\tau\alpha) - F_R U_L \left(\frac{T_i - T_a}{G_t} \right) \quad (4)$$

A thermal efficiency equation was performed with a convenient mathematical tool of a linear least-squares fit established with a 30 data points/sample. The performance curve of the ETC is presented as a straight line of the efficiency versus the estimation of different temperatures divided by solar irradiance as shown in Figure 8. The intercept of the line with vertical axis is the maximum efficiency of the collector ($F_R(\tau\alpha)$) and the slope of the line has no useful energy ($-F_R U_L$) [1]. The collector was tested according to ISO 9806-1 standard for an open loop system as shown in Figure 9.

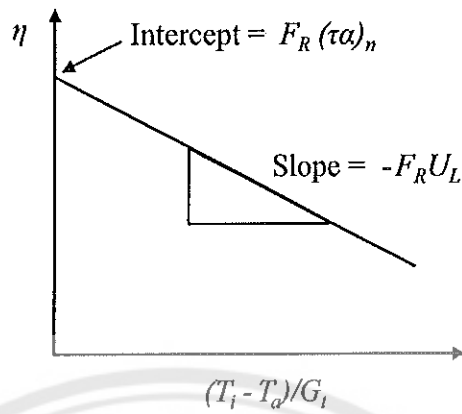


Figure 8 ETC performance curve

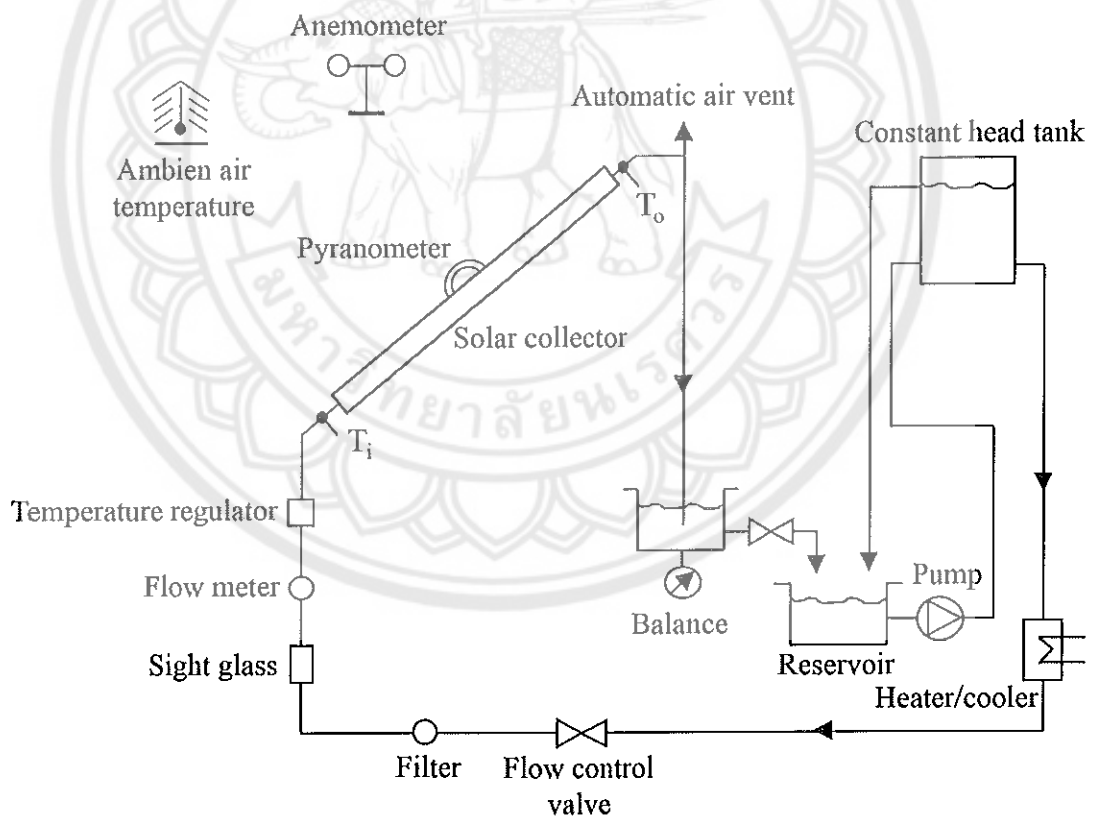


Figure 9 Open loop collector test system

Absorptance and emittance

The absorptance of substrates depends on the type of surface and the angle of incidence, that compare with the black body as an ideal absorber, and the emittance depends on the property of the surface and conductivity. Normally, metals have less emittance and smaller on the glossy surface (< 0.02), but may be increase on the coating surface by coating dyes or pigments, and oxidized metals. Calculation of absorptance (α) and amittance (ε) is similar (as equation 3), except the incident radiation must be specified [32]. In addition, the absorptance and emittance depend on the operating temperature. The solar absorptivity is expected to change a little at higher temperatures. In contrast, the thermal emissivity at different temperatures is strongly dependent on the position and sharpness of the cut-off edge from low reflectivity to high reflectivity at the operating temperature [33], they are defined as shown in equation 5.

$$\alpha, \varepsilon = \frac{\int_{\lambda_1}^{\lambda_2} (1 - R(\lambda)) I_s(\lambda) d\lambda}{\int_{\lambda_1}^{\lambda_2} I_s(\lambda) d\lambda} \quad (5)$$

Where

$R(\lambda)$ = The spectral reflectance, measured at a specific wavelength, λ

I_s = The solar spectra radiation

λ_1, λ_2 = Wavelength range

Thermal conductivity

The thermal conductivity (k) is calculated from thermal diffusivity (κ_d), which is measured by the laser flash analyser over the temperature range of 25 – 275°C according to ASTM 1461-13 standard, with density (ρ) and specific heat (C_p) as follow:

$$k = \kappa_d \rho C_p \quad (6)$$

Economic Analysis

1. Life cycle cost (LCC)

Life cycle cost (LCC) is the average energy price for lifetime using, which is a process for estimating the total cost and economic performance of the project over its whole life. It takes into account all costs of requiring, owning, and disposing of the project. LCC is based on assumptions of multiple project design options that diverge with respect to initial costs, operating costs, maintenance costs and possibly different life cycles, that have to be compared to select the maximizes net savings [34, 35], as shown in equation 7.

$$LCC = C_C + C_O + C_M + C_F - S \quad (7)$$

Where

C_C = Initial capital cost

C_O = Operating cost

C_M = Maintenance cost

C_F = energy cost

S = Residual values

2. Levelized cost of energy (LCOE)

Levelized cost of energy (LCOE) is defined as the total lifetime cost of an investment divided by the cumulated generated energy by investment [36], including operation and maintenance cost, operating results and fuel costs. Approach to definition by means of the net present value (NPV). The LCOE is the (average) internal price at which the energy is to be sold in order to achieve a zero NPV. Low LCOE, show the cost per energy prices are low, and if the LCOE is lower than the current cost of energy, shown to be highly effective technically and economically, as shown in equation 8.

$$LCOE = \frac{C_c + \sum_{n=1}^N \frac{C_n}{(1+i)^n}}{\sum_{n=1}^N \frac{E_n}{(1+i)^n}} \quad (8)$$

Where

C_c = Initial capital cost

C_n = Operating cost

E_n = Energy produced each year

i = Interest rate or discount rate

n = Project period

N = Year at the end of project

Literature Review

Many types of solar selective absorbers for concentrating solar power for high solar absorptance, and high reflection wavelengths of blackbody radiation at their operating temperature. Desirable characteristics for manufacturing are low cost and long-term stability.

Bermel, P. et al. [4] summarized selective solar absorbers in an overview. There are six types of selective absorbers; intrinsic absorbers, semiconductor-metal tandems, multilayer absorbers, cermets (ceramic-metal composite coatings), surface texturing and PhC-based designs. Cermets have good selectivity for using at high temperatures and can be successfully commercialized. A Cermet consists of one or more cermet layers, an anti-reflection layer and reflective substrate, to reduce absorption of undesired IR region. The solar selectivity of cermet can be optimized by varying the metal and constitute of the ceramic, particle and thickness of coating materials, particle concentration, size, shape and orientation. The high melting point metals are good candidates for cermet composition such as Au, Cu, Ni, Co, Mo, Cr, Pt, W and oxides such as SiO₂, MgO and Al₂O₃. The widely used solar selective coatings are black chrome, a graded Cr-Cr₂O₃ cermet, and Ni-pigmented Al₂O₃.

Various well known methods for anodizing aluminum to aluminum oxide (Al₂O₃) forming were proved many studied since preparation of aluminum plate, electrolytes, through to conditions of anodizing; electric current and temperature during operation.

Zhang, X. [37] determined the preparation of porous aluminum by anodization, cleaning or impurity removal from the surface aluminum plate is necessary. The two-step method of anodization is a general method for porous alumina preparation, electrolyte from any acids (e.g. sulfuric acid, oxalic acid, boric acid, phosphoric acid) and voltage is generated during this method. The lower voltage is an important factor for attraction to the advantage of pore density and porosity of alumina membrane fabrication and also the temperature offer to get more regular pore array if lower and vary under a small range.

Padwal, P., & Kulkarni, S. [38] prepared the aluminum oxide film by anodic oxidation and the effect of plasma etching on its surface by glow discharge plasma, and studied the surface using scanning electron microscope (SEM) and atomic force microscope (AFM) on 3 samples; untreated aluminum sample, Aluminum oxide film formed on Al substrate by the process of anodic oxidation and Aluminum Oxide film etched in Air Plasma. Different results of the oxide coating on the surfaces such as roughness, related to the parameters of the anodizing process selected and deposition conditions. The volume expansion of anodized aluminum oxide was and conducted with mixed solutions of phosphoric and oxalic acids. In the study it was revealed that the anodization conditions increase the volume expansion, when you increase the current density, aluminum consumption rate, anodizing voltage, temperature and pH values of electrolytes. The anodization time for coating the aluminum surface is an essential factor for different thicknesses of paint color.

Shaffei, M.F. et al. [18] compared the optical, protection from environmental aspects, and thickness of black Tin and Nickel as selective absorber coatings. Variation of anodization time from 10 to 60 minute at a constant coloring time of 5 minute. The study revealed that the thickness of the anodic coating was increased with increasing anodic oxidation time, but the anodic layer form the tin coating is higher than the nickel coating at all anodization times. The reflection percentage of anodized aluminum reduced lower than aluminum before processing markedly, and the tin coatings anodized for 45 minute is strongly recommended to produce more thermally efficient solar collectors.

The corrosion rate and corrosion resistance of anodized aluminum are sharply reduced compared to lower non-anodized aluminum. Moreover, the nickel coated samples are rapidly corroded higher than tin coated samples.

Djozan, D., & Amir-Zehni, M. [39] investigated a method for anodizing the inner surface of long and small-bore aluminum tubes, to indicate the optimum conditions of electrolyte solution, temperature, voltage and anodizing time for the Al_2O_3 layer during processing time in both dynamic and static modes. The study revealed that, a porous and stable layer, 45 μm thick. The inner surface of a long and small-bore aluminum tube using the dynamic anodizing process, could effectively be coated by Al_2O_3 , and the uniformity of the coated layer, chemical stability, and long durability are the main advantages of this coating.

Tsangaraki-Kaplanoglou, I. et al. [40] studied the effect of alloy types (AA 5083 and AA 6111, unheated and heat-treated) the anodizing process of aluminum to compare with pure aluminum, by SEM/EDS and XRD techniques. The results revealed that, the stage of porous structure development of AA 5083 alloy were considerably identical with that of pure aluminum. For AA 6111 alloy, the stage of readjustment of pores during the process before the current reaches a steady stage was missing, this is proof that modification of composition and morphology of the film, and oxide growth rate of AA 6111 alloy under standard anodizing conditions was similar to that of pure aluminum. And although under various operating conditions, both alloy types were also relative to that of pure aluminum. In addition, for AA 6111 alloy, the heat treatment affects anodizing kinetics and enhances slightly the anodizing current efficiency.

Belghith, M. et al. [5] studied the preparation of selective solar absorbers obtaining Ni pigment by anodization of 6060 aluminum surface, and measured the optical properties of the coated layer. They found that the optical properties depend on both the oxide film thickness and the Ni content. The thicknesses of the oxide film were 0.30, 0.50 and 0.70 μm . The pigmentation time took between 4 – 6 min. The α of 0.30, 0.50 and 0.70 μm of oxide thickness were 0.95, 0.95 and 0.94 respectively, and the normal ϵ at 100°C were 0.18, 0.13 and 0.22 respectively. The thermal stability was investigated in the optimized optical properties coated layer (0.5 μm) by varying the heat treatment in air and under vacuum conditions at 400 and 500°C for 5 and 10 days.

The optical properties of the coating at 400°C have no change. While at 500°C for 10 days, the α dropped to 0.92, but there is no significant change of the normal ϵ . Furthermore, the state of the coated surface was quit homogeneous up to about 450°C.

Sella, C. et al. [6] investigated the microstructure and growth mechanism of co-sputtering Pt -Al₂O₃ nanocermet films onto float-glass, stainless steel and silicon substrates. The volume fraction of Pt was fixed at 0.25. The film thickness, metal concentration and thermal annealing were considered by small-angle X-ray reflecometry (SAXS), transmission electron microscopy (TEM) and atomic force microscopy (AFM). The Pt -Al₂O₃ film is more compact in the growth direction than in a plane.

Kallithrakas-Kontos, N. et al. [29] studied two methods for investigation of the relationship between the specular reflectance in the visible region and the deposited amount of nickel and tin on aluminum oxide film surfaces. The coloring solution contained nickel borate and boric acid, another solution contained tin sulphate and sulphuric acid. Various organic additives were used as electrolytes in the coloring solutions to improve the efficiency of the electrolytic procedure. The absorbance was derived by an exponential relation, which was a function of the deposited metal density on the surface. The absorbance of anodized aluminum in nickel electrolytes increases with the increasing of amount of nickel contained within the oxide pores. A rather linear relation exists for the low density region, while the tendency of absorbance increases to the maximum value as the surface increases density. The absorbance of anodized aluminum in tin electrolytes were almost a linear relation. The lower absorbance indicating a lower metal filling in the aluminum oxide pores. The initial slope of nickel and tin deposited is similar at about 0.021 cm²/μg, and the slope increases in the nickel electrolytes with additive solutions.

Tesfamichael, T., & Roos, A. [41] succeeded in antireflection improvement of tin oxide (SnO₂) coated on nickel-pigmented anodic aluminum oxide (Ni-Al₂O₃) as a selective solar absorber. The solar absorptance of Ni-Al₂O₃ depends on the coating thickness and quantity of nickel particles embedded in the Al₂O₃ pores. The doping and deposition temperature of the pyrolytic sprayed SnO₂ coating can modify the solar absorptance and thermal emittance. Enough coating thickness also can be a good protecting layer. Dipping samples in silica sol was a further improvement of solar

absorptance without affecting to thermal emittance. The coated layer seems to be durable; resists high temperature, corrosion, chemical attacks and unaffected by outdoor exposure for 2 months.

Nuru, Z.Y. et al. [42] studied about Pt-Al₂O₃ nanocoatings for high temperature concentrated solar power applications (> 650 °C). This study focus on the optimization of Pt concentration in Pt-Al₂O₃ multilayer of cermet samples with and without reflection layers. The cermet layers were Pt-Al₂O₃/Mo/Stainless steel substrate and anti-reflection Pt-Al₂O₃/Mo/Stainless steel substrate. The samples with and without reflection layers demonstrated very low reflectance $\leq 0.05\%$ and optical absorption was high in the UV-vis-NIR regions (> 98%).

Wazwaz, A. et al. [43] determined the solar thermal performance of a nickel-pigmented aluminum oxide (Ni-Al₂O₃) selective absorber by using a prototype model of flat-plate collector with different volumes and different selective absorber samples. The models were tested outdoor under a clear sky during daylight. The collective flux was in the range of 590 – 699 W/m². They found that at constant emissivity, the net collective flux strongly increases as absorptivity increases, and conversion efficiency slightly increases. At constant absorptivity, the net collective flux decreases as emissivity increases, while conversion efficiency was not strongly affected. The maximum conversion efficiency was in range 0.73 – 0.78. The absorptivity was in the range 92.0 – 97.0%, while the emissivity was in the range 11.0 – 22.5%.

Ghoneim, A. A. et al. [44] analysed the performance of evacuated tube collector (ETC) in a hot climate (Kuwait). The model of ETC was validated by experimental data and provided by a manufacturer to investigate the thermal performance of the ETC for space heating, domestic water heating and air conditioning as required for typical house in the country. The optimum area of the collector was approximately 44 m². The annual life cycle saving (LCS) was 2,300 USD.

Ghoneim, A. A., & Mohammedein, A. M. [45] studied the effect of different parameters of a collector's thermal performance of a parabolic trough solar collector in a hot climate (Kuwait). The possibility and environmental impacts of integrating renewable energy in buildings were considered. The life cycle saving (LCS) and levelized cost of energy (LCOE) also were calculated. The calculation was based on

the estimated initial cost of the system and the discount rate adopted by the Kuwaiti government's plan for long-term use (6.5%). The optimum collector area was 850 m², which could avoid CO₂ emissions of approximately 980 t/year, and the cost of CO₂ saved was 0.024 USD/kWh. The LCS for the optimum conditions was 2,300 USD/kWh. The LCOE of the system after deducting the CO₂ cost exhibited approximately equal to 0.153 USD/kWh, which is similar to the current electricity producing cost in Kuwait (0.15 USD/kWh).



CHAPTER III

RESEARCH METHODOLOGY

Procedure and methodology

The procedure and methodology in this study are shown in Figure 10.

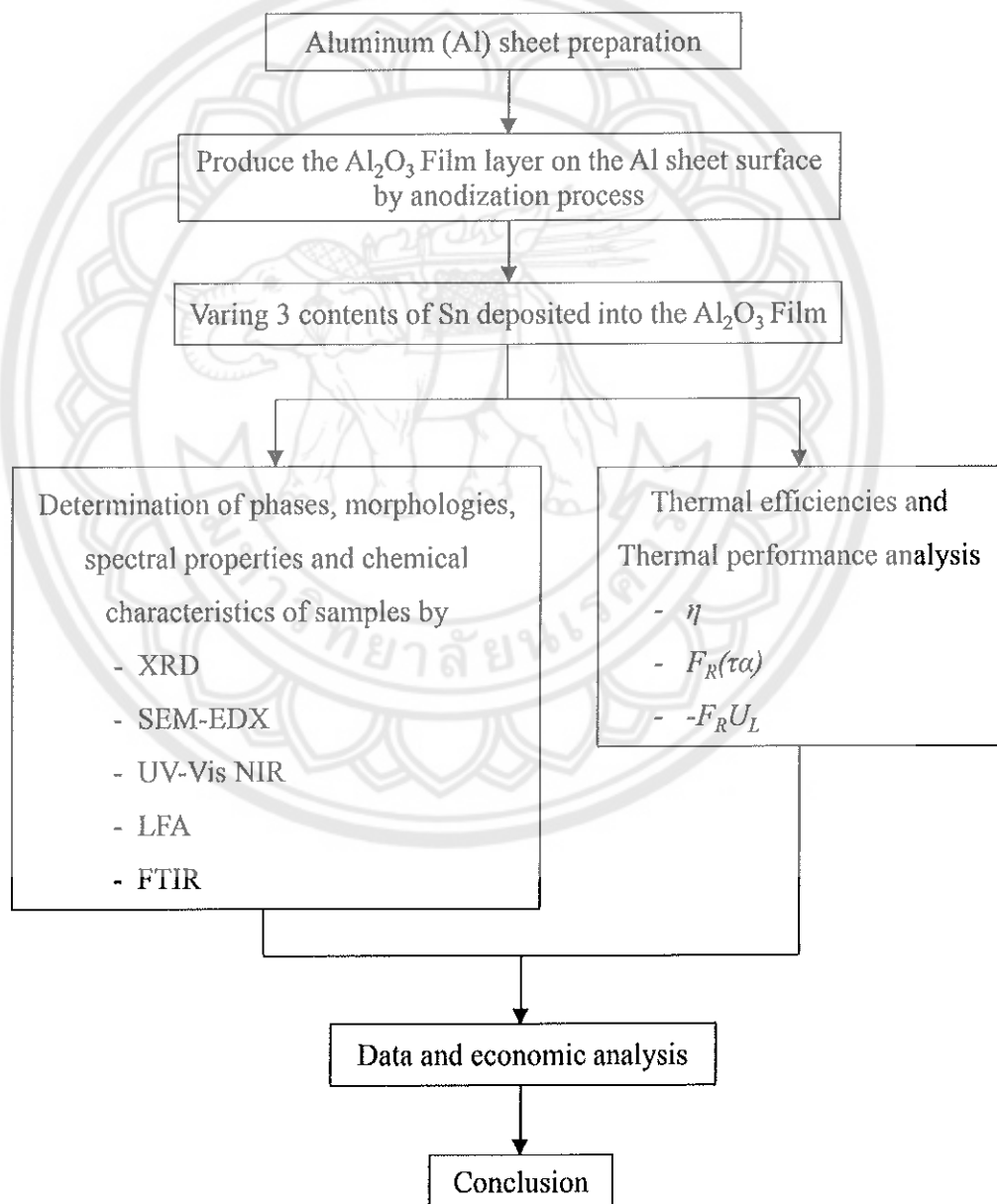


Figure 10 Flow chart of procedure and methodology of the study

Preparation of anodized aluminum sheet

Aluminum (Al) sheet of 9 cm wide \times 160 cm long with a thickness of 0.02 cm was used as a substrate. It was followed by the anodization process, under suitable conditions calculated by the surface area of the samples. Firstly, the aluminum sheet was degreased with a commercial cleaning solution, and then etched by NaOH solution, and immersed in 165 g/l sulfuric acid solution. The Al substrate was connected with an anode (+) and a lead plate was used as the cathode (-), and then a direct current of electrical density with 1,000 A at the constant potential of 15–17 V at 20°C was applied for 45 minutes to achieve the Al₂O₃ film thickness of 9.1 - 9.5 μ m. Subsequently, the formed Al₂O₃ film was directly transferred to the colouring bath containing tin (II) sulphate (SnSO₄). In this process, the deposition of tin pigmentation into the pores of translucent Al₂O₃ film (Sn-Al₂O₃) was carried out for 5, 7 and 10 minutes, which were coded as Sn-Al₂O₃-5, Sn-Al₂O₃-7 and Sn-Al₂O₃-10, respectively. Then, the porous Al₂O₃ was sealed in a hot water tank at 50-60°C for 30 minutes.

Characterization of Tin

Tin (Sn) is a chemical element in group IVA, period 5, atomic number is 50, atomic weight is 118.71 g/mol, density is 7.365 g/ m³ (for white, β -tin) and 5.769 g/ m³ (for gray, α -tin), thermal conductivity is 66.8 W/m.K.

Tin resists corrosion from water but can be attacked by acids and alkalis, high polished and is used as a protective coat for other metals. As prevent further oxidation in oxide layer form.

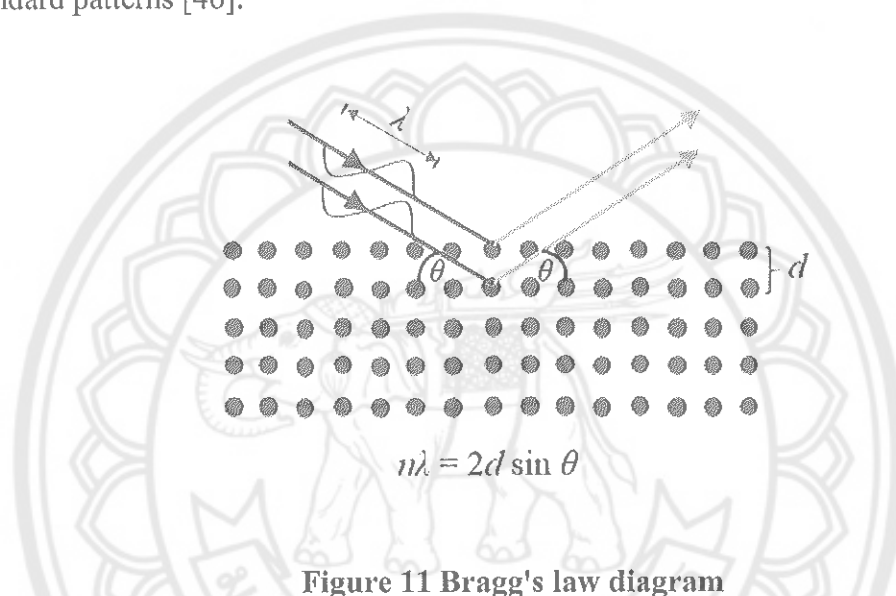
Apparatus for characterization of anodized aluminum sheet

The samples of the aluminum sheet characterized the phase, morphology, spectral reflectance (R) to calculate the solar absorptance (α_{sol}) and thermal emittance (ϵ_{therm}) and thermal diffusivity to calculate the thermal conductivity (k) by following instruments:

1. X-ray Diffractometer (XRD)

X-ray diffractometer (XRD) is a device for phase identification of a crystalline structure, atomic spacing and provides information for unit cell dimension. X-ray diffraction is based on the interaction between X-ray interference and crystalline

sample. Bragg's law ($n\lambda=2d \sin \theta$) was used to calculate the X-ray diffraction that scanned through a crystalline sample as shown in Figure 11. The wavelength of electromagnetic radiation related to the diffraction angle and lattice spacing in the crystalline structure. The diffracted X-rays are detected and counted. The diffraction peaks are converted to d-spacing provides the mineral identification because d-spacing of each mineral is unique. Typically, it is achieved by comparison with reference standard patterns [46].



The basic elements of X-ray diffractometer consist of an X-ray tube, an X-ray detector and a sample holder. The cathode ray tube can generate X-rays by heating a filament to produce electrons. The electrons are accelerated toward a target by using voltage and bombarding electrons on the target. When the electrons have adequate energy to exclude the inner shell electrons of the target, the X-ray's spectra is produced. The main component of these spectra are K_{α} and K_{β} , which are different in wavelength and intensity. The specific wavelengths identify each material (Cu, Mo, Fe, Cr). Copper (Cu) is the most common material as a target for single crystal diffraction ($\text{Cu-}K_{\alpha} = 1.54 \text{ \AA}$). These X-rays are directed at the sample and detector are rotated, then the intensity of the reflected X-rays is recorded. The impingement of incident X-rays on the sample satisfies the Bragg equation, then the interference and peak in intensity occurs. The X-rays signals are converted to a count rate, then output to a monitor or printer.

In this study, the XRD pattern is applied to find the phase of composition in the Sn-Al₂O₃ samples. The phase of the samples will be carried out on a Philips X'pert PANalytical X-ray diffractometer (Figure 12) with Cu-K_α radiation in the 2θ range of 10 - 100°.

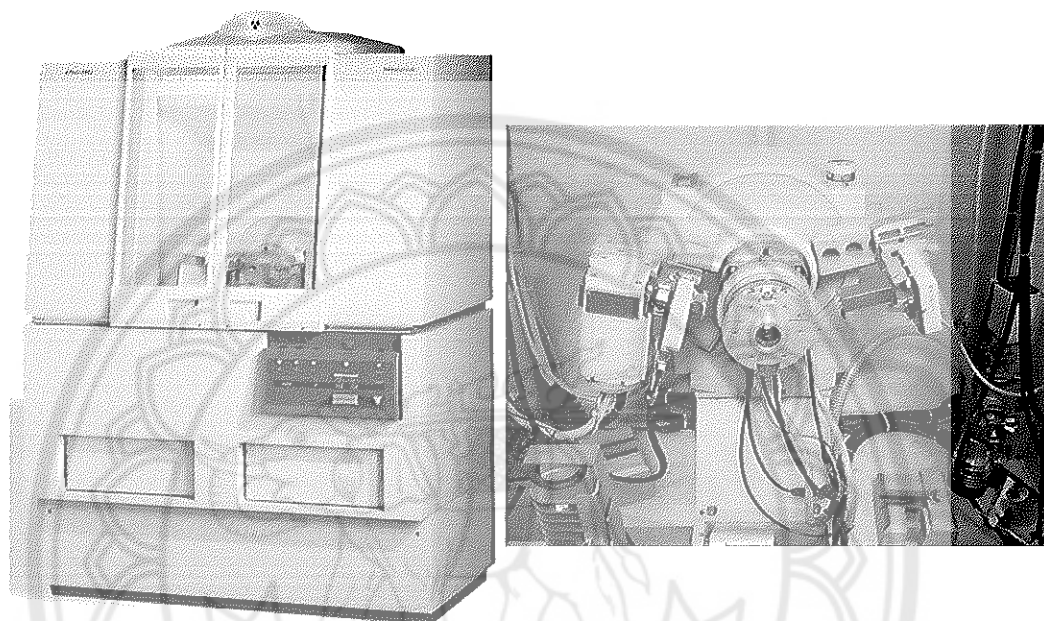


Figure 12 X-ray Diffractometer (XRD, PHILIPS X'Pert-MPD)

Sources: <https://www.icsp.nat.fau.eu/philipspanalytical-xpert-pro-mpd-powder-diffractometer/>
and http://www.x-ray.gatech.edu/images/mpd_HTK2000.JPG

2. Scanning Electron Microscope equipped with an Energy Dispersive X-ray analyser (SEM-EDX)

Scanning Electron Microscope (SEM) is a device that provides information about the surface, topography, chemical composition, crystalline structure and electric behavior of specimens by scanning the sample surface with a focused electron beam. Interaction between electrons with atoms at various depths in the sample can produce secondary electrons (SE), back scattered electrons (BSE), characteristic X-ray, diffracted backscattered electrons, visible light, and heat. The signals from the SE or BSE are the two most common types of images [47]. These

electrons are collected by detector and display the image on a cathode ray tube (CRT), computer monitor or TV screen. The secondary electron image (SEI) occurs from interaction of the primary electron beam with the specimen surface, then the secondary electrons are emitted from the surface, and the high resolution image is produced. The BSE image occurs from primary electrons impinging the specimen surface, which emerge from deep locations in the specimen, then reflected to the monitor. The SEI is higher resolution than the BSE image, but the intensity of the BSE signal is strongly related to the atomic number of the elements. Furthermore, the BSE image can provide the distribution of the elements in the specimen. For this reason a BSE image is often used in the SEM analysis along with the characteristic X-rays spectra. A schematic of the main component of SEM are shown in Figure 13. A typical SEM's parts consists of electron guns, electron lenses, column parameters, image formation and vacuum system [48]. The electron gun typically uses a tungsten filament thermionic emission type and the field emission guns are used for higher resolution. The electrons are accelerated to an energy between 1 - 30 keV. The condenser lenses consist of 2 or 3 lenses for controlling the electron beam to 2 – 10 nm [49]. The amount of electrons are controlled by an aperture. The fine electron beam is focused and scanned across the specimen surface by scanning coils. A detector counts the number of SE or BSE, then the signals are convert to topographic image of the sample.

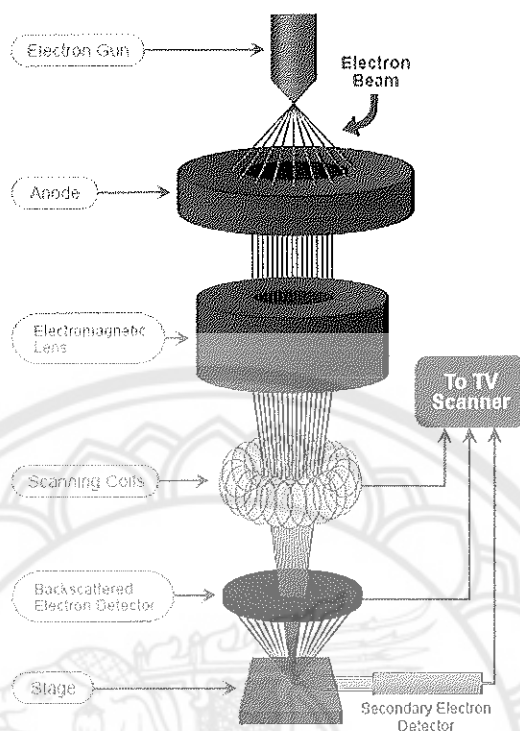


Figure 13 Internal component of Scanning Electron Microscope

Source: <http://www.nanoimages.com/sem-technology-overview/>

There are many types of SEM; Conventional (High vacuum) SEM, Low Vacuum SEM, Cryo on an SEM, Environmental SEM, Focused ion beam (FIB) and Electron-beam lithography. In this study the Low Vacuum SEM (LV-SEM) was used to characterize the morphology of the samples. The LV-SEM can be used to analyze a non-conductive sample surface. The back scattered electron (BSE) is used for imaging. BSE of non-conductive and uncoated samples can provide information about the composition via the contrast image: darker regions have a lower atomic number than brighter regions [50]. Furthermore, Energy Dispersive X-ray spectroscopy (EDX) can be coupled with SEM (SEM-EDX). The EDX is a technique to identify the elemental composition which is non-destructive to the specimen. The data generated by EDX provides mapping with their relative proportions (atomic % of elemental composition for example) [51]. The Low Vacuum Scanning Electron Microscope

equipped with an Energy Dispersive X-ray analyzer (LV-SEM-EDX) used for sample analysis in this study is shown in Figure 14.



Figure 14 Low Vacuum Scanning Electron Microscope equipped with an Energy Dispersive X-ray analyzer (LV-SEM-EDX, JSM-5910 JEOL)

3. Ultraviolet-Visible-Near Infrared Spectrophotometer (UV-Vis NIR Spectrophotometer)

Spectrophotometry is a measurement technique to measure the amount of intensity or concentration of a chemical substance. Ultraviolet-Visible-Near Infrared Spectrophotometer (UV-Vis NIR Spectrophotometer) is an instrument to measure the percentage of light reflected, transmitted or absorbed by the sample. The light source can be classified into 2 types: UV-Visible wavelengths are in the range of about 185 – 700 nm of the radiation spectrum and Near Infrared wavelength is in the range of about 700 – 2500 nm of the radiation spectrum [52]. When an incident light comes into a solid, many phenomena happen. The beam may be reflected, diffused, transmitted, absorbed, refracted or polarized as shown in Figure 15. Measurement of reflectance for a solid sample, there are 2 kinds of reflectance: specular and diffuse. Specular reflectance is the part of the reflected incident beam at the same angle as incident angle (as mirror reflectance). Diffuse reflectance is the part of reflected

incident beam in all directions (as occurs from powder reflectance). Most samples produce both types of reflectance [53].

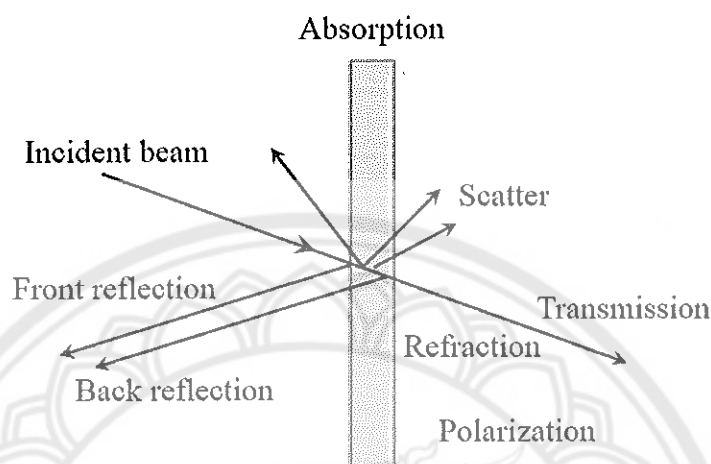


Figure 15 Light interaction with a solid

UV-Vis-NIR spectrometer consist of a means for sources of UV-Vis-NIR radiation, wavelength selector, sample containers, detector and signal processor and readout. The spectrometer operates by a light beam passing through a sample and the wavelength reaches a detector. The information from analysis can be revealed in transmittance or reflectance. Light is quantized into small packets of photons, the photon transferring occurs when the energy level of the photon is equal to the energy required to get the promoted electron to the next energy state. Normally, a certain wavelength of light and energy is irradiated on a sample, which absorbs from the incident light. The energy of the light transmitted from the sample can be measured using a photon detector. The Lambert-Beer rule is a principle of quantitative analysis. The relationship establishes when light intensity I_0 is directed to a material and light intensity I is transmitted. The value of I/I_0 is called transmittance (T), the value of $I/I_0 \times 100$ is transmission rate ($T\%$) and the value of $\log(1/T) = \log(I_0/I)$ is absorbance [54].

In order to characterize the performance of an absorber material, solar absorptance (α_{sol}) is one parameter that needs to be considered. The α_{sol} is defined as a fraction of incident radiation at a given wavelength on the surface that is absorbed.

It is calculated by weighting the spectral reflectance with the solar irradiation over the solar spectrum wavelength ($I_s(\lambda)$) [8] as indicated in Eq.5. In this study, the R of the samples is measured by UV-Vis NIR Spectrophotometer, Shimadzu UV-3101PC model as shown in Figure 16.

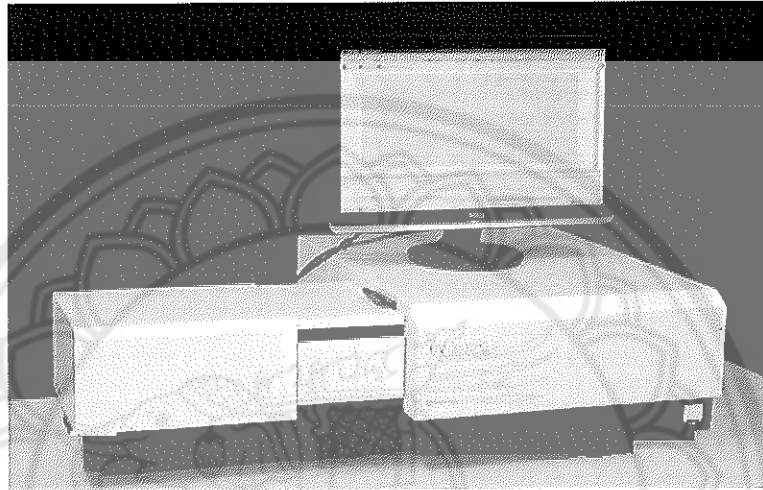


Figure 16 Ultraviolet-Visible-Near Infrared Spectrophotometer (UV-Vis-NIR Spectrophotometer, Shimadzu UV-3101PC)

Source: https://www.wotol.com/1-shimadzu-uv-3101pc-uv-vis-nir-w-isr-3100-integra/second-hand-machinery/prod_id/1272941

4. Laser Flash Analyzer (LFA)

A laser flash analyzer is an instrument used to measure the thermal diffusivity of materials. An energy or laser pulse heats from the back or bottom side surface of a sample and the temperature signal is detected versus time on the front or top side of the sample as shown in Figure 17. The laser flash measurement is supposed to have a single heat source. Supposing that the laser beam fits uniformly at the front of the sample, the heat source generates the thermal gradient in one direction [55].

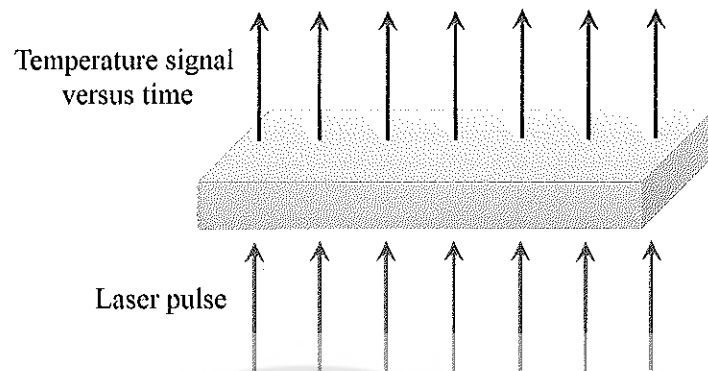


Figure 17 Principle thermal diffusivity analysis by laser flash method

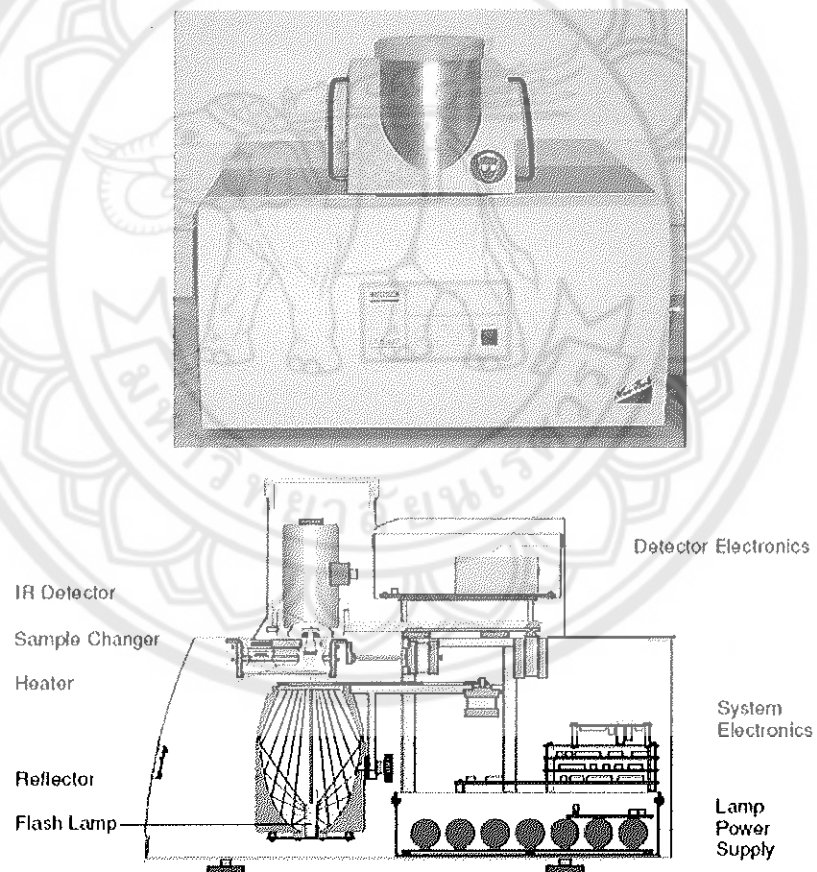


Figure 18 Laser Flash Analyzer (NETZSCH LFA 447 NanoFlash-A)

Sources: <https://scientificservices.eu/item/thermophysical-indicator-light-pulse-analysis-facility/534> and <https://www.sciencedirect.com/science/article/pii/S0008622307004009>

In this study, the laser flash analyzer model NETZSCH LFA 447 NanoFlash-A as shown in Figure 18 is used to measure the thermal diffusivity of the samples, over the temperature of 25 - 275°C according to ASTM 1461-13 standard. This laser flash analyzer generates the heat from the front side of the plane parallel with the short light pulse. The temperature rises from the back surface and it is detected by an infrared detector. The thermal diffusivity can be determined by the resulting temperature versus time curve analysis [56]. The thermal conductivity (k) was then calculated as the equation 6.

5. Fourier Transform Infrared spectrometer (FTIR)

Infrared spectroscopy is a measurement of interaction between a substance and the electromagnetic fields in the IR region. The molecule of the substance has specific frequencies of internal vibrations, and a higher vibration of the molecule occurs from absorbing IR radiation. The absorbed particular IR frequency depends on the vibrational frequencies of the molecule, but transmit all other frequencies [54]. Fourier Transform Infrared spectrometer (FTIR) is an instrument which uses the interferometer to identify about material placed in the IR region.

The IR light source passes through a Michelson interferometer and the sample. The interferometer consists of a beam splitter, fixed mirror, and moving mirror as shown in Figure 19. When the light passes through the beam splitter, it is divided to 2 optical beams. One beam reflects to a fixed mirror then back to a beam splitter, and another beam reflects to a moving mirror. The 2 beams reflect off their 2 reflective mirrors and meet up again and recombine at the beam splitter, but the path length of these 2 beams are interfering with each other (constructive and destructive interference). This signal is called an interferogram, which is a unique property depending on the position of the moving mirror, which makes the different IR frequencies, and all these frequencies are measured simultaneously [57].

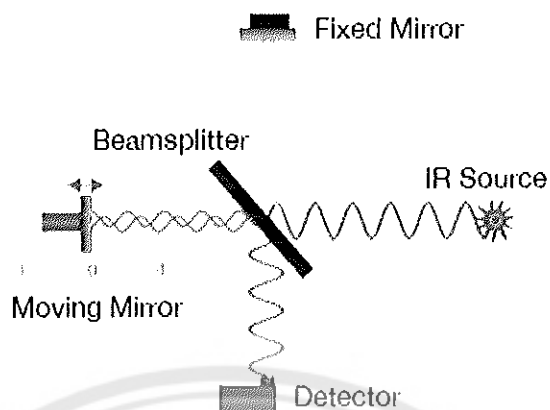


Figure 19 Schematic of a Michelson interferometer

Source: <https://www.thermofisher.com/us/en/home/industrial/spectroscopy-elemental-isotope-analysis/spectroscopy-elemental-isotope-analysis-learning-center/molecular-spectroscopy-information/ftir-information/ftir-basics.html>



Figure 20 Fourier Transform Infrared spectrometer (FTIR, Bruker Tensor 27)

Sources: <http://www.uakron.edu/cpspe/research-centers-facilities/equipment-polymer-science.dot>
and <https://www.cnyn.unam.mx/~wencel/departamento/irbruker>

In this study, the FTIR, Bruker Tensor 27 model (as in Figure 20) is used to measure the reflectance (R) of all samples in IR region (2.5 – 25 μm) to calculate the thermal emittance (ϵ_{therm}) as define in equation 5.

Sample preparation for analysis

1. XRD analysis

The X-ray Diffraction (XRD) was used to measure the phase of the samples. The samples for the XRD analysis were prepared to 1×1 square centimeter as shown in Figure 21.

2. Morphology characterization

The morphology was measured by Low Vacuum Scanning Electron Microscope equipped with an Energy Dispersive X-ray analyser (SEM-EDX). The samples for the morphology characterization were formed in Bakelite as shown in Figure 22.

3. Spectral reflectance measurement

The spectral reflectance (R) was measured by Ultraviolet-Visible-Near Infrared Spectrophotometer (UV-Vis NIR Spectrophotometer) to calculate the solar absorptance (α_{sol}), and by Fourier Transform Infrared spectrometer (FTIR) to calculate the thermal emittance (ϵ_{therm}). The samples for investigation of the R were prepared to 1×1 square centimeter as shown in Figure 21.

4. Thermal diffusivity measurement

The thermal diffusivity was measured by Laser Flash Analyzer (LFA) to calculate the thermal conductivity (k). The samples for investigation of the thermal diffusivity were prepared to 1.25×1.25 square centimeters as shown in Figure 23.

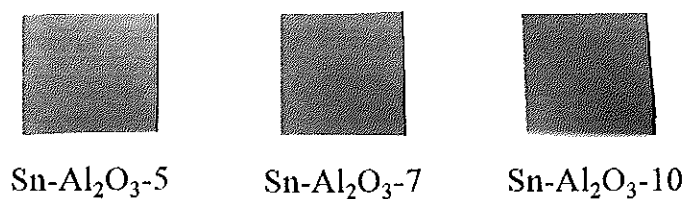


Figure 21 The 1x1 square centimeter samples for phase and reflectance characterizations

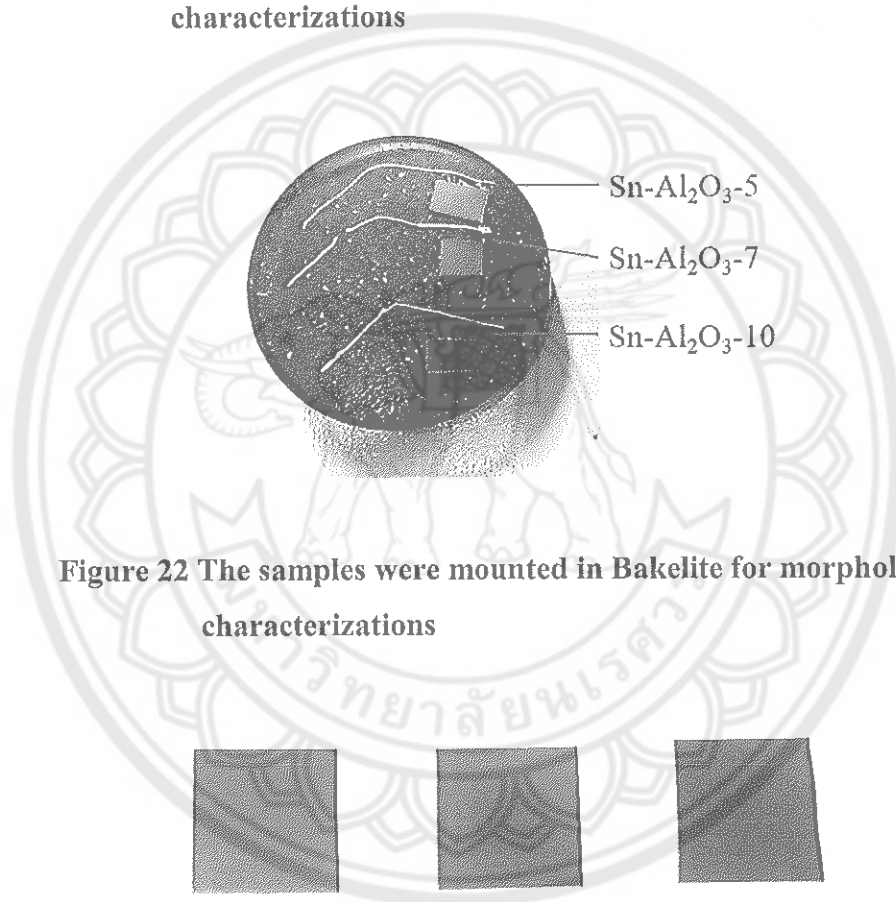


Figure 22 The samples were mounted in Bakelite for morphologies characterizations

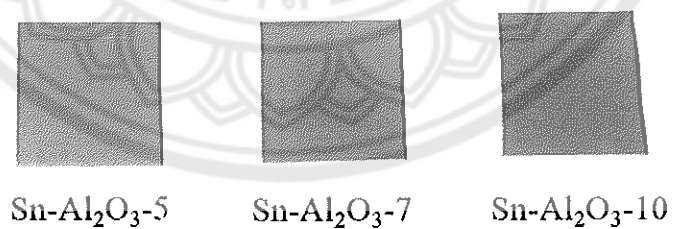


Figure 23 The 1.25x1.25 square centimeter samples for thermal diffusivity characterizations

Thermal efficiency

The Sn-Al₂O₃ selective solar absorber coated on Al fin was assembled with a heat pipe and transparent double layer borosilicate evacuated tube as one set of solar receiver tubes. Then, the new prototype of ETC was obtained by using 15 tubes of solar receiver tube sets mounted with a header and manifold as shown in Figure 24. The thermal efficiency test of the ETC was measured under steady-state conditions as prescribed by the ISO 9806-1 standard. The collector area is 1.08 m². The parameters for the thermal efficiency test consists of ambient temperature (T_a), fluid mass flow rate (\dot{m}) and global solar irradiance (G_T) at the collector plane, as summarized in Table 3. The inlet temperature (T_i) was controlled to be at 30, 40, 50 and 60 °C, while the outlet temperature (T_o) was collected. The thermal efficiency (η) was calculated by the first-degree equation (linear regression) according the equation 1.

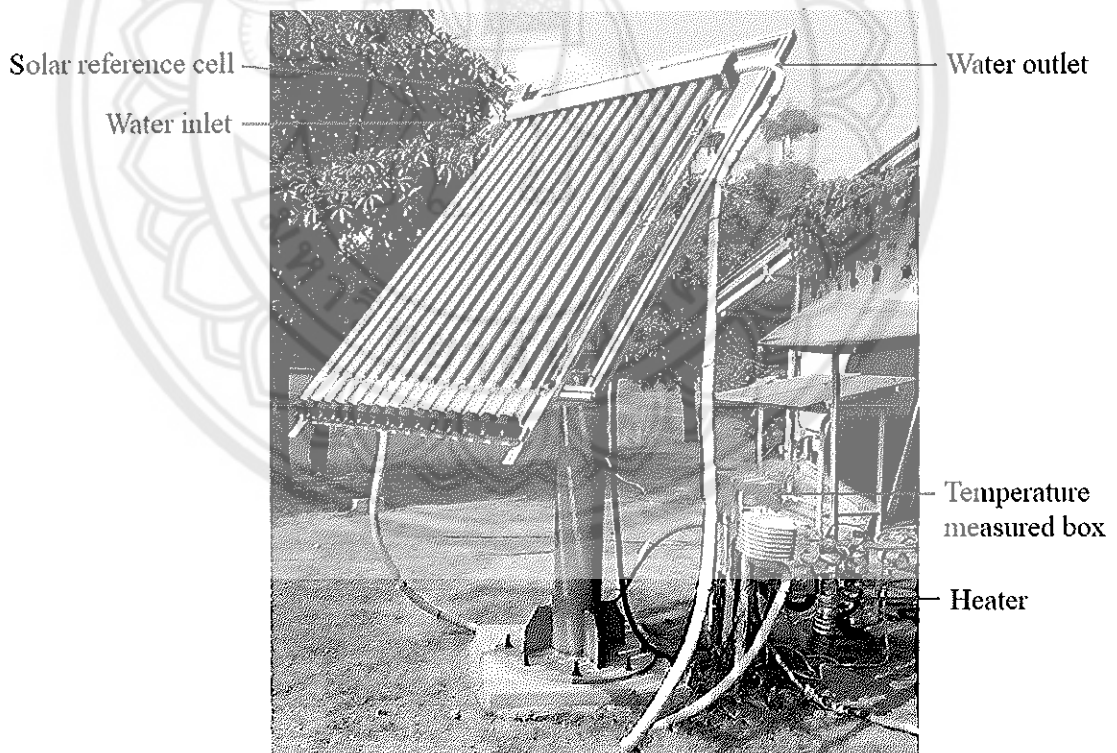


Figure 24 The evacuated tube collector equipped with header and stand as a solar water heater system for thermal efficiency test

Table 3 Parameters for the thermal efficiency test

Parameters	Factors
Solar irradiance (G_i)	$800 \pm 50 \text{ W/m}^2$
Ambient or surrounding air temperature (T_a)	29 - 31 °C
Fluid mass flow rate (m)	0.216 kg/s, $\pm 1\%$
Fluid temperature at the collector inlet (T_i)	30 - 60 °C, ± 0.1 °C

Economic analysis

Life Cycle Cost (LCC) and Levelized Cost of Energy (LCOE).

The Life Cycle Cost (LCC) and Levelized Cost of Energy (LCOE) of the evacuated tube collector (ETC) applied the Sn-Al₂O₃ coatings with 3 different Sn contents on the Al surface as a solar selective absorber were calculated by equation 7 and 8, respectively. The data for calculations were as follow;

1. Initial investment costs

The initial investment costs of the system or project includes;

1.1 Initial capital costs, consist of

1.1.1 Cost of the glass tube for evacuated collector

1.1.2 Cost of the aluminum sheet

1.1.3 Cost of the anodization coating

1.1.4 Cost of transportation fee

1.2 Operating and Maintenance cost

The Operating and Maintenance cost were calculated by 0.5% of the initial capital costs [58] for a 16 year project life time [59].

2. Benefits

The benefits from the project includes;

2.1 Salvage value

The salvage values were calculated by 10% of the initial capital costs [58] at the end of project.

2.2 Energy production

The energy production was calculated from the efficiency equation.

CHAPTER IV

RESULT AND DISCUSSION

This chapter presents 3 sections of the tin-pigmented aluminum oxide film ($\text{Sn-Al}_2\text{O}_3$) base solar selective absorbers. It was successfully prepared in 3 contents of Sn by the anodization process. The first section is characterization of phase and morphology. The second section is the thermal efficiency of the evacuated tube collector (ETC), and the last section is an economic analysis to evaluate the feasibility of using $\text{Sn-Al}_2\text{O}_3$ as a solar selective absorber material.

As received Al sheet in the Figure 25(a) was successfully prepared by anodic anodization. The the $\text{Sn-Al}_2\text{O}_3$ coating with variation of time in the coloring bath was shown in Figure 25(b). It was observed that the coatings reached a darker black with increasing coloring time. The $\text{Sn-Al}_2\text{O}_3$ -5 was dark brown, the $\text{Sn-Al}_2\text{O}_3$ -7 was black and brown and the $\text{Sn-Al}_2\text{O}_3$ -10 was dark black.

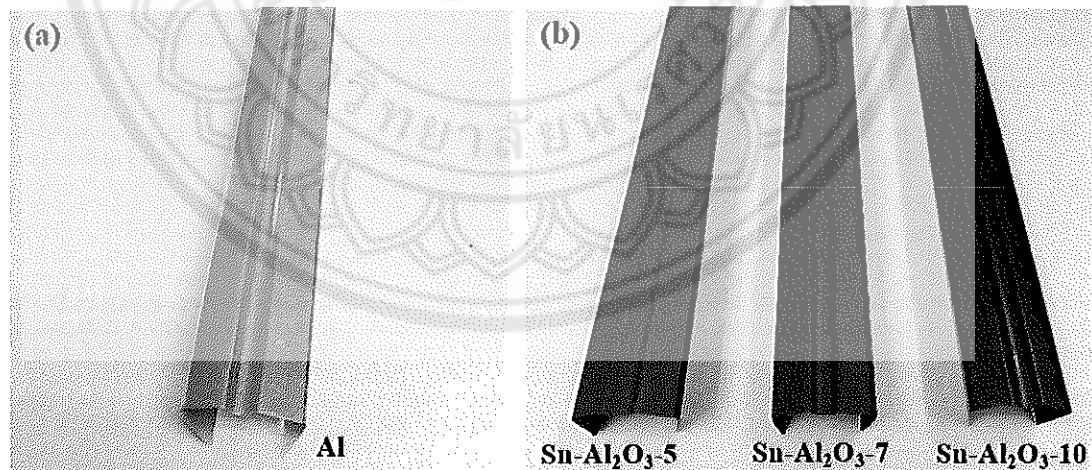


Figure 25 (a) Aluminum sheet and (b) $\text{Sn-Al}_2\text{O}_3$ coating on Al fin with variation of coloring times

Characterization of phase and morphology of the Sn-Al₂O₃

The methods for characterization of phase and morphology of the Sn-Al₂O₃ were;

1. The phase of the Sn-Al₂O₃

Figure 26 shows the XRD patterns of Sn-Al₂O₃ with various Sn contents, compared with the JCPDS database No. 01-1176, 01-1243 and 01-0926 for the elemental Al, Al₂O₃ and Sn, respectively. The phases of Al and Sn were indexed for all samples, and the phase intensity of Sn was increased by increasing the Sn contents. The crystallite size was also calculated by Scherrer's equation [60] (equation 9) using the Sn (200) peak in the XRD spectrum.

$$D = \frac{K\lambda}{\beta \cos\theta} \quad (9)$$

K is the crystallite shape factor which usually takes a value of 0.9, λ is the X-ray wavelength of Cu-K α radiation (0.15406 nm), β is the full width at half maximum (FWHM) in radians and θ is the Bragg's angle of the (200) peak of Sn. The calculated results for the Sn-Al₂O₃-5, Sn-Al₂O₃-7 and Sn-Al₂O₃-10 were 23.24, 23.24 and 46.48 nm, respectively. It was observed that the crystallite size of the Sn-Al₂O₃-10 sample is double the size of the others, indicating that the crystal nucleation of Sn inside the Al₂O₃ pores continuously occurs by the higher nucleation sites than other conditions during the coloring process beyond 7 min. According to the double intensity for (200) plane of Sn, the crystallinity of the highest content of Sn is also improved due to the sufficient time in the colouring process. However, the Al₂O₃ phase was not found in the XRD patterns because its structure is the amorphous phase, which is consistent with previous studies of W-Al₂O₃ [14], Pt-Al₂O₃ [42] and Mo-Al₂O₃ [16].

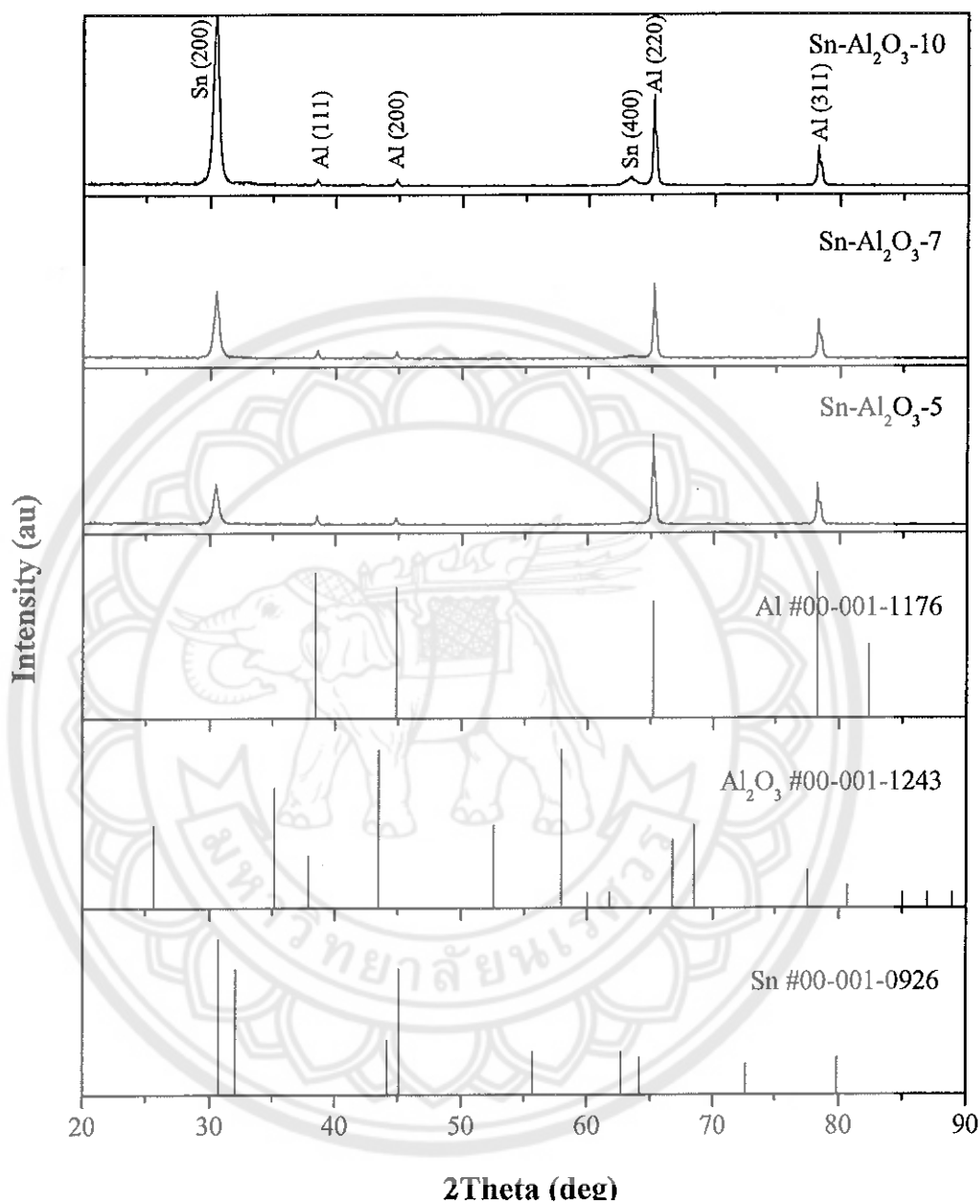


Figure 26 The XRD patterns of the Sn-Al₂O₃ at different Sn contents

2. The morphology of the Sn-Al₂O₃

The surface morphologies of the Sn-Al₂O₃ solar absorbers prepared by the anodization process were presented by SEM images. The anodized Al surface was heterogeneous nucleation like ordinary anodized aluminum substrate prepared to be solar absorber black coatings (Fig. 27 (a-c)) [5, 61, 62]. The coating samples consist of

2 layers; a compact Al_2O_3 barrier layer close to the interface of the Al substrate and a porous Al_2O_3 layer. The shallow marks of the surfaces occurred during the phenomenon of sealing the Al_2O_3 pores. Fig. 27 (d-f) indicates that the Al_2O_3 films were formed with a thickness of 9.1 – 9.5 μm , with a perpendicular pore structure and compact Al_2O_3 barrier on Al substrate, corresponding with Ni- Al_2O_3 selective absorbers [63].

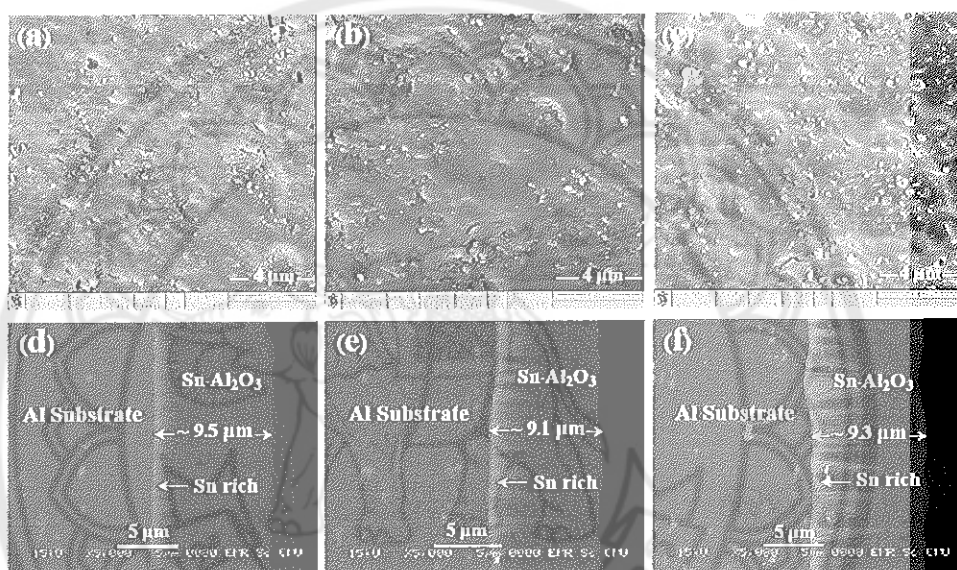


Figure 27 LV-SEM images of a-c) surface and d-f) sectional image of Sn- Al_2O_3 -5, Sn- Al_2O_3 -7 and Sn- Al_2O_3 -10

In addition, it detected different contrast regions on the Sn- Al_2O_3 films, due to the different atomic numbers of the elements. The Al_2O_3 phase presented contrast regions, according to the atomic number of the elements. Elements with higher atomic numbers caused more reflection of the electron beam during the SEM measurement, making the colour appear lighter in that area. Sn has its highest atomic number in the Al_2O_3 phase, the Sn rich revealed a spike shape and light region close to the interface of Al substrate, corresponding with a previous study [64]. The light gray area was the Sn pigment rich area which exhibited a high content near the Al substrate interface of the Al fin. The length of the spike shape or Sn pigment rich area increased when increasing the coloring time in the order Sn- Al_2O_3 -10 > Sn- Al_2O_3 -7 > Sn- Al_2O_3 -

5. This is due to the increasing time for electrochemical deposition in the coloring process leading to increasing the Sn content deposited into the pores of Al_2O_3 . The phase structure of $\text{Sn-Al}_2\text{O}_3$ of all coatings was not changed with increasing the coloring time.

3. The chemical composition and distribution of the $\text{Sn-Al}_2\text{O}_3$

In order to ascertain the increase of Sn content in the porous Al_2O_3 films, SEM-EDX with line scan analysis techniques were used (as shown in Figure 28). All the samples consist of detected Al, O and Sn elements, corresponding to the XRD pattern. The Sn content exhibited a high count rate close to the interface of the Al substrate, and the accumulation of Sn according to the incremental deposition time.

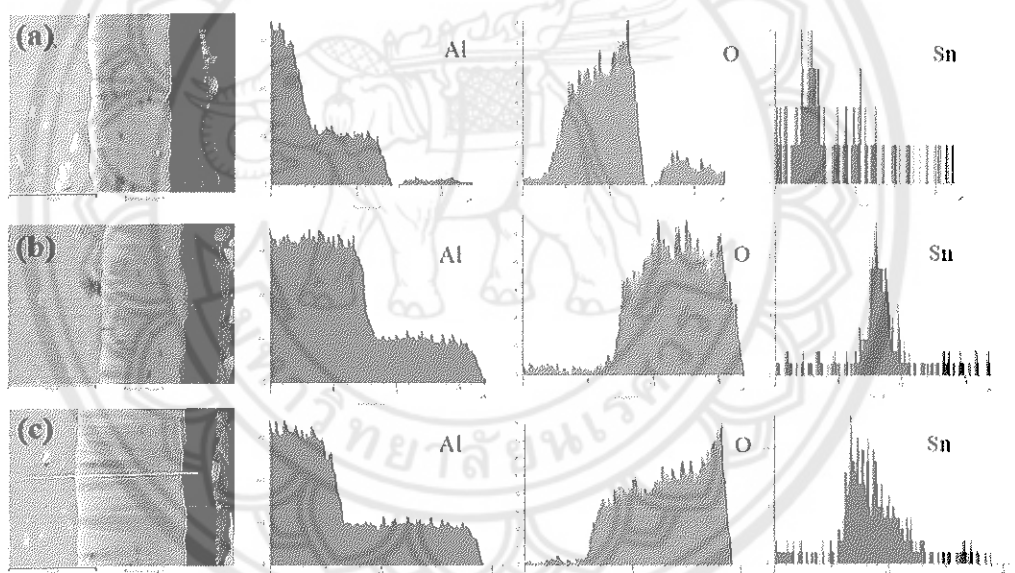


Figure 28 SEM-EDX line scanning of (a) $\text{Sn-Al}_2\text{O}_3$ -5, (b) $\text{Sn-Al}_2\text{O}_3$ -7 and (c) $\text{Sn-Al}_2\text{O}_3$ -10

In addition, the chemical distribution over a cross section of the surface of the $\text{Sn-Al}_2\text{O}_3$ coatings indicated the different chemical distributions in each layer, as presented by the EDX mapping images in Figure 29. The fundamental elements of these samples were dispersed in different densities in each region. Al displayed the highest density in the Al substrate, while the O revealed the highest density in the

Al_2O_3 layer, and the Sn also appeared in the Al_2O_3 layer but the highest density is at the interface of the Al substrate, consistent with the EDX line scanning images.

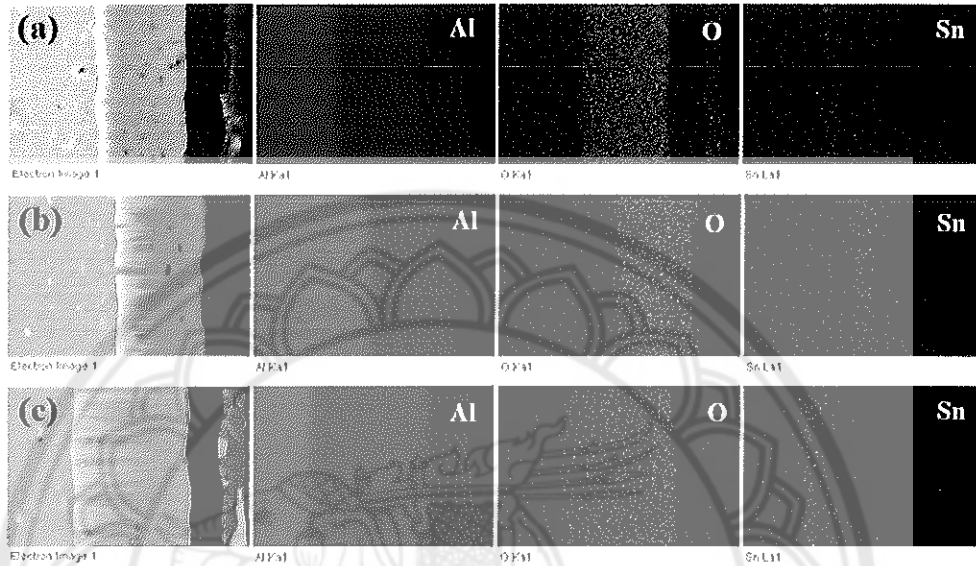


Figure 29 SEM-EDX Mapping of the (a) Sn- Al_2O_3 -5, (b) Sn- Al_2O_3 -7 and (c) Sn- Al_2O_3 -10

Figure 30 presents the elemental distribution profiles in the cross-section of the Sn- Al_2O_3 coatings on Al fin samples which characterized by SEM-EDX with the line scan analysis. The Al, O and Sn elements were found in all coatings. The highest content of Al was found at the Al substrate, the content immediately decreased at the interface between the Al_2O_3 layer and Al substrate, and kept relatively constant through the oxide film layer. The O exhibited a larger content in the Al_2O_3 film in all the samples, indicating that Al_2O_3 was formed by anodic anodization. The Sn presented high content in the Al_2O_3 film layer near the Al substrate interface. The increasing amount of Sn in the Al_2O_3 film lead to an increasing length of the spike-like Sn layer. This is due to the increasing time for electrochemical deposition in coloring process leading to increasing the Sn content deposited into the pores of Al_2O_3 .

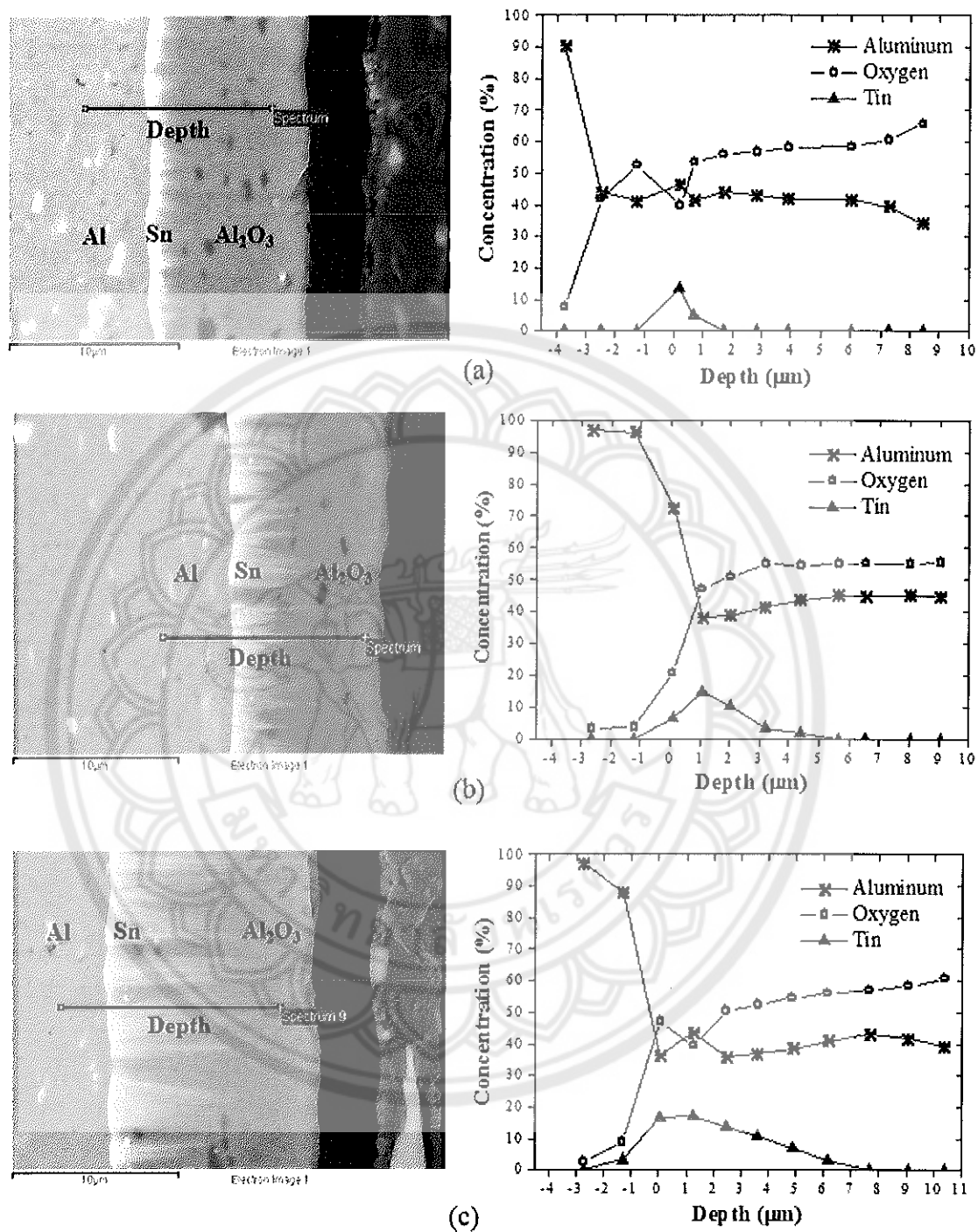


Figure 30 Elemental distributions of the (a) Sn-Al₂O₃-5, (b) Sn-Al₂O₃-7 and (c) Sn-Al₂O₃-10 on Al substrate

4. The reflectance (R) in the Ultraviolet-Visible-Near Infrared (UV-VIS-Near IR) region

According to the theoretical properties to achieve high performance in selective solar absorbers, the coatings require a high α_{sol} ($\alpha_{sol} \approx 1$) or low R ($R \approx 0$) in the solar spectrum region ($0.3 < \lambda \leq 3 \mu\text{m}$) and low ε_{therm} ($\varepsilon_{therm} \approx 0$) or high R ($R \approx 1$) in the infrared region ($\lambda \geq 3 \mu\text{m}$) at the operational temperature of the solar thermal applications [3]. As the cermet selective solar absorbers, ceramic matrix or dielectric layers increase the absorption in the UV-VIS regions, and metal layers and a highly IR-reflective metal substrate effectively increase the R in the IR region [4].

Figure 31 presents the measured R of all the Sn-Al₂O₃ coatings in the UV-VIS-NIR region, according to the whole wavelength interval of the solar spectrum at AM 1.5 (0.3 - 2.5 μm). All the Sn-Al₂O₃ samples exhibit low R in the whole wavelength range. However, the R of all samples gradually increased with the increasing wavelength due to the maximum of the scattering and reflectance efficiencies at high wavelength [3]. With increasing the Sn content in the pores of Al₂O₃, the spectral R of the samples relatively decreased in the wavelength range of UV-VIS-NIR regions due to the thickness of Al₂O₃ layer behaved as an anti-reflection (AR) layer reducing the reflection between the air and the Sn pigment layer [42, 65]. The α_{sol} of the samples was calculated from equation 5 and summarized in Table 4, together with the previous reports. The α_{sol} of the Sn-Al₂O₃-5, Sn-Al₂O₃-7 and Sn-Al₂O₃-10 were 0.89, 0.93 and 0.94, respectively. All are close to commercial solar absorbers (0.85-0.95) [3], and consistent with solar absorbers with related metal-Al₂O₃ film such as Co-Al₂O₃, W-Al₂O₃, Ag-Al₂O₃, Mo-Al₂O₃, Pt-Al₂O₃ and Ni-Al₂O₃ [11, 14, 15, 16, 42, 63]. In addition, α_{sol} of the Sn-Al₂O₃ samples increased according to the increase of Sn content as a result of the solar radiation trapped inside the Al₂O₃ pores by the light resonant scattering with Sn particles. The light scatter caused more solar radiation to be trapped in the absorber materials [3, 63]. It corresponds to a previous study which found that the Al₂O₃ layer plays the role of antireflection, obstructing the reflection of solar radiation from the Sn particles, as a result of the reflective index mismatch between air and the Sn-Al₂O₃ layer and the amount of Sn pigment filling in the Al₂O₃ pores affect the α_{sol} [19].

These results indicate that the Sn pigment in the pores of Al_2O_3 film forms a structure that facilitates solar radiation trapping and the conversion of solar radiation for solar thermal applications. The great increase of Sn in the coating leads to a significant increase in absorptance capacity. It is therefore clear that, the increase of the Sn content in the $\text{Sn-Al}_2\text{O}_3$ solar absorber can result in a good solar selective absorber in solar collectors.

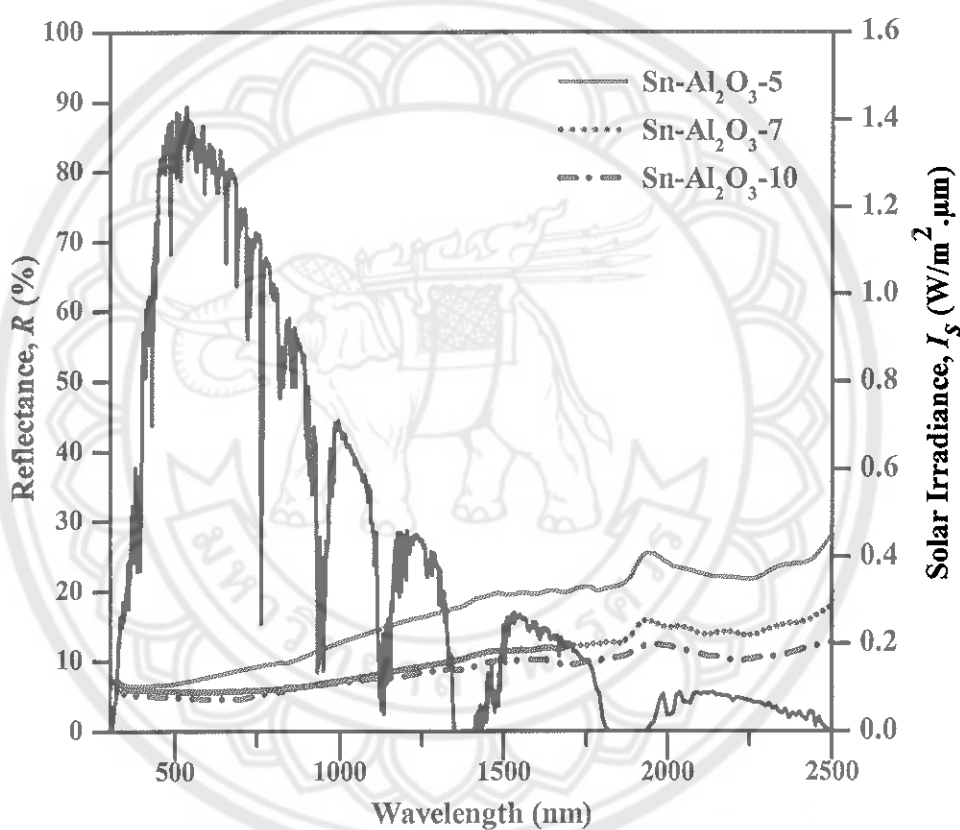


Figure 31 Spectral reflectance (R) of the $\text{Sn-Al}_2\text{O}_3$ solar absorber, compared with the sun spectrum at AM 1.5 in the wavelength range of 300 – 2500 nm

Table 4 The solar absorptance (α_{sol}) and thermal emittance (ϵ_{therm}) of the Sn- Al_2O_3 samples with different Sn contents compared with the previous studies

Solar selective absorber	Preparation	Solar Absorptance (α_{sol})	Thermal Emittance (ϵ_{therm})
Present study			
Sn- Al_2O_3 -5	Anodization	0.89	0.23 (100°C)
Sn- Al_2O_3 -7	Anodization	0.93	0.24 (100°C)
Sn- Al_2O_3 -10	Anodization	0.94	0.21 (100°C)
Previous studies			
Co- Al_2O_3 [11]	Anodization/ Electrodeposition	> 0.98	0.03 (100°C)
W- Al_2O_3 [14]	Sputtering	0.94	0.10 (400°C)
Ag- Al_2O_3 [15]	Sputtering	0.93	0.04-0.05 (82°C)
Ni- Al_2O_3 [63]	Anodization	0.92-0.97	0.14-0.23 (70°C)
Pt- Al_2O_3 [66]	Evaporation	0.98	0.36 (200°C)
Mo- Al_2O_3 [67]	Sputtering	0.91-0.93	0.19-0.27 (80°C)

5. The reflectance (R) in the Infrared (IR) region

The measured spectral R in the wavelength range of the IR region is presented in Figure 32. The spectral R was above 0.95 for all the samples in the wavelengths of 2.5-8.0 μm , and there was no display of the spectral R beyond 17.5 μm due to extreme noise. It is observed that the spectral R has little effect on Sn content in the wavelength range of the IR region. The ϵ_{therm} was calculated by equation 2, on the Planck blackbody distribution at 100°C, as shown in Table 5. The ϵ_{therm} was 0.23, 0.24 and 0.21 for Sn-Al₂O₃-5, Sn-Al₂O₃-7 and Sn-Al₂O₃-10, respectively. It seems that the ϵ_{therm} is insignificantly changed with the increasing Sn content. When considering previous studies, the ϵ_{therm} of this study was lower than the Pt-Al₂O₃ coating ($\epsilon_{therm} = 0.36$) [66] and close to the Ni-Al₂O₃ coatings ($\epsilon_{therm} = 0.14-0.23$) [63] and Mo-Al₂O₃ coating ($\epsilon_{therm} = 0.19-0.27$) [67].

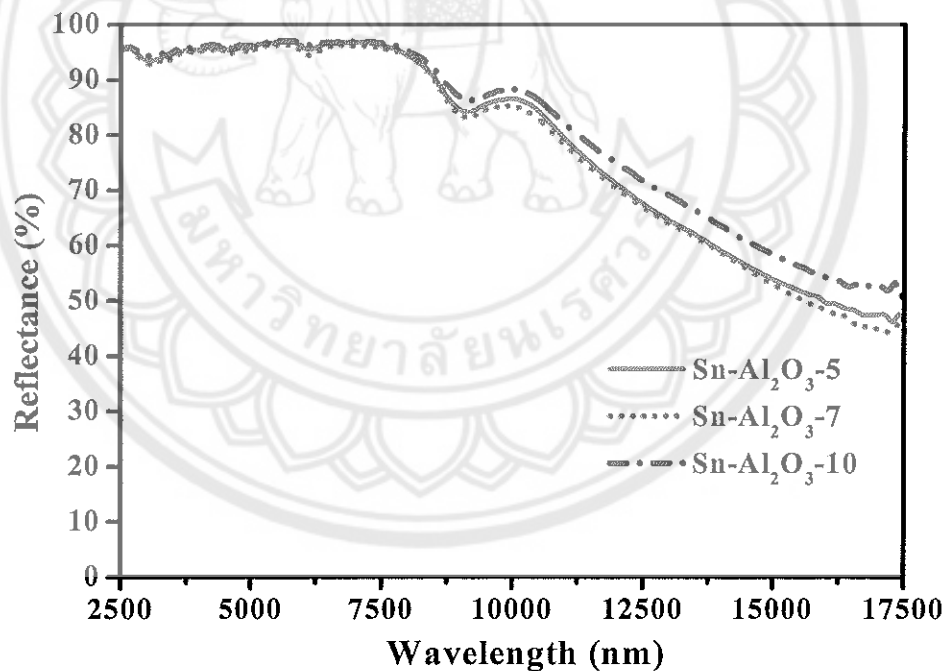


Figure 32 Reflectance of non-anodized Al and anodized Al at different Sn contents in the IR region

As the results shown in Figure 31 and 32, all the Sn-Al₂O₃ samples exhibit low R in the wavelength range of 0.3 – 2.5 μm , and high R in the wavelength range of 2.5-17.5 μm , according to the theoretical property of solar absorber materials for achieving a high solar selectivity. Therefore, the increasing Sn content in the pores of Al₂O₃ leads to a significant increase in the α_{sol} , but has little effect on the ε_{therm} . To consider the morphology of the segregated Sn at the interface, the α_{sol} is dependent on the morphology (spike size and length) of the spike-like Sn layer, while the ε_{therm} has little effect.

To consider the morphology of the segregated Sn at the interface, the α_{sol} is dependent on the morphology (spike size and length) of spike-like Sn layer, while the ε_{therm} has little effect.

6. Solar spectral selectivity ($\alpha_{sol}/\varepsilon_{therm}$)

In order to discuss in the spectral solar selectivity of the Sn-Al₂O₃ solar absorber materials in more detail, the solar selectivity ($\alpha_{sol}/\varepsilon_{therm}$) of the samples should be evaluated. Although there is no theoretical limit for the maximum $\alpha_{sol}/\varepsilon_{therm}$, in order to maximize the $\alpha_{sol}/\varepsilon_{therm}$ of solar absorber materials, the α_{sol} is required to be at the highest, but ε_{therm} should be reduced as much as possible. The $\alpha_{sol}/\varepsilon_{therm}$ of the samples are summarized in Table 5.

The $\alpha_{sol}/\varepsilon_{therm}$ of the Sn-Al₂O₃ samples were 3.87 - 4.48. With increasing the Sn content, the $\alpha_{sol}/\varepsilon_{therm}$ of the Sn-Al₂O₃ coatings increased. The $\alpha_{sol}/\varepsilon_{therm}$ of the coatings was relatively lower than that of the related coatings prepared using various sputtering techniques such as Ag-Al₂O₃ [15], AlNi-Al₂O₃ [65], Pt-Al₂O₃ [68] and Al₂O₃-WC [69]. The $\alpha_{sol}/\varepsilon_{therm}$ of the Sn-Al₂O₃-10 sample is close to that of the Mo-Al₂O₃ deposited by the magnetron sputtering technique [67], and the Ni-Al₂O₃ coating prepared using an anodization process [43].

Table 5 The solar selectivity ($\alpha_{sol}/\epsilon_{therm}$) of the Sn-Al₂O₃

Samples	Solar absorptance (α_{sol})	Thermal emittance (ϵ_{therm})	Solar selectivity ($\alpha_{sol}/\epsilon_{therm}$)
Present study			
Sn-Al ₂ O ₃ -5	0.89	0.23	3.87
Sn-Al ₂ O ₃ -7	0.93	0.24	3.88
Sn-Al ₂ O ₃ -10	0.94	0.21	4.48
Related and previous studies			
Ag-Al ₂ O ₃ [15]	0.93	0.04 - 0.05	18.8 - 23.5
AlNi-Al ₂ O ₃ [65]	0.94 - 0.95	0.07 - 0.078	12.18 - 13.43
Pt-Al ₂ O ₃ [68]	0.97	0.05	19.4
Al ₂ O ₃ -WC [69]	0.94	0.08	11.75
Mo-Al ₂ O ₃ [67]	0.92	0.19	4.84
Ni-Al ₂ O ₃ [43]	0.92-0.97	0.11-0.22	4.41-8.36

7. Thermal conductivity (k)

Figure 33 presents the temperature dependences of thermal conductivity for non-anodized Al and Sn-Al₂O₃ solar absorbers with various Sn contents to propose the quantity of heat transmitted through a unit thickness of the samples at interval temperatures from 25 - 275°C. The thermal conductivity of non-anodized Al was the highest related to the thermal conductivity of pure Al which was reported by National Standard Reference Data Series-National Bureau of Standards [70]. While, the thermal conductivity of the Sn-Al₂O₃ samples was lower than that of the non-anodized Al because Al₂O₃ film on the surface acts like an insulator and imperfections in the atomic structure as ceramic behavior. It was observed that the thermal conductivity of all the samples slightly decreased with increasing the temperature, indicating that the Sn-Al₂O₃ coatings are able to be used in special thermal applications by maintaining the thermal conductivity of materials over the operational temperature range (50 - 275°C). Furthermore, the thermal conductivity in each sample decreased with increasing

Sn content as a result of the increasing thickness of the Sn layer at the interface leading to obstruct free electrons and phonon contributions.

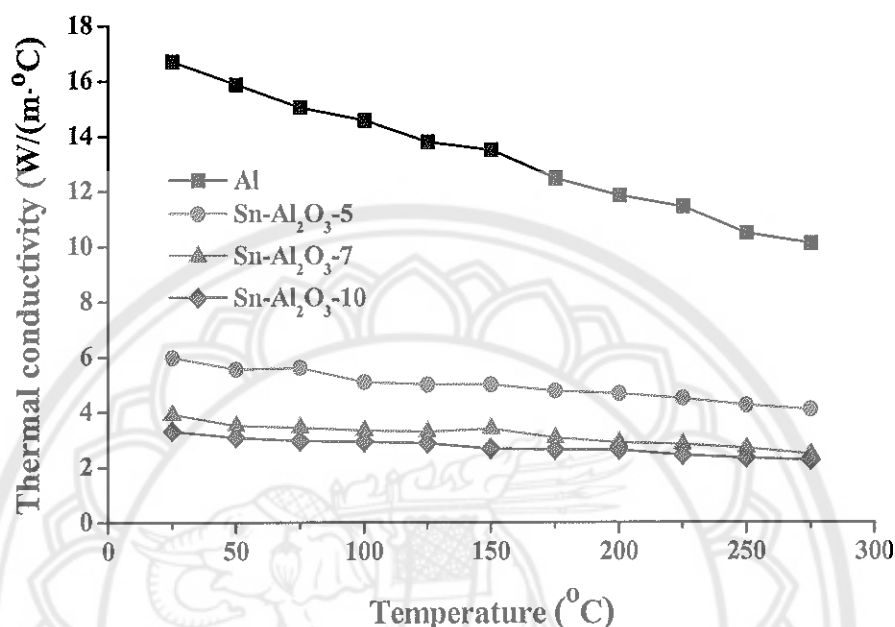


Figure 33 Thermal conductivity of anodized Al with different Sn contents

Figure 34 represents a diagram of the heat flow in the sample for thermal conductivity measurement indicating the thermal direction from Al substrate to the Al₂O₃ layer. In the Sn-Al₂O₃ samples, thermal conduction in the Al substrate occurs from free electrons, where heat is transferred through kinetic energy in the elements but is easily scattered [71]. The heat transferred through the Al₂O₃ layer by lattice vibration (phonons), which is directly transmitted from high to low temperature regions. It is well known that free electrons are predominant in the thermal conductivity of metals and non-anodized Al, causing high thermal conductivity. However, the thermal conductivity of all Sn-Al₂O₃ samples was higher than commercial hard anodic coatings (0.7 W/m K) and also greater than previous studies with Al anodic coatings using several electrolytes (no more than 1.33 W/m K) [72]. The solar spectrum is converted to thermal energy at the Sn-Al₂O₃ solar absorber, then, useful heat is easily transferred through the Al substrate to the exchanger. It implies that the heat loss from the Sn-Al₂O₃ solar absorber to its surroundings is

blocked and reduced by the Al_2O_3 layer, as illustrated in Figure 35. Therefore, the low thermal conductivity of the Sn- Al_2O_3 solar absorber (Al_2O_3 layer) has advantages in solar thermal applications.

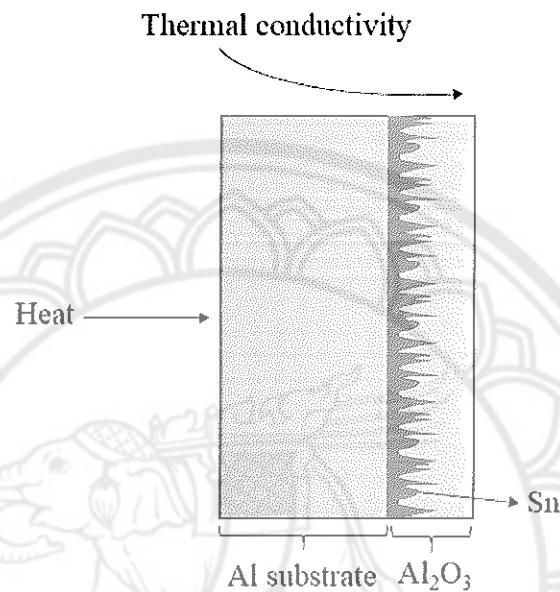


Figure 34 Heat flow in the thermal conductivity measurement on the Sn- Al_2O_3 specimen

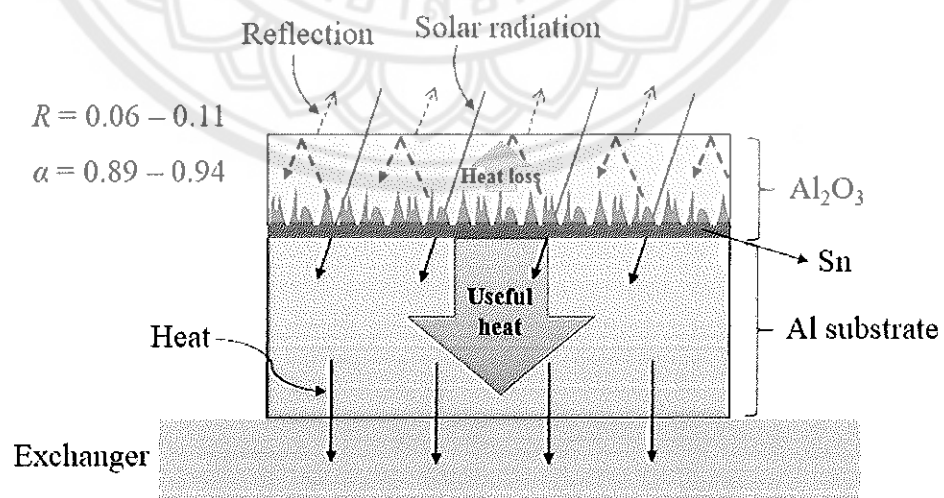


Figure 35 Solar radiation and heat transfer through the Sn- Al_2O_3 specimen

Thermal efficiency of the evacuated tube collector (ETC)

The Sn-Al₂O₃ with different Sn contents were applied as selective solar absorbers in the new prototype of ETC. According to the collected data from the thermal efficiency testing system, the η were calculated by equation 1 and 4. The thermal performance curve, of η verses $(T_i - T_a)/G_t$, was plotted, as shown in Figure 36. To consider determine the thermal efficiency equations, the interception on the vertical efficiency, $F_R (\tau\alpha)$, was 0.42, 0.54, and 0.61 for the Sn-Al₂O₃-5, Sn-Al₂O₃-7 and Sn-Al₂O₃-10, respectively. While, the slope ($-F_R U_L$), which is defined as no useful energy, was -9.62, -11.64 and -11.49 W/m².°C for the Sn-Al₂O₃-5, Sn-Al₂O₃-7 and Sn-Al₂O₃-10, respectively.

In order to consider determine the influence of different Sn content impregnated Sn-Al₂O₃ selective solar absorbers on the thermal performance of ETC, the parameters related to the thermal efficiency equation should be performed. Table 6 presents the summary of the thermal performance parameters of ETC using Sn-Al₂O₃ selective solar absorbers. It is clearly observed that not only the F_R increase with increasing the Sn content into the pores of Al₂O₃, but also the U_L decreases. The F_R increased with increasing Sn content, indicating that the actual useful energy gains of the new prototype ETC also increased. It implies the solar radiation is directly converted to thermal energy at the Sn-Al₂O₃ solar absorbers, after that useful heat is easily transferred through the Al fin and exchanger, respectively. According to the $\alpha_{sol}/\epsilon_{therm}$ of Sn-Al₂O₃ coatings, the U_L of the new prototype of ETC decreased with the increasing amount of Sn. Among the thermal performance testing, the new prototype ETC using the Sn-Al₂O₃-10 solar absorber exhibits the highest thermal performance. It is clearly seen, that the higher Sn content into the Al₂O₃ porous layer leads to enhancing the thermal performance of the new prototype ETC as a result of increasing F_R , together with decreasing the U_L .

However, the thermal performance curve of the ETC prototype using Sn-Al₂O₃ with different Sn content over an Al fin as a solar absorber was slightly lower than in previous studies with several approaches for enhancing the thermal performance [2, 44, 73, 74], but using Sn-Al₂O₃-10 seems higher than applying the ETC with a mini-CPC prototype [75]. So, the new prototypes of ETC with changing the position of the solar absorber from the inner double glass tube to Al fin coated with

the Sn-Al₂O₃ selective solar absorber is considered as a good competitor to commercially available solar collectors, indicating that the role of the Al fin is a solar receiver and heat transfer medium at the same time.

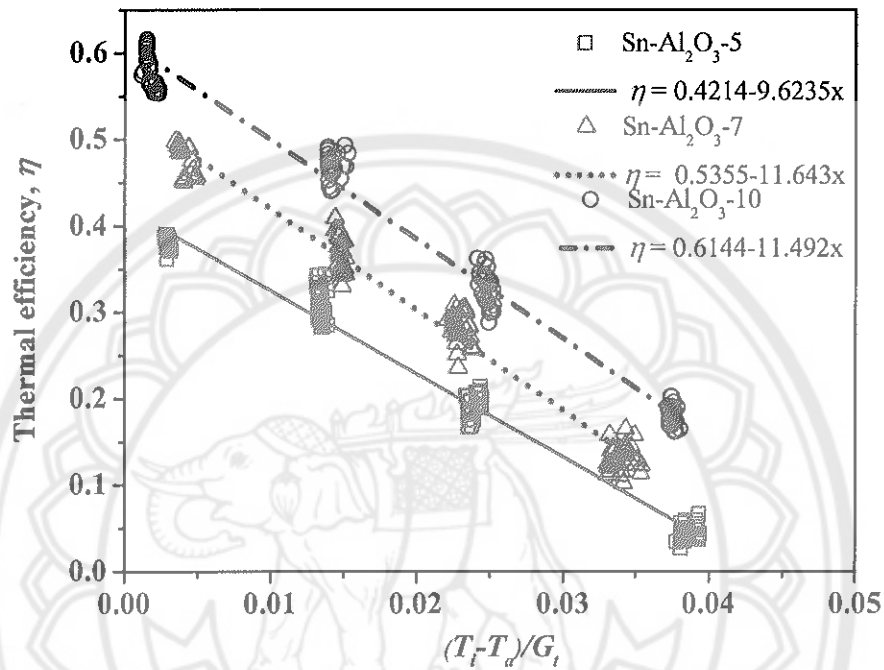


Figure 36 Thermal performance curve of the new prototype ETC using (a) Sn-Al₂O₃-5, (b) Sn-Al₂O₃-7 and (c) Sn-Al₂O₃-10 as a selective solar Absorber

Table 6 Summary of thermal performance parameters of the new ETC prototype using Sn-Al₂O₃ as a selective solar absorber

Samples	$\eta = F_R(\tau\alpha) - F_R U_L \left(\frac{T_i - T_a}{G_i} \right)$	$F_R(\tau\alpha)$	F_R	U_L	$-F_R U_L$
Sn-Al ₂ O ₃ -5	$\eta = 0.4214 - 9.6235x$	0.42	0.52	18.35	-9.62
Sn-Al ₂ O ₃ -7	$\eta = 0.5355 - 11.644x$	0.54	0.64	18.04	-11.64
Sn-Al ₂ O ₃ -10	$\eta = 0.6144 - 11.492x$	0.61	0.72	15.94	-11.49

Table 7 The thermal efficiency of the ETC using Sn-Al₂O₃ as solar selective absorber compared with previous studies

Samples	Equations
Present study	
Sn-Al ₂ O ₃ -5	$\eta = 0.4214 - 9.6235(T_i - T_a)/G_t$
Sn-Al ₂ O ₃ -7	$\eta = 0.5355 - 11.644(T_i - T_a)/G_t$
Sn-Al ₂ O ₃ -10	$\eta = 0.6144 - 11.492(T_i - T_a)/G_t$
Previous studies	
Ni- Al ₂ O ₃ [2]	$\eta = 0.722 - 15.825(T_i - T_a)/G_t$
ETC with U-pipe [73]	$\eta = 0.708 - 3.516(T_i - T_a)/G_t$
ETC with U-tube [44]	$\eta = 0.696 - 3.31(T_i - T_a)/G_t$
Flat micro-heat pipe collector [74]	$\eta = 0.75 - 6.36(T_i - T_a)/G_t$
ETC with mini-CPC [75]	$\eta = 0.555 - 0.9679(T_i - T_a)/G_t$

Economic analysis

The economic analysis of an evacuated tube collector applied the Sn-Al₂O₃ coating on the surface as solar selective absorber was calculated by Life Cycle Cost (LCC) and Levelized Cost of Energy (LCOE)

The LCC and LCOE of this project were calculated bases on assumptions of multiple project design options are shown in Tables 8 and 9. This project was calculated for 16 years of the project life time including initial capital cost (C_C), operating cost (C_O), maintenance cost (C_M), fuel or energy cost (C_F) and also disposal cost (S). The projected costs for years 1 - 15 were discounted back to present value by calculation of a NPV formula with a discount rate of 8.17 [76].

The initial capital costs at year 0 was 21,491.71 THB for the Sn-Al₂O₃-5 and 22,091.71 THB for the Sn-Al₂O₃-7 and Sn-Al₂O₃-10. Operating and maintenance costs were calculated at 0.5% and salvage value was calculated at 10% of the initial capital costs. The operating and maintenance costs for the whole project lifespan were 889.69 THB for the Sn-Al₂O₃-5 and 914.53 THB for the Sn-Al₂O₃-7 and Sn-Al₂O₃-10.

Table 8 The investment costs and benefits of the project

Parameters	Details	Costs (THB)
1. Initial capital cost [59]	1. The glass tube for evacuated collector	12,053.60
	1) The aluminum sheet (30 pcs/set × 0.81 USD × 34.49 THB) [77, 78]	838.11
	2) The shipping and tax [59]	9,600.00
	3) The anodization cost for 3 sample coatings	5,400.00
	3.1 Sn-Al ₂ O ₃ -5	6,000.00
	3.2 Sn-Al ₂ O ₃ -7	6,000.00
	3.3 Sn-Al ₂ O ₃ -10	
2. Operating and maintenance costs (THB/Year) [79]	1) Sn-Al ₂ O ₃ -5	107.46
	2) Sn-Al ₂ O ₃ -7	110.46
	3) Sn-Al ₂ O ₃ -10	110.46
3. Salvage value, S	1) Sn-Al ₂ O ₃ -5	627.80
	2) Sn-Al ₂ O ₃ -7	645.33
	3) Sn-Al ₂ O ₃ -10	645.33
4. Energy production (MJ)	1) Sn-Al ₂ O ₃ -5	38,206.34
	2) Sn-Al ₂ O ₃ -7	48,575.02
	3) Sn-Al ₂ O ₃ -10	56,957.35

The estimated benefits of the project included the salvage value and energy production. The salvage value was 2,149.17 THB for the Sn-Al₂O₃-5 system and 2,209.17 THB for the Sn-Al₂O₃-7 and Sn-Al₂O₃-10 systems. The energy production was calculated from the equation of thermal efficiency with parameters as shown in Table 9. It was 38,206.34 MJ, 48,575.02 MJ and 56,957.35 MJ, and electric hot water production consumed 707.52 kWh/year, 899.54 kWh/year and 1054.77 kWh/year for the Sn-Al₂O₃-5, Sn-Al₂O₃-7 and Sn-Al₂O₃-10 systems respectively. If converted, these energy to the annual electricity cost multiplied with the current electricity tariff in

Thailand at 4.42 THB/unit (for electricity consumed over 400 unit/month) [80] there will be savings of 3,127.26 THB, 3975.96 THB and 4662.06 THB respectively.

Table 9 The parameters for calculation

Parameter	Symbol	Sample			Unit
		Sn-Al ₂ O ₃ -5	Sn-Al ₂ O ₃ -7	Sn-Al ₂ O ₃ -10	
1. Initial capital costs	C_c	21,491.71	22,091.71	22,091.71	THB
2. Operating and maintenance costs	C_n	107.46	110.46	110.46	THB
3. Salvage value	S	2,149.17	2,209.17	2,209.17	THB
4. Annual Energy production	E_n	707.52	899.54	1054.77	kWh/ Year
5. Interest rate or discount rate	i	8.17	8.17	8.17	Percent
6. Project period	n	16	16	16	Year
7. Year at the end of project	N	15	15	15	Year

Table 10 Parameters for calculation the annual energy of the ETC [81]

Parameter	Symbol	Variable value	Unit
Solar irradiance	G_t	800	W/m ²
Ambient or surrounding air temperature	T_a	30	°C
Fluid temperature at the collector inlet	T_i	35	°C
Fluid temperature at the collector outlet	T_o	60	°C
Average annual solar energy of Thailand	E	1,800	kWh/m ² ·year

The annual energy from the new prototypes of ETC with different Sn content in the Al_2O_3 pores as the Sn- Al_2O_3 solar selective absorbers was calculated using the parameters mentioned in Table 10 and were used in the following equations:

The sample annual energy calculation from the thermal efficiency equation of the Sn- Al_2O_3 -10;

$$\eta = 0.61 - 11.49 \left(\frac{T_i - T_a}{G_t} \right)$$

Substituted the variables in the Table 10 to the equation;

$$\eta = 0.61 - 11.49 \left(\frac{35 - 30}{800} \right)$$

$$\eta = 0.54$$

$$\begin{aligned} \text{Annual energy calculations} &= 0.54 \times E \text{ kWh/m}^2 \cdot \text{Year} \\ &= 0.54 \times 1,800 \text{ kWh/m}^2 \cdot \text{Year} \\ &= 976.64 \text{ kWh/m}^2 \cdot \text{Year} \end{aligned}$$

The annual energy output for each Sn- Al_2O_3 sample for the new ETC prototypes are shown in Table 11.

Table 11 The annual energy from the new prototypes of ETC with different Sn content coatings

Samples	Annual Energy Yield (kWh/m ²)	Annual Energy Yield (kWh)	Annual Energy Yield (MJ)
Sn- Al_2O_3 -5	655.12	707.52	38,206.34
Sn- Al_2O_3 -7	832.90	899.54	48,575.02
Sn- Al_2O_3 -10	976.64	1,054.77	56,957.35

The LCC and LCOE of this project were calculated from equations 7 and 8 respectively, and the net present value (NPV) was considered. The results are shown in Table 12 and Figure 37. The LCC of the projects were 21,753.60 THB for the system using the Sn-Al₂O₃-5 as a solar selective absorber, and 22,360.91 THB for the system using Sn-Al₂O₃-7 and Sn-Al₂O₃-10 as solar selective absorbers. The LCOE were 2.05 THB/kWh, 1.66 THB/kWh and 1.14 THB/kWh for the system using the Sn-Al₂O₃-5, Sn-Al₂O₃-7 and Sn-Al₂O₃-10 as solar selective absorbers respectively. All are similar to previous studies using Ni-Al₂O₃ and solar paint on Al fins as a selective solar absorber for the ETC [59, 82].

Table 12 The LCC and LCOE of the Sn-Al₂O₃ solar absorbers

Sample	LCC (THB)	LCOE (THB/kWh)
Sn-Al ₂ O ₃ -5	21,753.60	2.05
Sn-Al ₂ O ₃ -7	22,360.91	1.66
Sn-Al ₂ O ₃ -10	22,360.91	1.41

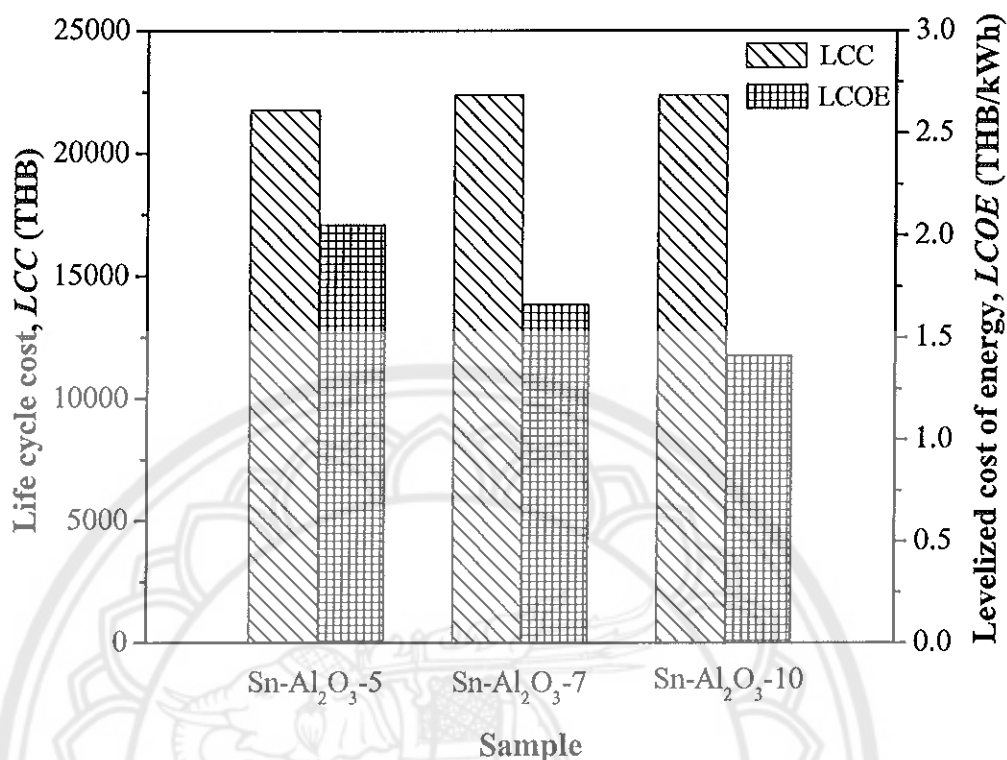


Figure 37 The LCC and LCOE of the new prototype of ETC using Sn-Al₂O₃ as solar selective absorbers

The results of this study, it was found that tin (Sn) is one of the pigments which is able to deposit into the Al₂O₃ film layer as the metal-dielectric composite (cermet) coating for applying as a solar absorber material in solar thermal applications [18, 19]. In addition, the tin pigmented-Al₂O₃ (Sn-Al₂O₃) coating prepared by the anodization process has been considered due to an eco-innovative production method for sustainable development.

CHAPTER V

CONCLUSION

The Sn-Al₂O₃ selective solar absorber was successfully prepared by the anodic anodization process onto Al fin with different Sn contents in the pores of the Al₂O₃ layer. The conclusions and recommendations for studying the Sn-Al₂O₃ are described in this chapter.

The characteristics of the Sn-Al₂O₃ solar selective absorbers

The Al₂O₃ film layer for all samples was formed with a perpendicular pore structure and compact Al₂O₃ barrier on Al substrate, and the film thickness was controlled identically. Different contents of Sn were deposited into the pores of the Al₂O₃ layer as the Sn-Al₂O₃ solar selective absorbers. The Sn-Al₂O₃ coatings achieved a darker black with increasing coloring time and their surfaces were quite homogeneous. The XRD pattern found the Al and Sn phases composed in the samples, which corresponds to the SEM-EDX results. The Al, O and Sn distributions were found in the cross section of the specimens. The Sn impregnated into the pores of Al₂O₃ appeared spike shaped and expanded into the oxide film layer. The Sn content exhibited a high count rate close to the interface of the Al substrate, and the accumulation of Sn according to the incremental deposition time.

Spectral and thermal properties of the Sn-Al₂O₃ solar selective absorbers

The spectral reflectance (R) in the wavelength range of 0.3 - 2.5 μm was measured in the wavelength range of UV-Vis-NIR regions (0.3 - 2.5 μm). The R of Sn-Al₂O₃ samples exhibited low in the whole wavelength range, and relatively decreased with increasing the Sn content in the pores of the Al₂O₃ film, which correlates with the solar absorptance (α_{sol}). The increasing Sn content, the α_{sol} of all samples gradually increased ($\alpha_{sol} = 0.89 - 0.94$), which is close to commercial panels. While the R in the infrared region (2.5 - 17 μm) presented high ($R > 95\%$) corresponding with the theoretical property of the solar absorber materials. The thermal emittance (ϵ_{therm}) of all samples was relatively low (0.21 - 0.24), but it was insignificant when compared to the increasing Sn content. The solar selectivity

$(\alpha_{sol}/\epsilon_{therm})$ of the Sn-Al₂O₃ coatings increased with increasing Sn content. The thermal conductivity (k) of anodized Al samples was relatively lower than non-anodized Al, especially with Sn filling in the pores leading to the decrease in heat loss from the Al substrate in the surroundings. It can be concluded that the increased Sn contents in Sn-Al₂O₃ is able to enhance the solar selective properties and hence is considered to be a candidate for good solar absorber materials for solar collectors.

The thermal performance of an ETC applied the Sn-Al₂O₃ as selective solar absorbers

The thermal performance curve of the new ETC prototype, the higher Sn content into the pores of Al₂O₃ leads to the enhancement of the thermal performance of the new prototype ETC as the result of increasing F_R , together with decreasing U_L . The maximum thermal efficiency ($F_R (\tau\alpha)$) increased according to the increasing Sn content, that was 0.42, 0.54, and 0.61 for the Sn-Al₂O₃-5, Sn-Al₂O₃-7 and Sn-Al₂O₃-10, respectively. Therefore, the new prototype of ETC using the Sn-Al₂O₃ selective solar absorber is considered as a good competitor to commercial solar collectors, indicating the role of the Al fin is a solar receiver and heat transfer medium at the same time. Also, it is a guideline for enhancing thermal performance and developing the new eco-innovative ETC prototype.

The economic analysis

The Life Cycle Cost (LCC) and Levelized Cost of Energy (LCOE) were indicators for economic evaluation. The LCC of the ETC with the Sn-Al₂O₃ as solar selective absorbers were 21,753.60 THB for applying Sn-Al₂O₃-5 and 22,360.91 THB for applying the Sn-Al₂O₃-7 and Sn-Al₂O₃-10. The higher LCC came from the higher cost in the anodization process. The LCOE of this project were 2.05 THB/kWh, 1.66 THB/kWh and 1.41 THB/kWh for the Sn-Al₂O₃-5, Sn-Al₂O₃-7 and Sn-Al₂O₃-10 respectively. It was observed that the LCOE decreased with the thermal efficiency of collectors increased.

From the results and worthiness of this study, using Sn-Al₂O₃ as solar selective absorbers with different Sn contents in the pores of the Al₂O₃ film layer demonstrated that the spectral and thermal properties of the Sn-Al₂O₃ samples were close to solar selective materials in the market. The increasing of the Sn content also

affect to improve many better properties, including well worth economics for energy producing cost.

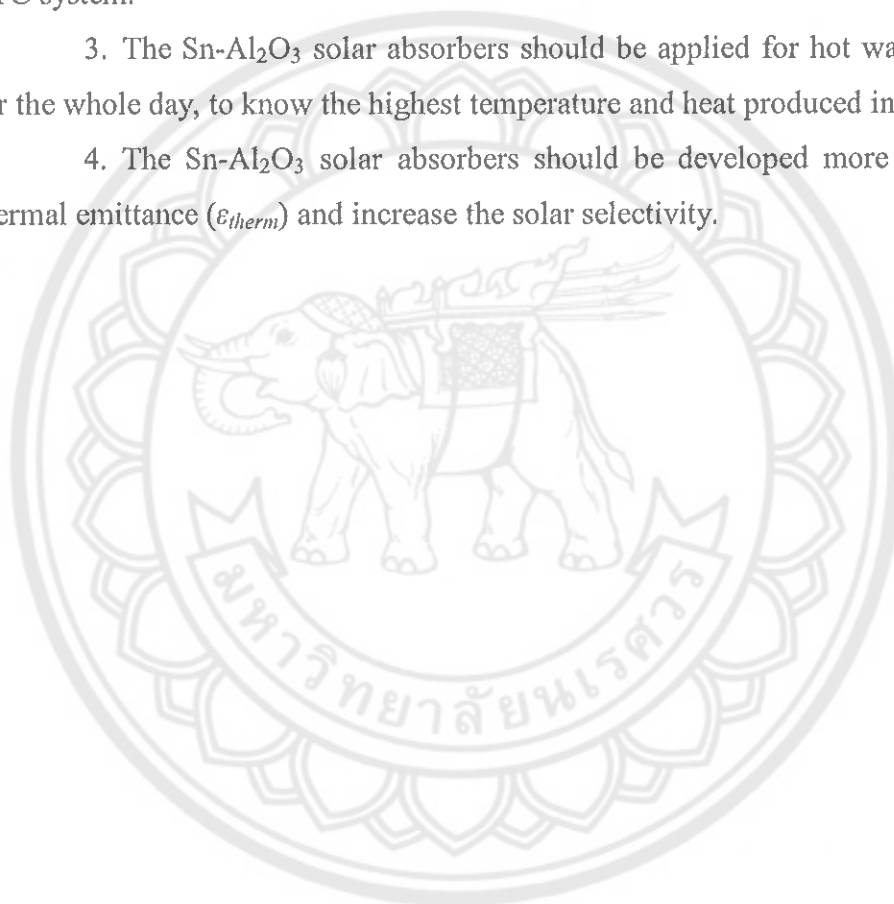
Recommendations

1. Further experiments are recommended to test the thermal stability of the Sn-Al₂O₃ solar absorbers for long term use as collectors.

2. Reducing the anodization cost could reduce the investment costs of the ETC system.

3. The Sn-Al₂O₃ solar absorbers should be applied for hot water production for the whole day, to know the highest temperature and heat produced in one day.

4. The Sn-Al₂O₃ solar absorbers should be developed more to reduce the thermal emittance (ϵ_{therm}) and increase the solar selectivity.





REFERENCES

- [1] Kalogirou, S.A. (2009). *Solar Energy Engineering Processes and Systems*. United State of America: Elsevier.
- [2] Nunocha, P., Suriwong, T., & Threrujirapong, T. (2014). Development and Application of Anodized Aluminum for Selective Absorber in Evacuated Tube Collector (ETC). *Naresuan University Journal: Science and Technology*, 22(2), 75-84.
- [3] Kennedy, C.E. (2002). *Review of Mid-to High-Temperature Solar Selective Absorber Materials*. Colorado: National Renewable Energy Laboratory (NREL).
- [4] Bermel, P., Lee, J., Joannopoulos, J.D., Celanovic, I., & Soljačić, M. (2012). Selective Solar Absorbers (Chapter 7). *Annual Review of Heat Transfer*, 15, 231-254.
- [5] Belghith, M., Arurault, L., & Bes, R.S. (2013). Selective Absorber Obtained by Nickel-Pigmented Anodized 6060 Aluminum Surface. *Arabian Journal for Science and Engineering*, 38(4), 751-757.
- [6] Sella, C., Mâaza, M., Pardo, B., Dunsteter, F., Martin, J.C., & Sainte Catherine, M.C. (1997). Microstructure and growth mechanism of Pt-Al₂O₃ co-sputtered nanocermet films studied by SAXS, TEM and AFM. *Physica A: Statistical Mechanics and its Applications*, 241(1), 192-198.
- [7] Maaza, M., Nemraoui, O., Sella, C., Lafait, J., Gibaud, A., Baruch-Barak, B., & Beye, A.C. (2006). Thickness induced transversal percolation in Pt-Al₂O₃ nano-composites. *Solid State Communications*, 137(3), 166-170.
- [8] Tesfamichael, T. (2000). *Characterization of Selective Solar Absorbers* (Doctoral dissertation). Sweden: Uppsala University.
- [9] Shashikala, A.R., Sharma, A.K., & Bhandari, D.R. (2007). Solar selective black nickel-cobalt coatings on aluminum alloys. *Solar Energy Materials and Solar Cells*, 91(7), 629-635.
- [10] Tharamani, C.N., & Mayanna, S.M. (2007). Low-cost black Cu-Ni alloy coatings for solar selective applications. *Solar Energy Materials and Solar Cells*, 91(8), 664-669.

- [11] Karoro, A., Nuru, Z.Y., Kotsedi, L., Bouziane, K., Mothudi, B.M., & Maaza, M. (2015). Selective Solar Absorbers' Properties of Laser Treated Electrodeposited Tubular Co-Al₂O₃ Nanocomposites. *Materials Today: Proceedings*, 2(7), 4028-4037.
- [12] Ding, D., Cai, W., Long, M., Wu, H., & Wu, Y. (2010). Optical, structural and thermal characteristics of Cu-CuAl₂O₄ hybrids deposited in anodic aluminum oxide as selective solar absorber. *Solar Energy Materials and Solar Cells*, 94(10), 1578-1581.
- [13] Katumba, G., Makiwa, G., Baisitse, T.R., Olumekor, L., Forbes, A., & Wäckelgård, E. (2008). Solar selective absorber functionality of carbon nanoparticles embedded in SiO₂, ZnO and NiO matrices. *Physica Status Solidi (c)*, 5(2), 549-551.
- [14] Antonaia, A., Castaldo, A., Addonizio, M.L., & Esposito, S. (2010). Stability of W-Al₂O₃ cermet based solar coating for receiver tube operating at high temperature. *Solar Energy Materials and Solar Cells*, 94(10), 1604-1611.
- [15] Barshilia, H.C., Kumar, P., Rajam, K.S., & Biswas, A. (2011). Structure and optical properties of Ag-Al₂O₃ nanocermet solar selective coatings prepared using unbalanced magnetron sputtering. *Solar Energy Materials and Solar Cells*, 95(7), 1707-1715.
- [16] Cheng, J., Wang, C., Wang, W., Du, X., Liu, Y., Xue, Y., ... Chen, B. (2013). Improvement of thermal stability in the solar selective absorbing Mo-Al₂O₃ coating. *Solar Energy Materials and Solar Cells*, 109, 204-208.
- [17] Wu, L., Gao, J., Liu, Z., Liang, L., Xia, F., & Cao, H. (2013). Thermal aging characteristics of CrN_xO_y solar selective absorber coating for flat plate solar thermal collector applications. *Solar Energy Materials and Solar Cells*, 114, 186-191.
- [18] Shaffei, M.F., Khattab, N., Awad, A.M., & Hussein, H.S. (2014). Characterization of Black Ni and Sn as Optically Selective Absorber Coatings in Thermal Solar Collectors Mainly (Part I). *Research Journal of Pharmaceutival, Biological and Chemical Science*, 5(1), 173-182.

- [19] Chorchong, T., Suriwong, T., Sukchai, S., & Threrujirapapong, T. (2015). Characterization and Spectral Selectivity of Sn-Al₂O₃ Solar Absorber. *Key Engineering Materials*, 675-676, 467-472.
- [20] Alternative Energy Tutorials. (2017). *Evacuated Tube Collector*. Retrieved November 26, 2017, from <http://www.alternative-energy-tutorials.com/solar-hot-water/evacuated-tube-collector.html>.
- [21] The international society for optics and photonics, SPIE. (2009). *High-performance absorbers for solar thermal applications*. Retrieved March 30, 2015, from <http://spie.org/newsroom/1835-high-performance-absorbers-for-solar-thermal-applications?SSO=1>
- [22] Garg, H.P., & Prakash, J. (1997). *Solar Energy, Fundamental and Applications*. New Delhi, India: Tata Mc graw Hill Pub.
- [23] Choudhury, M.G.M. (2000). Selective Surface for efficient Solar Thermal Conversion. *Bangladesh Renewable Energy Newsletter*, 1, 1-3.
- [24] Garg, H.P., & Prakash, J. (2004). *Solar Energy Fundamentals and Applications*. New Dehli, India: Tata McGraw-Hill.
- [25] Supasitmongkol, S., & Pungwiwat, N. (2002). Polymer Coating on Aluminum 6061 for Corrosion Protection by Electrochemical Technique. *Journal of KMITNB*, 12(3), 40-47.
- [26] Zhu, D., & Zhao, S. (2010). Chromaticity and optical properties of colored and black solar-thermal absorbing coatings. *Solar Energy Materials and Solar Cells*, 94(10), 1630-1635.
- [27] Ebnesajjad, S., & Ebnesajjad, C.F. (2014). *Surface Treatment of Materials for Adhesive Bonding* (2nd ed.). Massachusetts, USA: Elsevier.
- [28] Kopeliovich, D. (2013). *Anodizing*. Retrieved December 12, 2013, from <http://www.substech.com/dokuwiki/doku.php?id=anodizing>
- [29] Kallithrakas-Kontos, N., Moshohoritou, R., Ninni, V., & Tsangarakis-Kaplanoglou, I. (1998). Investigation of the relationship between the reflectance and the deposited nickel and tin amount on the aluminum anodic oxide film. *Thin Solid Films*, 326(1-2), 166-170.
- [30] Pennisi, M.S. (2001). *Anodising*. Retrieved October 10, 2014, from <http://www.coatfab.com/anodising.htm>.

- [31] Oliver, W.C., & Pharr, G.M. (2004). Measurement of hardness and elastic modulus by instrumented indentation: Advances in understanding and refinements to methodology. *Journal of Materials Research*, 19(1), 1-20.
- [32] Datcheva, M., Cherneva, S., Stoycheva, M., Iankov, R., & Stoychev, D. (2011). Determination of Anodized Aluminum Material Characteristics by Means of Nanoindentation Measurements. *Materials Sciences and Applications*, 2, 1452-1464.
- [33] Liu, Y., Wang, Z., Lei, D., & Wang, C. (2014). A new solar spectral selective absorbing coating of SS-(Fe₃O₄)/Mo/TiZrN/TiZrON/SiON for high temperature application. *Solar Energy Materials and Solar Cells*, 127, 143-146.
- [34] Reidy, R., Provost, V., Davis, M., Coony, R., Gould, S., Mann, C., & Sewak, B. (2005). *Guidelines for Life Cycle Cost Analysis*. USA: Stanford University.
- [35] Fuller, S. (2015). *Life-Cycle Cost Analysis (LCCA)*. Retrieved September 19, 2016, from <http://www.wbdg.org/resources/lcca.php>
- [36] Pawel, I. (2014). The Cost of Storage – How to Calculate the Levelized Cost of Stored Energy (LCOE) and Applications to Renewable Energy Generation. *Energy Procedia*, 46, 68-77.
- [37] Zhang, X.S. (2014). *Preparation of Porous Alumina by Anodization*. Retrieved October 16, 2014, from http://www3.ntu.edu.sg/eee/urop/congress2003/Proceedings/abstract/NTU_EEE/XiaoSong%20Zhang.pdf
- [38] Padwal, P., & Kulkarni, S. (2013). Preparation of aluminum oxide film by anodic oxidation and effect of plasma etching on its surface. *International Journal of Applied Engineering and Technology*, 3(1), 69-72.
- [39] Djozan, D., & Amir-Zehni, M. (2003). Anodizing of inner surface of long and small-bore aluminum tube. *Surface and Coatings Technology*, 173(2-3), 185-191.
- [40] Tsangaraki-Kaplanoglou, I., Theohari, S., Dimogerontakis, T., Wang, Y.M., Kuo, H.H., & Kia, S. (2006). Effect of alloy types on the anodizing process of aluminum. *Surface and Coatings Technology*, 200(8), 2634-2641.

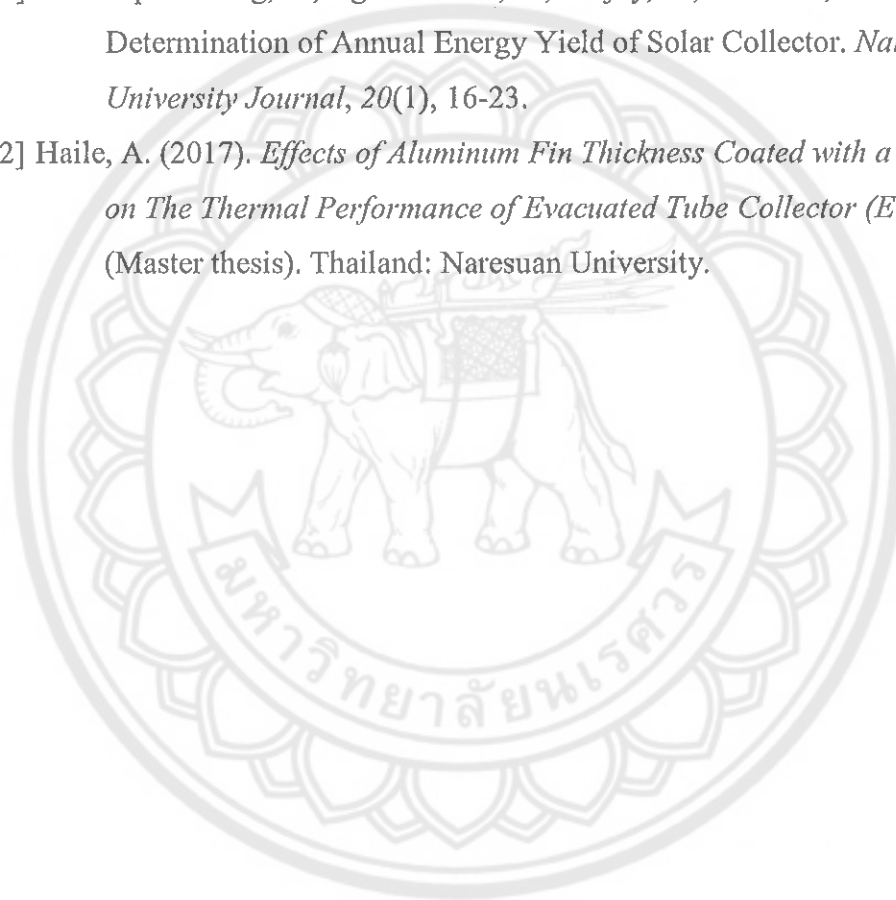
- [41] Tesfamichael, T., & Roos, A. (1998). Treatment of antireflection on tin oxide coated anodized aluminum selective absorber surface. *Solar Energy Materials and Solar Cells*, 54(1–4), 213-221.
- [42] Nuru, Z.Y., Arendse, C.J., Nemutudi, R., Nemraoui, O., & Maaza, M. (2012). Pt–Al₂O₃ nanocoatings for high temperature concentrated solar thermal power applications. *Physica B: Condensed Matter*, 407(10), 1634-1637.
- [43] Wazwaz, A., Salmi, J., Hallak, H., & Bes, R. (2002). Solar thermal performance of a nickel-pigmented aluminum oxide selective absorber. *Renewable Energy*, 27(2), 277-292.
- [44] Ghoneim, A.A., Shabana, H.M., Shaaban, M.S., & Mohammedein, A.M. (2016). Performance Analysis of Evacuated Tube Collector in Hot Climate. *European International Journal of Science and Technology*, 5(3), 8-20.
- [45] Ghoneim, A.A., & Mohammedein, A.M. (2016). Parabolic Trough Collector Performance in a Hot Climate. *Journal of Energy Engineering*, 142(1), 1-11.
- [46] Geochemical Instrumentation and Analysis. (2007). *X-ray Powder Diffraction (XRD)*. Retrieved January 9, 2018, from https://serc.carleton.edu/research_education/geochemsheets/techniques/XRD.html
- [47] Vernon-Parry, K.D. (2000). Scanning electron microscopy: an introduction. *III-Vs Review*, 13(4), 40-44.
- [48] Zhou, W., & Wang, Z.L. (2006). *Scanning Microscopy for Nanotechnology Techniques and applications*. New York, USA: Springer Science+Business Media, LCC.
- [49] Goodhew, P.J., Humphreys, J., & Beanland, R. (2001). *Electron Microscopy and Analysis* (3rd ed.). London, UK: Tayler & Francis.
- [50] Handbook of Analytical Methods for Materials. (2014). *Scanning electron microscopy*. Retrieved January 10, 2018, from https://www.mee-inc.com/files/1014/2118/3300/HAMM_2014-ScanningElectronMicroscopy.pdf
- [51] Hafner, B. (2015). *Energy Dispersive Spectroscopy on the SEM: A Primer*. Retrieved January 10, 2018, from http://www.charfac.umn.edu/instruments/eds_on_sem_primer.pdf

- [52] Sanda, F.M., Victor, M.E., Monica, T.A., & Alina, C. (2012). Spectrophotometric Measurement Techniques for Fermentation Process (Part one). *Hungary-Romania Cross-Border Co-operation Programme 2007-2013*, HURO 1001/121/2.2.2.
- [53] Tams, C., & Enjalbert, N. (2009). *The Use of UV/Vis/NIR Spectroscopy in the Development of Photovoltaic Cells*. Retrieved November 20, 2017, from https://www.perkinelmer.com/lab-solutions/resources/docs/APP_UseofUVVisNIRinDevelopmentPV.pdf
- [54] Patel, N.H. (2015). *Basic Principle, Working and Instrumentation of Experimental Techniques* (Doctoral dissertation). India: Sardar Patel University.
- [55] Penco, G., Barni, D., Michelato, P., & Pagani, C. (2001). Thermal properties measurements using laser flash technique at cryogenic temperature. *PACS2001. Proceedings of the 2001 Particle Accelerator Conference*, 2, 1231-1233.
- [56] NETZSCH. (2014). *Thermal Diffusivity – Thermal Conductivity Method, Technique, Applications*. Germany: NETZSCH-Gerätebau GmbH. Retrived November 19, 2017, from https://pec.engr.wisc.edu/Assets/Machines/LFA/LFA447_Brochure.pdf
- [57] Spires, T. (2001). *Introduction to Fourier Transform Infrared Spectrometry*. Wisconsin, USA: Thermo Nicolet Corporation.
- [58] Kongcharoen, K., & Jitsanguan, T. (2006). *Economic Analysis of Project Investment on Hot Water Production from Integrated Solar Energy System: Case Study of Klang Hospital, Rayong Province* (Master thesis). Thailand: Kasetsart University.
- [59] Nunocha, P., & Suriwong, T. (12-14 November 2014). Economic Evaluation of Applying Anodized Aluminum as Solar Absorber in Evacuated Tube Collector (ETC). In *The 7th Thailand Renewable Energy for Community Conference (TREC-7)* (pp. 131-137). Prachuapkhirikhan, Thailand: Rajamangala University Of Technology Rattanakosin Hua Hin campus.

- [60] Suriwong, T., Thongtem, S., & Thongtem, T. (2009). Solid-state synthesis of cubic ZnTe nanocrystals using a microwave plasma. *Materials Letters*, 63, 2103-2106.
- [61] Zemanová, M., Chovancová, M., Gáliková, Z., & Krivošík, P. (2008). Nickel electrolytic colouring of anodic alumina for selective solar absorbing films. *Renewable Energy*, 33(10), 2303-2310.
- [62] Aggerbeck, M., Canulescu, S., Dirscherl, K., Johansen, V.E., Engberg, S., Schou, J., & Ambat, R. (2014). Appearance of anodised aluminum: Effect of alloy composition and prior surface finish. *Surface and Coatings Technology*, 254, 28-41.
- [63] Wazwaz, A., Salmi, J., & Bes, R. (2010). The effects of nickel-pigmented aluminum oxide selective coating over aluminum alloy on the optical properties and thermal efficiency of the selective absorber prepared by alternate and reverse periodic plating technique. *Energy Conversion and Management*, 51(8), 1679-1683.
- [64] Chorchong, T. (2015). *Characterization and application of anodized aluminum for selective solar absorber in parabolic trough collector (PTC)* (Doctoral dissertation). Thailand: Naresuan University.
- [65] Xue, Y., Wang, C., Wang, W., Liu, Y., Wu, Y., Ning, Y. & Sun, Y. (2013). Spectral properties and thermal stability of solar selective absorbing AlNi–Al₂O₃ cermet coating. *Solar Energy*, 96, 113-118.
- [66] Craighead, H.G., Howard, R.E., Sweeney, J.E., & Buhrman, R.A. (1981). Graded-index Pt–Al₂O₃ composite solar absorbers. *Applied Physics Letters*, 39(1), 29-31.
- [67] Xinkang, D., Cong, W., Tianmin, W., Long, Z., Buliang, C., & Ning, R. (2008). Microstructure and spectral selectivity of Mo–Al₂O₃ solar selective absorbing coatings after annealing. *Thin Solid Films*, 516(12), 3971-3977.
- [68] Nuru, Z.Y., Motaung, D.E., Kaviyarasu, K., & Maaza, M. (2016). Optimization and preparation of Pt–Al₂O₃ double cermet as selective solar absorber coatings. *Journal of Alloys and Compounds*, 664, 161-168.

- [69] Gao, X., Wang, C., Guo, Z., Geng, Q., Theiss, W., & Liu, G. (2016). Structure, optical properties and thermal stability of Al₂O₃-WC nanocomposite ceramic spectrally selective solar absorbers. *Optical Materials*, 58, 161-168.
- [70] National Standard Reference Data Series-National Bureau of Standard-8. (1966). *Thermal Conductivity of Selected Materials*. Washington D.C., USA: United State Department of Commerce.
- [71] Vincent, C., Silvain, J.F., Heintz, J.M., & Chandra, N. (2012). Effect of porosity on the thermal conductivity of copper processed by powder metallurgy. *Journal of Physics and Chemistry of Solids*, 73(3), 499-504.
- [72] Ogden, T.R. (June 29 - July 2, 1987). Thermal Conductivity of Hard Anodized Coatings on Aluminum. In *AIAA/SAE/ASME/ASEE 23rd Joint Propulsion Conference*,. California, USA: Naval Ocean Systems Center.
- [73] Gao, Y., Fan, R., Zhang, X.Y., An, Y.J., Wang, M.X., Gao, Y.K., & Yu, Y. (2014). Thermal performance and parameter analysis of a U-pipe evacuated solar tube collector. *Solar Energy*, 107, 714-727.
- [74] Zhu, T.T., Diao, Y.H., Zhao, Y.H., & Deng, Y.C. (2015). Experimental study on the thermal performance and pressure drop of a solar air collector based on flat micro-heat pipe arrays. *Energy Conversion and Management*, 94, 447-457.
- [75] Pei, G., Li, G., Zhou, X., Ji, J., & Su, Y. (2012). Comparative Experimental Analysis of the Thermal Performance of Evacuated Tube Solar Water Heater Systems With and Without a Mini-Compound Parabolic Concentrating (CPC) Reflector($C < 1$). *Energy*, 5, 911-924.
- [76] Bank of Thailand. (2017). *Loan Rates of Commercial Banks registered in Thailand*. Retrieved March 18, 2017, from https://www.bot.or.th/english/statistics/_layouts/application/interest_rate/in_rate.aspx
- [77] Bank of Thailand. (2017). *Weighted-average Interbank Exchange Rate*. Retrieved May 18, 2017, from https://www.bot.or.th/english/financialmarkets/_layouts/application/exchangerate/exchangerate.aspx.
- [78] Haining Sunshine Trade Co., Ltd. (2013). *Commercial Invoice*. Zhejiang, China: 122 Lianhong RD, Yuan Hua Town, Haining City.

- [79] Kongcharoen, K., & Jitsanguan, T. (2006). *Economic Analysis of Project Investment on Hot Water Production from Integrated Solar Energy System: Case Study of Klang Hospital, Rayong Province*. Thailand: Kasetsart University.
- [80] Provincial Electricity Authority. (2017). *Electricity Tariff*. Retrived July 26, 2017, from <http://www.solarhub.co.th/document/rate-pea-summary.pdf>
- [81] Sirisamphanwong, C., Ngoenmeesri, R., Ketjoy, N., & Sa-ard, W.C. (2012). Determination of Annual Energy Yield of Solar Collector. *Naresuan University Journal*, 20(1), 16-23.
- [82] Haile, A. (2017). *Effects of Aluminum Fin Thickness Coated with a Solar Paint on The Thermal Performance of Evacuated Tube Collector (ETC)* (Master thesis). Thailand: Naresuan University.





APPENDIX

มหาวิทยาลัยนครสวรรค์

APPENDIX A

Powder –Diffract-File from JCPDS-ICDD

Name and formula

Reference code:	00-001-1176
PDF index name:	Aluminum
Empirical formula:	Al
Chemical formula:	Al

Crystallographic parameters

Crystal system:	Cubic
Space group:	Fm3m
Space group number:	225
a (?):	4.0406
b (?):	4.0406
c (?):	4.0406
Alpha (?):	90.0000
Beta (?):	90.0000
Gamma (?):	90.0000
Measured density (g/cm ³):	2.69
Volume of cell (10 ⁶ pm ³):	65.97
Z:	4.00
RIR:	-

Status, subfiles and quality

Status:	Marked as deleted by ICDD
Subfiles:	Inorganic
Quality:	Blank (B)

Comments

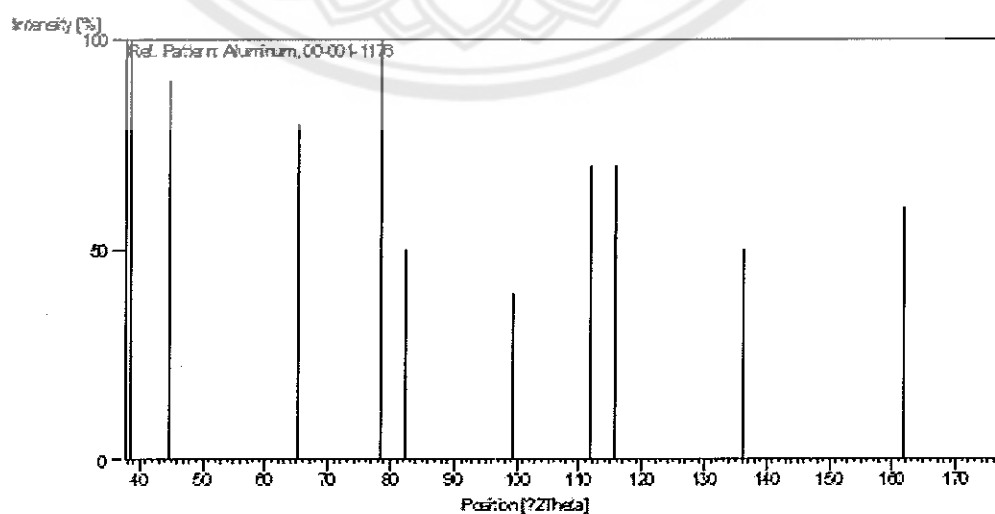
Deleted by:	Deleted by NBS card.
Color:	White
Melting point:	660

References

Primary reference: Davey., *Phys. Rev.*, **25**, 753, (1925)
 Optical data: *Data on Chem. for Cer. Use, Natl. Res. Council Bull. 107*
 Unit cell: *The Structure of Crystals, 1st Ed.*

Peak list

No.	h	k	l	d [Å]	2Theta[deg]	I [%]
1	1	1	1	2.34000	38.439	100
2	2	0	0	2.02000	44.833	90
3	2	2	0	1.43000	65.186	80
4	3	1	1	1.22000	78.306	100
5	2	2	2	1.17000	82.352	50
6	4	0	0	1.01000	99.401	40
7	3	3	1	0.93000	111.845	70
8	4	2	0	0.91000	115.662	70
9	4	2	2	0.83000	136.273	50
10	5	1	1	0.78000	161.909	60
11				0.72000		20

Stick Pattern

Name and formula

Reference code: 00-001-1243
 PDF index name: Aluminum Oxide
 Empirical formula: Al_2O_3
 Chemical formula: Al_2O_3

Crystallographic parameters

Crystal system: Rhombohedral
 Space group: R-3c
 Space group number: 167
 a (?): 4.7500
 b (?): 4.7500
 c (?): 12.9700
 Alpha (?): 90.0000
 Beta (?): 90.0000
 Gamma (?): 120.0000
 Measured density (g/cm^3): 4.02
 Volume of cell (10^6 pm^3): 253.43
 Z: 2.00
 RIR: -

Status, subfiles and quality

Status: Marked as deleted by ICDD
 Subfiles: Inorganic Alloy, metal or intermetallic
 Quality: Blank (B)

Comments

Deleted by: Deleted by NBS.
 Color: Various
 Optical data: $A=1.7604$, $B=1.7686$, $\text{Sign}=-$
 Melting point: 2050
 Unit cell: Rhombohedral cell: $a=5.120$, $a=55.28$.

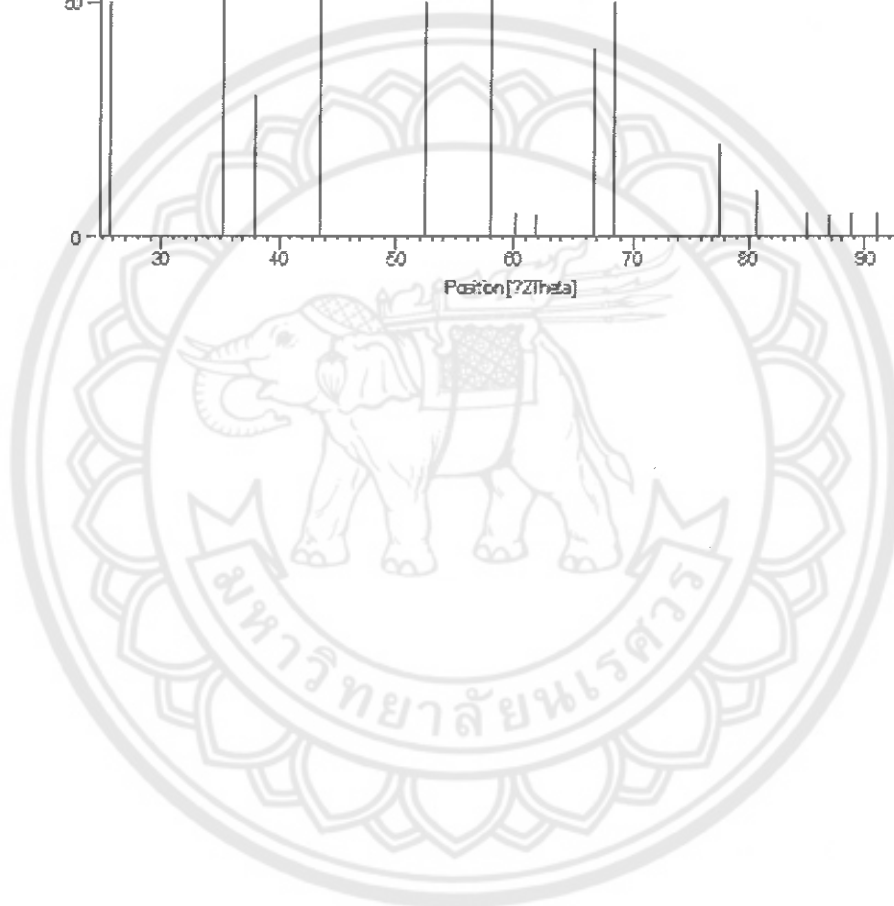
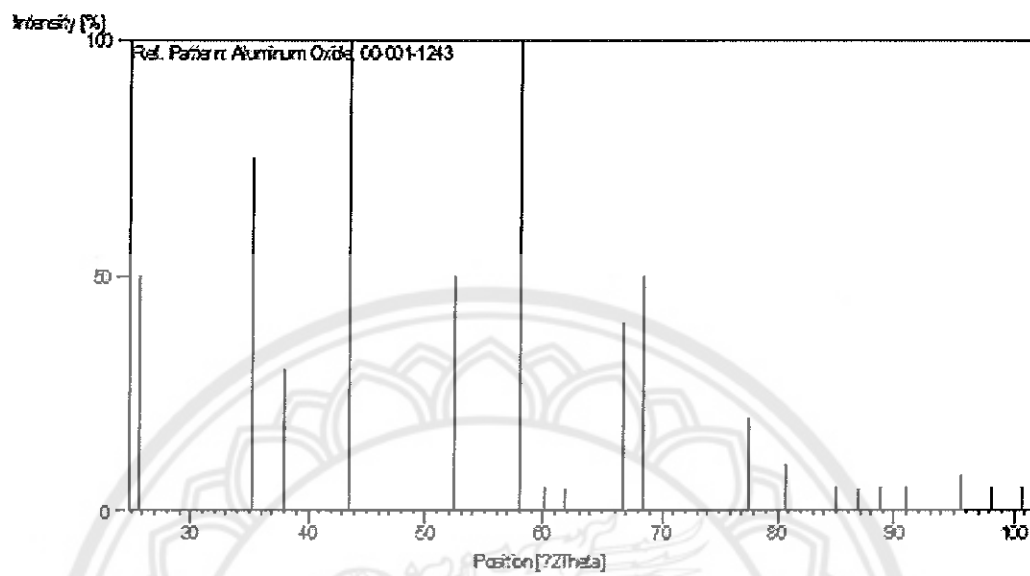
References

Primary reference: Hanawalt et al., *Anal. Chem.*, **10**, 475, (1938)

Unit cell: *Dana's System of Mineralogy, 7th Ed.*

Peak list

<u>No.</u>	h	K	I	d [Å]	2Theta[deg]	I [%]
1	0	1	2	3.47000	25.652	50.0
2	1	0	4	2.55000	35.165	75.0
3	1	1	0	2.37000	37.934	30.0
4	1	1	3	2.08000	43.473	100.0
5	0	2	4	1.74000	52.553	50.0
6	1	1	6	1.59000	57.955	100.0
7	2	1	1	1.54000	60.026	5.0
8	0	1	8	1.50000	61.799	5.0
9	2	1	4	1.40000	66.763	40.0
10	3	0	0	1.37000	68.425	50.0
11	1	1	9	1.23000	77.549	20.0
12	2	1	7	1.19000	80.678	10.0
13	1	3	1	1.14000	85.017	5.0
14	1	2	8	1.12000	86.907	5.0
15	0	2	10	1.10000	88.898	5.0
16	0	0	12	1.08000	90.998	5.0
17	2	2	6	1.04000	95.578	8.0
18	0	4	2	1.02000	98.085	5.0
19	2	1	10	1.00000	100.762	5.0

Stick Pattern

Name and formula

Reference code:	00-001-0926
PDF index name:	Tin
Empirical formula:	Sn
Chemical formula:	Sn

Crystallographic parameters

Crystal system:	Tetragonal
Space group:	I41/amd
Space group number:	141
a (?):	5.8190
b (?):	5.8190
c (?):	3.1753
Alpha (?):	90.0000
Beta (?):	90.0000
Gamma (?):	90.0000
Measured density (g/cm ³):	7.31
Volume of cell (10 ⁶ pm ³):	107.52
Z:	4.00
RIR:	-

Status, subfiles and quality

Status:	Marked as deleted by ICDD
Subfiles:	Inorganic
Quality:	Blank (B)

Comments

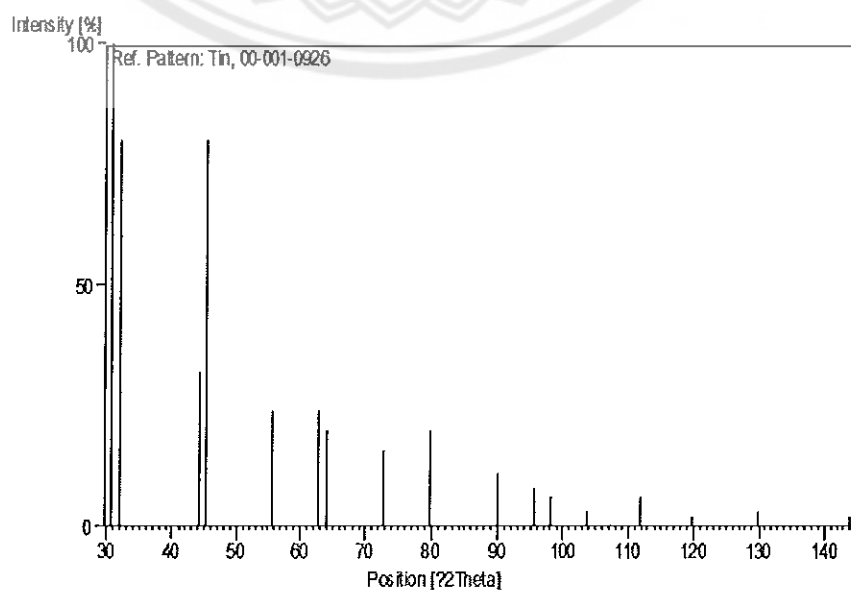
Deleted by:	Deleted by NBS card.
Color:	Tin-white
Melting point:	231.8

References

Primary reference:	Hanawalt et al., <i>Anal. Chem.</i> , 10 , 475, (1938)
Unit cell:	<i>Dana's System of Mineralogy, 7th Ed.</i>

Peak list

<u>No.</u>	h	K	I	d [Å]	2Theta[deg]	I [%]
1	2	0	0	2.91000	30.699	100.0
2	1	0	1	2.79000	32.054	80.0
3	2	2	0	2.05000	44.142	32.0
4	2	1	1	2.01000	45.068	80.0
5	3	0	1	1.65000	55.660	24.0
6	1	1	2	1.48000	62.728	24.0
7	4	0	0	1.45000	64.179	20.0
8	4	2	0	1.30000	72.675	16.0
9	3	1	2	1.20000	79.870	20.0
10	4	3	1	1.09000	89.934	11.0
11	1	0	3	1.04000	95.578	8.0
12	5	2	1	1.02000	98.085	6.0
13	2	1	3	0.98000	103.630	3.0
14	3	0	3	0.93000	111.845	6.0
15	3	2	3	0.89000	119.881	2.0
16	4	1	3	0.85000	129.980	3.0
17	6	4	0	0.81000	143.974	2.0

Stick Pattern

APPENDIX B

Table 13 The calculation of the solar absorptance of the Sn-Al₂O₃-5

Wavelength mm	Direct circumsolar W*m ⁻² *mm ⁻¹	I _{sol} W*m ⁻²	Reflectance	Integrate $\int_{300}^{2500} I_{sol} * (1-R(\lambda)) d\lambda$	Integrate I _{sol}	Absorptance (%)	Absorptance*I _{sol} W/sq.m
λ	I _{sol}	I _{sol} (λ)	R	$\int_{300}^{2500} I_{sol} (1-R(\lambda)) d\lambda$	$\int_{300}^{2500} I_{sol}(\lambda) d\lambda$	α	$\alpha \cdot I_{sol}$
300	4.56E-04	1.37E-01	0.07677	0.001913	0.127729	66.75803	2.94E-01
302	1.46E-03	4.40E-01	0.07681	0.006554	0.006051	92.31511	1.43E+00
304	5.10E-03	1.55E+00	0.07686	0.015247	0.014077	92.32199	2.87E+00
306	1.02E-02	3.11E+00	0.07674	0.030903	0.028535	92.33674	5.90E+00
308	2.08E-02	6.39E+00	0.07658	0.048579	0.044867	92.35918	7.97E+00
310	2.78E-02	8.63E+00	0.07628	0.078724	0.072732	92.38881	1.47E+01
312	5.09E-02	1.59E+01	0.07602	0.116164	0.107358	92.41935	1.89E+01
314	6.53E-02	2.05E+01	0.07564				

Table 13 (cont.)

Wavelength nm	Direct		I _{sol} W*m ⁻²	Reflectance	Integrate	Integrate I _{sol}	Absorbance (%)	Absorbance* I _{sol} W/sq.m
	W*m ⁻² *nm ⁻¹	circumsolar						
λ	I _{sol}	I _{sol} (λ)	1-R(λ)	$I_{sol} * (1-R(\lambda))$	$\int_{300}^{2500} I_{sol}(\lambda) d\lambda$	$\int_{300}^{2500} I_{sol}(\lambda) d\lambda$	α	α · I _{sol}
316	6.71E-02	2.12E+01	0.0753	0.925	0.132354	0.122366	92.45323	1.96E+01
318	9.58E-02	3.05E+01	0.07483	0.925	0.162903	0.150681	92.49764	2.82E+01
320	1.13E-01	3.61E+01	0.07423	0.926	0.208585	0.193044	92.54944	3.34E+01
.
2480	8.00E-03	1.98E+01	0.26826	0.732	0.123173	0.090624	73.57443	1.46E+01
2490	3.50E-03	8.70E+00	0.27472	0.725	0.057477	0.041945	72.97755	6.35E+00
2500	7.03E-03	1.76E+01	0.28026	0.720	0.052643	0.037986	72.15794	1.27E+01
Total						0.7956	0.8923	

Table 14 The calculation of the solar absorptance of the Sn-Al₂O₃-7

Wavelength nm	Direct circumsolar		Reflectance	Integrate	Integrate I_{sol}	Absorptance (%)	Absorptance* I_{sol} W/sq.m
	I_{sol} W*m ⁻² *nm ⁻¹	I_{sol} W*m ⁻²					
λ			1	$I_{sol} * (1 - R(\lambda))$	$\int_{300}^{2500} I_{sol}(\lambda) d\lambda$	α	$\alpha \cdot I_{sol}$
			R	$\int_{300}^{2500} I_{sol} (1 - R(\lambda)) d\lambda$			
300	4.56E-04	1.37E-01	0.07211	0.928	0.12837364	67.09505505	2.95E-01
302	1.46E-03	4.40E-01	0.07207	0.928	0.00191331	92.79222223	1.44E+00
304	5.10E-03	1.55E+00	0.07208	0.928	0.0065543	92.80398245	2.88E+00
306	1.02E-02	3.11E+00	0.0719	0.928	0.0152473	92.82544572	5.93E+00
308	2.08E-02	6.39E+00	0.07167	0.928	0.030903	92.85304796	8.01E+00
310	2.78E-02	8.63E+00	0.07132	0.929	0.048579	92.89192188	1.48E+01
312	5.09E-02	1.59E+01	0.07095	0.929	0.078724	92.92129346	1.90E+01
314	6.53E-02	2.05E+01	0.07066	0.929	0.116164	92.95528909	1.97E+01
316	6.71E-02	2.12E+01	0.07024	0.930	0.132354	93.00423226	2.83E+01
18	9.58E-02	3.05E+01	0.06976	0.930	0.162903		

Table 14 (cont.)

Wavelength nm	Direct circumsolar $W \cdot m^{-2} \cdot nm^{-1}$	I_{sol} $W \cdot m^{-2}$	Reflectance	$1-R(\lambda)$	Integrate $I_{sol} \cdot (1-R(\lambda))$ $\int_{300}^{2500} I_{sol} (1-R(\lambda)) d\lambda$	Integrate I_{sol} $\int_{300}^{2500} I_{sol}(\lambda) d\lambda$	Absorbance (%)	Absorbance* I_{sol} W/sq.m
λ	I_{sol}	$I_{sol}(\lambda)$	R	$1-R(\lambda)$	$\int_{300}^{2500} I_{sol} (1-R(\lambda)) d\lambda$	$\int_{300}^{2500} I_{sol}(\lambda) d\lambda$	α	$\alpha \cdot I_{sol}$
320	1.13E-01	3.61E+01	0.06911	0.931	0.208585	0.194107411	93.05914179	3.36E+01
322	1.22E-01	3.93E+01	0.06854	0.931	0.23477	0.218614585	93.11862048	3.66E+01
.
.
.
2480	8.00E-03	1.98E+01	0.17412	0.826	0.123173	0.101964829	82.78180242	1.64E+01
2490	3.50E-03	8.70E+00	0.17702	0.823	0.0574765	0.047418004	82.49981152	7.18E+00
2500	7.03E-03	1.76E+01	0.17996	0.820	0.0526425	0.043220342	82.10161465	1.44E+01
Total						0.8917	0.8285	0.9292

Table 15 The calculation of the solar absorptance of the Sn-Al₂O₃-10

Wavelength nm	Direct		Reflectance	Integrate	Integrate I_{sol}	Absorptance (%)	Absorptance* I_{sol} W/sq.m
	I_{sol} W*m ⁻² *nm ⁻¹	I_{sol} W*m ⁻²					
λ			1	$I_{sol} * (1 - R(\lambda))$	$\int_{300}^{2500} I_{sol}(\lambda) d\lambda$	α	$\alpha \cdot I_{sol}$
			R	$\int_{300}^{2500} I_{sol} (1 - R(\lambda)) d\lambda$			
300	4.56E-04	1.37E-01	0.06445	0.936			
302	1.46E-03	4.40E-01	0.06435	0.936	0.129433488	67.64898955	2.98E-01
304	5.10E-03	1.55E+00	0.06424	0.936	0.006133091	93.57355474	1.45E+00
306	1.02E-02	3.11E+00	0.06409	0.936	0.0152473	93.58598537	2.91E+00
308	2.08E-02	6.39E+00	0.06387	0.936	0.030903	93.60577416	5.98E+00
310	2.78E-02	8.63E+00	0.06354	0.936	0.048579	93.63190237	8.08E+00
312	5.09E-02	1.59E+01	0.06322	0.937	0.078724	93.66668919	1.49E+01
314	6.53E-02	2.05E+01	0.06273	0.937	0.116164	93.70553034	1.92E+01
316	6.71E-02	2.12E+01	0.06236	0.938	0.132354	93.74575467	1.99E+01
318	9.58E-02	3.05E+01	0.06181	0.938	0.162903	93.79634947	2.86E+01

Table 15 (cont.)

Wavelength nm	Direct circumsolar		Reflectance	Integrate	Integrate I_{sol}	Absorptance (%)	Absorptance* I_{sol} W/sq.m
	I_{sol} W*m ⁻² *nm ⁻¹	I_{sol} W*m ⁻²					
λ	I_{sol}	$I_{sol}(\lambda)$	1 R	$I_{sol} * (1 - R(\lambda))$ $\int_{300}^{2500} I_{sol} (1 - R(\lambda)) d\lambda$	$\int_{300}^{2500} I_{sol}(\lambda) d\lambda$	α	$\alpha \cdot I_{sol}$
320	1.13E-01	3.61E+01	0.06134	0.208585	0.195745363	93.84441022	3.39E+01
322	1.22E-01	3.93E+01	0.06076	0.23477	0.220439968	93.89614014	3.69E+01
.
.
.
2480	8.00E-03	1.98E+01	0.12611	0.123173	0.107738631	87.4693571	1.74E+01
2490	3.05E-03	8.70E+00	0.12685	0.0574765	0.050215204	87.36649673	7.60E+00
2500	7.03E-03	1.76E+01	0.1282	0.0526425	0.045917327	87.22482305	1.53E+01
Total				0.8917	0.8367	0.9383	

APPENDIX C

Table 16 The thermal efficiency of ETC with the Sn-Al₂O₃-5 as solar selective absorber

T_{in} (°C)	T_{out} (°C)	T_{am} (°C)	G_t (W/m ²)	$(T_{in}-T_{am})/G_t$	η
30.37	32.33	27.80	808.54	0.00318	0.3739
30.41	32.33	28.03	821.32	0.00289	0.3619
30.44	32.39	27.88	815.28	0.00314	0.3712
30.48	32.45	28.02	815.47	0.00302	0.3729
30.52	32.46	28.06	800.28	0.00307	0.3759
30.54	32.52	28.09	800.42	0.00306	0.3828
30.56	32.50	28.14	802.02	0.00302	0.3739
30.57	32.57	28.20	805.99	0.00294	0.3828
30.60	32.60	28.20	822.07	0.00292	0.3778
30.63	32.59	28.23	818.86	0.00292	0.3723
30.65	32.63	28.19	811.09	0.00304	0.3770
30.67	32.68	28.22	811.04	0.00302	0.3835
30.69	32.72	28.28	811.81	0.00297	0.3867
30.70	32.74	28.32	807.88	0.00295	0.3904
30.72	32.76	28.34	814.18	0.00292	0.3879
30.73	32.79	28.38	820.88	0.00287	0.3868
30.75	32.77	28.41	824.37	0.00285	0.3788
30.77	32.79	28.46	821.45	0.00282	0.3805
30.79	32.82	28.45	818.35	0.00286	0.3838
30.81	32.85	28.58	818.80	0.00272	0.3867
30.83	32.90	28.54	818.44	0.00279	0.3906
30.85	32.92	28.55	823.40	0.00280	0.3883
30.88	32.93	28.50	825.32	0.00288	0.3840
30.90	32.91	28.55	825.95	0.00285	0.3754
30.92	32.93	28.52	830.87	0.00290	0.3747

Table 16 (cont.)

T_{in} (°C)	T_{out} (°C)	T_{am} (°C)	G_t (W/m ²)	$(T_{in}-T_{am})/G_t$	η
30.94	32.96	28.52	836.02	0.00289	0.3755
30.95	33.03	28.54	836.35	0.00289	0.3854
30.97	33.04	28.63	836.83	0.00280	0.3828
30.98	33.07	28.57	836.05	0.00288	0.3865
30.99	33.02	28.50	834.94	0.00298	0.3775
41.10	42.73	29.73	860.57	0.01321	0.2941
41.04	42.70	29.65	860.25	0.01324	0.2986
41.21	42.80	29.29	859.84	0.01386	0.2861
41.09	42.76	29.42	860.31	0.01356	0.2998
41.02	42.83	29.52	855.29	0.01345	0.3276
41.03	42.87	29.64	854.90	0.01332	0.3345
41.00	42.66	29.48	847.56	0.01360	0.3028
41.05	42.83	29.34	844.45	0.01386	0.3254
41.04	42.86	29.38	845.70	0.01379	0.3335
41.08	42.64	29.74	843.78	0.01343	0.2877
41.00	42.61	29.82	840.81	0.01328	0.2970
41.04	42.61	29.79	840.62	0.01339	0.2886
41.06	42.94	29.52	842.10	0.01370	0.3445
41.00	42.74	29.61	842.98	0.01351	0.3186
41.24	42.83	29.87	837.02	0.01358	0.2948
41.03	42.83	29.93	834.40	0.01330	0.3349
41.04	42.82	30.04	837.37	0.01314	0.3289
41.14	42.68	29.89	839.67	0.01340	0.2830
41.03	42.89	30.01	840.61	0.01311	0.3431
41.03	42.85	30.07	839.58	0.01306	0.3350
41.03	42.77	30.00	836.71	0.01318	0.3221
41.11	42.76	30.16	830.84	0.01318	0.3069
41.19	42.71	29.89	830.76	0.01360	0.2836

Table 16 (cont.)

T_{in} (°C)	T_{out} (°C)	T_{am} (°C)	G_t (W/m ²)	$(T_{in}-T_{am})/G_t$	η
41.07	42.83	29.95	835.12	0.01331	0.3250
41.10	42.74	29.89	832.26	0.01347	0.3049
41.23	42.85	29.81	834.34	0.01369	0.3000
41.11	42.68	29.97	837.24	0.01330	0.2912
41.02	42.88	29.86	841.64	0.01326	0.3425
41.07	42.63	29.78	838.96	0.01345	0.2879
41.08	42.75	29.89	837.08	0.01337	0.3087
50.29	51.34	30.83	819.17	0.02375	0.1982
50.37	51.35	30.98	817.85	0.02370	0.1863
50.35	51.32	30.85	819.30	0.02380	0.1820
50.36	51.35	30.91	820.41	0.02370	0.1866
50.34	51.34	30.94	820.06	0.02366	0.1884
50.45	51.42	31.08	816.68	0.02372	0.1833
50.54	51.44	31.10	818.75	0.02375	0.1689
50.55	51.47	30.99	820.22	0.02384	0.1746
50.63	51.56	30.97	822.58	0.02390	0.1760
50.65	51.62	31.01	825.94	0.02377	0.1828
50.67	51.61	31.08	829.86	0.02360	0.1748
50.63	51.64	31.03	834.60	0.02349	0.1861
50.67	51.73	30.89	835.24	0.02368	0.1963
50.58	51.68	30.93	836.07	0.02350	0.2028
50.59	51.69	31.04	836.02	0.02338	0.2039
50.69	51.68	31.00	837.19	0.02351	0.1838
50.79	51.69	31.14	835.26	0.02352	0.1672
50.73	51.73	31.22	829.40	0.02352	0.1861
50.79	51.81	31.09	813.55	0.02422	0.1935
50.79	51.79	31.15	810.03	0.02425	0.1907
50.82	51.82	31.03	810.22	0.02443	0.1897

Table 16 (cont.)

T_{in} (°C)	T_{out} (°C)	T_{am} (°C)	G_t (W/m ²)	$(T_{in}-T_{am})/G_t$	η
50.79	51.88	31.19	805.74	0.02433	0.2090
50.80	51.84	31.13	812.16	0.02422	0.1992
50.81	51.91	31.06	817.04	0.02417	0.2082
50.76	51.85	30.91	816.13	0.02432	0.2066
50.78	51.84	30.84	815.98	0.02444	0.2015
50.74	51.87	30.83	818.53	0.02433	0.2145
50.78	51.80	30.93	819.48	0.02422	0.1927
50.76	51.86	31.03	820.34	0.02404	0.2078
50.81	51.83	31.03	821.45	0.02408	0.1919
60.29	60.51	28.75	823.61	0.03829	0.0419
60.23	60.53	28.77	825.58	0.03810	0.0566
60.19	60.43	28.79	822.59	0.03817	0.0452
60.23	60.42	28.82	820.06	0.03831	0.0353
60.16	60.41	28.73	820.22	0.03832	0.0479
60.08	60.33	28.84	819.84	0.03810	0.0474
60.14	60.33	28.90	821.73	0.03802	0.0358
60.12	60.31	28.89	826.84	0.03777	0.0345
60.21	60.36	28.74	826.48	0.03808	0.0272
60.18	60.38	28.75	824.74	0.03812	0.0362
60.23	60.44	28.80	822.38	0.03822	0.0390
60.25	60.47	28.96	813.91	0.03845	0.0424
60.23	60.49	28.87	813.35	0.03855	0.0504
60.25	60.48	28.89	811.07	0.03867	0.0437
60.20	60.44	28.90	812.46	0.03853	0.0469
60.15	60.40	28.92	812.80	0.03842	0.0478
60.19	60.41	28.94	813.88	0.03840	0.0409
60.19	60.38	28.96	815.73	0.03828	0.0376
60.09	60.35	28.81	815.71	0.03835	0.0492

Table 16 (cont.)

T_{in} (°C)	T_{out} (°C)	T_{am} (°C)	G_t (W/m ²)	$(T_{in}-T_{am})/G_t$	η
60.02	60.33	28.76	814.95	0.03837	0.0589
60.08	60.31	28.74	815.49	0.03843	0.0435
60.31	60.66	28.86	800.64	0.03928	0.0669
60.40	60.63	28.85	802.03	0.03934	0.0436
60.34	60.57	28.88	801.65	0.03925	0.0433
60.28	60.49	28.75	803.34	0.03925	0.0409
60.24	60.45	28.72	803.13	0.03925	0.0393
60.24	60.49	28.76	804.94	0.03910	0.0483
60.41	60.70	28.92	802.90	0.03922	0.0555
60.41	60.72	28.97	804.21	0.03910	0.0597
60.45	60.64	29.00	801.14	0.03926	0.0377

Table 17 The thermal efficiency of ETC with the Sn-Al₂O₃-7 as solar selective absorber

T_{in} (°C)	T_{out} (°C)	T_{am} (°C)	G_t (W/m ²)	$(T_{in}-T_{am})/G_t$	η
28.10	30.83	25.16	847.63	0.00348	0.4979
28.13	30.84	25.06	848.78	0.00362	0.4930
28.17	30.87	25.01	848.40	0.00372	0.4927
28.21	30.93	25.06	848.36	0.00371	0.4969
28.24	30.94	25.04	847.71	0.00377	0.4936
28.28	30.99	25.11	848.71	0.00373	0.4945
28.31	31.00	25.09	849.66	0.00378	0.4909
28.34	31.05	25.15	849.37	0.00376	0.4943
28.38	31.04	25.18	847.43	0.00377	0.4870
28.41	31.10	25.17	847.06	0.00382	0.4918
28.43	31.10	25.20	849.22	0.00380	0.4866
28.47	31.12	25.25	847.89	0.00380	0.4846

Table 17 (cont.)

T_{in} (°C)	T_{out} (°C)	T_{am} (°C)	G_t (W/m ²)	$(T_{in}-T_{am})/G_t$	η
28.50	31.15	25.24	848.10	0.00384	0.4848
28.53	31.21	25.26	848.38	0.00386	0.4891
28.57	31.23	25.32	847.79	0.00383	0.4874
28.60	31.30	25.39	848.00	0.00379	0.4938
28.64	31.31	25.42	849.24	0.00379	0.4875
28.83	31.31	25.44	848.38	0.00400	0.4509
28.85	31.33	25.45	848.37	0.00400	0.4540
28.88	31.37	25.37	847.44	0.00413	0.4553
29.05	31.57	25.30	847.92	0.00443	0.4596
29.05	31.74	25.34	849.01	0.00438	0.4894
29.07	31.76	25.36	848.71	0.00437	0.4911
29.09	31.76	25.42	846.92	0.00432	0.4893
29.20	31.81	25.29	849.65	0.00460	0.4754
29.24	31.79	25.25	851.72	0.00468	0.4646
29.30	31.81	25.22	852.76	0.00479	0.4550
29.34	31.86	25.23	852.99	0.00481	0.4577
29.40	31.92	25.24	853.24	0.00488	0.4574
29.44	31.97	25.31	851.47	0.00485	0.4589
40.33	42.34	27.63	876.32	0.01450	0.3540
40.33	42.39	27.61	869.62	0.01463	0.3667
40.50	42.36	27.58	870.73	0.01484	0.3303
40.15	42.38	27.65	872.84	0.01431	0.3955
40.40	42.41	27.71	874.28	0.01451	0.3559
40.34	42.46	27.49	874.53	0.01468	0.3767
40.45	42.42	27.42	876.26	0.01487	0.3475
40.34	42.49	27.28	871.15	0.01499	0.3833
40.45	42.50	27.32	871.85	0.01506	0.3631
40.56	42.49	27.46	870.00	0.01506	0.3442

Table 17 (cont.)

T_{in} (°C)	T_{out} (°C)	T_{am} (°C)	G_t (W/m ²)	$(T_{in}-T_{am})/G_t$	η
40.40	42.53	27.58	863.23	0.01485	0.3825
40.66	42.58	27.67	863.98	0.01503	0.3451
40.69	42.64	27.74	862.88	0.01500	0.3509
40.63	42.72	27.78	879.14	0.01461	0.3680
40.57	42.71	27.72	883.19	0.01455	0.3758
40.79	42.74	27.76	881.53	0.01478	0.3423
40.70	42.82	27.74	884.11	0.01467	0.3711
40.61	42.82	27.75	884.25	0.01454	0.3878
40.80	42.83	27.66	884.74	0.01485	0.3557
40.57	42.84	27.75	887.58	0.01444	0.3956
40.46	42.81	27.68	888.40	0.01439	0.4093
40.76	42.88	27.53	888.35	0.01489	0.3700
40.66	42.84	27.48	886.81	0.01486	0.3814
40.54	42.78	27.55	885.80	0.01466	0.3915
40.25	42.59	27.55	885.98	0.01433	0.4096
40.53	42.79	27.61	883.96	0.01462	0.3956
40.72	42.73	27.47	884.85	0.01498	0.3522
40.57	42.59	27.44	884.51	0.01484	0.3530
40.63	42.60	27.46	885.24	0.01488	0.3447
40.44	42.66	27.48	886.76	0.01462	0.3864
50.88	52.64	29.95	898.00	0.02331	0.3026
50.78	52.54	29.93	895.38	0.02328	0.3050
50.84	52.58	29.95	895.52	0.02334	0.2998
50.76	52.39	29.77	891.26	0.02355	0.2828
50.87	52.36	29.78	890.68	0.02368	0.2592
50.77	52.40	29.79	889.88	0.02357	0.2848
50.73	52.28	29.77	887.12	0.02362	0.2717
50.74	52.21	29.81	882.34	0.02372	0.2572

Table 17 (cont.)

T_{in} (°C)	T_{out} (°C)	T_{am} (°C)	G_t (W/m ²)	$(T_{in}-T_{am})/G_t$	η
50.77	52.23	29.90	875.31	0.02384	0.2582
50.78	52.25	29.95	878.78	0.02370	0.2595
50.63	52.22	30.02	881.68	0.02338	0.2794
50.59	52.22	30.10	884.26	0.02318	0.2850
50.46	52.18	30.18	881.40	0.02301	0.3026
50.59	52.20	30.39	885.21	0.02282	0.2821
50.51	52.21	30.46	890.02	0.02253	0.2941
50.73	52.25	30.53	889.43	0.02271	0.2639
50.63	52.07	30.36	890.13	0.02277	0.2515
50.30	52.03	30.32	880.33	0.02270	0.3039
50.27	52.03	30.37	882.36	0.02255	0.3083
50.43	51.99	30.33	881.45	0.02281	0.2731
50.34	51.89	30.34	877.26	0.02280	0.2748
50.27	51.84	30.27	876.07	0.02283	0.2774
50.21	51.83	30.35	881.64	0.02253	0.2850
50.17	51.83	30.59	884.99	0.02212	0.2911
50.25	51.84	30.45	884.30	0.02239	0.2777
50.46	51.81	30.29	883.08	0.02284	0.2360
50.25	51.83	30.17	882.67	0.02274	0.2773
50.24	51.80	30.21	883.10	0.02268	0.2733
50.11	51.76	30.22	882.67	0.02254	0.2889
50.13	51.82	30.21	885.68	0.02249	0.2956
59.08	59.74	30.72	826.73	0.03428	0.1234
59.00	59.76	30.79	832.21	0.03392	0.1416
59.06	59.84	30.87	822.48	0.03412	0.1459
59.23	59.83	30.92	834.83	0.03374	0.1107
59.26	59.81	30.92	830.63	0.03328	0.1023
59.19	59.88	30.90	838.61	0.03339	0.1266

Table 17 (cont.)

T_{in} (°C)	T_{out} (°C)	T_{am} (°C)	G_t (W/m ²)	$(T_{in}-T_{am})/G_t$	η
59.14	59.92	30.77	852.38	0.03328	0.1404
59.18	59.93	30.72	852.52	0.03339	0.1364
59.11	59.98	30.73	855.74	0.03316	0.1579
59.14	59.92	30.70	850.96	0.03342	0.1426
59.20	59.89	30.72	853.34	0.03338	0.1255
59.25	59.89	30.97	850.55	0.03324	0.1163
59.23	59.93	30.99	854.57	0.03305	0.1255
59.32	59.94	30.94	857.86	0.03309	0.1123
59.29	59.96	30.96	855.83	0.03310	0.1212
59.35	60.02	30.90	856.95	0.03321	0.1205
59.34	60.02	30.80	852.96	0.03346	0.1236
59.34	60.04	30.80	849.51	0.03359	0.1287
59.29	60.04	30.73	846.98	0.03373	0.1356
59.36	60.08	30.83	848.49	0.03363	0.1319
59.44	60.07	30.84	841.04	0.03401	0.1162
59.46	60.05	30.91	808.08	0.03533	0.1138
59.32	60.04	30.88	827.53	0.03436	0.1347
59.22	60.10	30.82	828.44	0.03428	0.1652
59.38	60.15	30.74	826.04	0.03467	0.1439
59.34	60.09	30.81	832.52	0.03427	0.1397
59.39	60.04	30.77	816.76	0.03504	0.1243
59.39	60.06	30.76	815.66	0.03509	0.1287
59.41	60.05	30.78	809.46	0.03536	0.1228
59.27	60.10	30.90	812.74	0.03491	0.1575

Table 18 The thermal efficiency of ETC with the Sn-Al₂O₃-10 as solar selective absorber

T_{in} (°C)	T_{out} (°C)	T_{am} (°C)	G_t (W/m ²)	$(T_{in}-T_{am})/G_t$	η
35.05	38.24	33.83	805.15	0.00151	0.6124
35.05	38.23	33.85	804.68	0.00149	0.6116
35.04	38.21	33.81	805.17	0.00152	0.6087
35.04	38.23	33.80	804.44	0.00154	0.6132
35.05	38.26	33.82	806.71	0.00152	0.6160
35.05	38.26	33.80	810.23	0.00154	0.6124
35.05	38.21	33.81	808.15	0.00153	0.6054
35.05	38.24	33.83	807.00	0.00151	0.6125
35.06	38.22	33.88	808.99	0.00146	0.6045
35.09	38.23	33.89	810.73	0.00148	0.6009
35.10	38.21	33.89	812.25	0.00149	0.5922
35.13	38.24	33.82	809.48	0.00162	0.5950
35.16	38.22	33.81	808.82	0.00167	0.5853
35.20	38.23	33.79	807.08	0.00175	0.5805
35.23	38.29	33.81	806.70	0.00175	0.5867
35.27	38.32	33.94	808.97	0.00163	0.5850
35.00	38.00	34.04	808.74	0.00118	0.5749
35.05	38.07	33.98	809.69	0.00131	0.5782
35.09	38.07	33.71	810.16	0.00170	0.5695
35.14	38.10	33.77	811.59	0.00168	0.5646
35.19	38.16	33.75	808.94	0.00178	0.5678
35.25	38.20	33.79	812.99	0.00180	0.5614
35.31	38.23	33.71	815.14	0.00197	0.5550
35.37	38.33	33.66	814.08	0.00210	0.5627
35.44	38.42	33.67	814.59	0.00217	0.5662
35.51	38.48	33.79	815.46	0.00210	0.5637
35.58	38.49	33.82	812.64	0.00217	0.5536

Table 18 (cont.)

T_{in} (°C)	T_{out} (°C)	T_{am} (°C)	G_t (W/m ²)	$(T_{in}-T_{am})/G_t$	η
35.65	38.59	33.85	815.81	0.00221	0.5581
35.72	38.66	33.78	813.46	0.00238	0.5582
35.79	38.70	33.89	813.83	0.00234	0.5534
45.46	47.97	33.23	802.14	0.01524	0.4842
45.25	47.80	33.20	801.13	0.01504	0.4934
45.32	47.75	33.23	800.69	0.01510	0.4687
45.20	47.63	33.28	801.08	0.01487	0.4694
45.18	47.54	33.34	803.55	0.01473	0.4551
45.02	47.53	33.35	801.88	0.01455	0.4846
44.91	47.41	33.45	805.46	0.01423	0.4809
44.99	47.41	33.47	808.83	0.01424	0.4621
44.94	47.38	33.41	806.15	0.01430	0.4670
44.86	47.33	33.43	807.10	0.01416	0.4746
44.89	47.31	33.45	807.76	0.01417	0.4632
44.87	47.27	33.48	806.21	0.01414	0.4609
44.67	47.22	33.50	804.53	0.01387	0.4913
44.80	47.19	33.42	804.98	0.01414	0.4596
44.63	47.18	33.45	807.55	0.01384	0.4883
44.67	47.11	33.49	806.13	0.01387	0.4682
44.49	47.03	33.37	800.16	0.01389	0.4916
44.53	47.03	33.38	802.05	0.01390	0.4831
44.46	46.93	33.35	802.84	0.01383	0.4771
44.57	46.86	33.19	801.59	0.01420	0.4421
44.44	46.92	33.04	802.55	0.01421	0.4788
44.43	46.86	32.98	804.19	0.01424	0.4688
44.41	46.83	33.02	803.89	0.01417	0.4647
44.44	46.83	33.07	800.11	0.01420	0.4615
44.38	46.79	33.12	801.92	0.01405	0.4656

Table 18 (cont.)

T_{in} (°C)	T_{out} (°C)	T_{am} (°C)	G_t (W/m ²)	$(T_{in}-T_{am})/G_t$	η
44.27	46.72	33.08	801.89	0.01396	0.4742
44.30	46.72	33.12	804.58	0.01390	0.4653
44.40	46.70	33.08	806.32	0.01404	0.4406
44.29	46.65	33.07	805.86	0.01392	0.4534
44.31	46.62	33.06	805.14	0.01397	0.4451
55.41	57.10	35.19	802.85	0.02518	0.3259
55.20	56.92	35.16	802.03	0.02499	0.3316
55.22	56.89	35.18	802.09	0.02498	0.3223
55.14	56.97	35.23	802.02	0.02483	0.3525
55.04	56.91	35.18	803.70	0.02470	0.3614
55.07	56.84	35.20	802.08	0.02477	0.3413
55.08	56.79	35.25	801.01	0.02476	0.3319
54.71	56.44	35.27	802.94	0.02421	0.3328
54.75	56.52	35.29	800.82	0.02430	0.3408
54.67	56.55	35.33	800.58	0.02416	0.3628
55.12	56.74	35.33	800.56	0.02472	0.3129
55.14	56.79	35.32	804.85	0.02463	0.3185
55.29	56.84	35.29	802.10	0.02494	0.2997
55.40	56.89	35.37	804.18	0.02491	0.2884
55.18	56.83	35.24	800.38	0.02491	0.3188
55.41	56.97	35.23	802.57	0.02514	0.3011
55.31	56.88	35.25	802.96	0.02499	0.3017
54.99	56.83	35.27	802.52	0.02457	0.3559
55.29	56.84	35.09	801.02	0.02522	0.3009
55.24	56.84	35.00	801.99	0.02524	0.3079
55.14	56.87	35.06	801.67	0.02504	0.3354
55.23	56.88	35.15	805.24	0.02494	0.3174
55.42	56.98	35.27	804.46	0.02504	0.3010

Table 18 (cont.)

T_{in} (°C)	T_{out} (°C)	T_{am} (°C)	G_t (W/m ²)	$(T_{in}-T_{am})/G_t$	η
55.25	56.86	35.33	800.41	0.02489	0.3112
55.15	56.90	35.35	805.06	0.02459	0.3373
55.16	56.95	35.36	804.77	0.02460	0.3443
55.15	56.93	35.41	804.90	0.02452	0.3410
55.19	56.86	35.52	804.32	0.02445	0.3220
55.02	56.82	35.49	804.54	0.02427	0.3456
55.16	56.80	35.39	803.89	0.02459	0.3164
65.40	66.30	35.47	800.25	0.03740	0.1743
65.49	66.37	35.64	801.02	0.03727	0.1701
65.68	66.55	35.70	802.20	0.03736	0.1689
65.62	66.58	35.74	801.69	0.03728	0.1850
65.66	66.53	35.74	801.38	0.03733	0.1685
65.56	66.54	35.73	801.53	0.03722	0.1889
65.59	66.50	35.74	801.05	0.03727	0.1749
65.50	66.49	35.74	800.28	0.03719	0.1905
65.53	66.40	35.60	800.39	0.03739	0.1683
65.43	66.39	35.38	800.79	0.03752	0.1842
65.49	66.39	35.28	800.30	0.03775	0.1737
65.48	66.37	35.28	800.98	0.03771	0.1724
65.47	66.31	35.28	801.94	0.03764	0.1622
65.41	66.36	35.37	801.36	0.03749	0.1835
65.49	66.33	35.27	800.68	0.03774	0.1626
65.38	66.43	35.32	802.38	0.03746	0.2024
65.42	66.39	35.22	802.59	0.03763	0.1869
65.45	66.30	35.25	802.18	0.03765	0.1639
65.31	66.27	35.12	802.40	0.03762	0.1850
65.40	66.25	34.98	800.54	0.03800	0.1650
65.29	66.27	35.01	800.86	0.03781	0.1896

Table 18 (cont.)

T_{in} (°C)	T_{out} (°C)	T_{am} (°C)	G_t (W/m ²)	$(T_{in}-T_{am})/G_t$	η
65.32	66.21	35.14	800.81	0.03768	0.1721
65.22	66.23	35.09	801.73	0.03758	0.1960
65.30	66.20	35.14	801.19	0.03764	0.1753
65.19	66.18	35.11	802.29	0.03749	0.1912
65.19	66.11	35.13	800.79	0.03754	0.1773
65.21	66.14	35.06	800.90	0.03764	0.1796
65.10	66.15	35.12	801.42	0.03741	0.2028
65.13	66.06	35.18	800.01	0.03744	0.1798
65.12	66.06	35.10	800.19	0.03752	0.1823

APPENDIX D

The Parameter of annual energy calculation

$$T_a (\text{°C}) = 30$$

$$T_o (\text{°C}) = 60$$

$$T_i (\text{°C}) = 35$$

$$G_t = 800$$

$$E (\text{kWh/m}^2) = 1800$$

Table 19 The calculation of annual energy

Sample	Thermal efficiency equations	η_o	F_{RUL}	$(T_f - T_o)/G_t$	Efficiency	Annual energy yield (kWh/m ²)
Sn-Al ₂ O ₃ -5	$\eta = 0.4241 - 9.6235 [(Ti - Ta)/Gt]$	0.42	9.62	0.00625	0.3640	655.12
Sn-Al ₂ O ₃ -7	$\eta = 0.5355 - 11.6440 [(Ti - Ta)/Gt]$	0.54	11.64	0.00625	0.4627	832.90
Sn-Al ₂ O ₃ -10	$\eta = 0.6144 - 11.4920 [(Ti - Ta)/Gt]$	0.61	11.49	0.00625	0.5426	976.64

APPENDIX E

Table 20 The LCC and LCOE of the new prototype of ETC using the Sn-Al₂O₃-5 as a solar selective absorber

Year	Initial cost	O&M (0.5%)	Salvage value (10%)	O&M cost (NPV)	Salvage value (NPV)	Energy Production (kWh)
0	21491.71					
1		107.46		98.99		707.52
2		107.46		91.20		707.52
3		107.46		84.01		707.52
4		107.46		77.40		707.52
5		107.46		71.30		707.52
6		107.46		65.68		707.52
7		107.46		60.51		707.52
8		107.46		55.74		707.52
9		107.46		51.35		707.52
10		107.46		47.31		707.52
11		107.46		43.58		707.52
12		107.46		40.15		707.52
13		107.46		36.99		707.52
14		107.46		34.07		707.52
15		107.46	2,149.17	31.39	627.80	707.52
Total	21,491.71	1,611.88		889.69		10,612.87
LCC	21,753.60 THB					
LCOE	2.05 THB/kWh					

Table 21 The LCC and LCOE of the new prototype of ETC using the Sn-Al₂O₃-7 as a solar selective absorber

Year	Initial cost	O&M (0.5%)	Salvage value (10%)	O&M cost (NPV)	Salvage value (NPV)	Energy Production (kWh)
0	22091.71					
1		110.46		101.76		899.5374
2		110.46		93.74		899.5374
3		110.46		86.36		899.5374
4		110.46		79.56		899.5374
5		110.46		73.29		899.5374
6		110.46		67.52		899.5374
7		110.46		62.20		899.5374
8		110.46		57.30		899.5374
9		110.46		52.79		899.5374
10		110.46		48.63		899.5374
11		110.46		44.80		899.5374
12		110.46		41.27		899.5374
13		110.46		38.02		899.5374
14		110.46		35.03		899.5374
15		110.46	2,209.17	32.27	645.33	899.5374
Total	22,091.71	1,656.88		914.53		13493.061
LCC	22,360.91 THB					
LCOE	1.66 THB/kWh					

Table 22 The LCC and LCOE of the new prototype of ETC using the Sn-Al₂O₃-10 as a solar selective absorber

Year	Initial cost	O&M (0.5%)	Salvage value (10%)	O&M cost (NPV)	Salvage value (NPV)	Energy Production (kWh)
0	22091.71					
1		110.46		101.76		1054.77
2		110.46		93.74		1054.77
3		110.46		86.36		1054.77
4		110.46		79.56		1054.77
5		110.46		73.29		1054.77
6		110.46		67.52		1054.77
7		110.46		62.20		1054.77
8		110.46		57.30		1054.77
9		110.46		52.79		1054.77
10		110.46		48.63		1054.77
11		110.46		44.80		1054.77
12		110.46		41.27		1054.77
13		110.46		38.02		1054.77
14		110.46		35.03		1054.77
15		110.46	2,209.17	32.27	645.33	1054.77
Total	22,091.71	1,656.88		914.53		15821.49
LCC	22,360.91 THB					
LCOE	1.41 THB/kWh					

APPENDIX F

Publications and conference

Materials for Renewable and Sustainable Energy (2018) 7:2
<https://doi.org/10.1007/s40243-017-0109-1>

ORIGINAL PAPER



Influence of tin content on spectral selectivity and thermal conductivity of Sn–Al₂O₃ solar selective absorber

Warisa Wamae¹ · Tawat Surlwong¹ · Thotsaphon Threrujirapong²

Received: 23 August 2017 / Accepted: 30 December 2017
© The Author(s) 2018. This article is an open access publication

Abstract

The tin-pigmented aluminium oxide film (Sn–Al₂O₃) based solar selective absorber was successfully prepared with three different contents of tin by an anodization process. The phase and morphology of the Sn–Al₂O₃ were measured by X-ray diffractometer and a scanning electron microscope equipped with an energy dispersive X-ray analyser. The reflectance (*R*) of the coating was determined by Ultraviolet–visible–near infrared spectrophotometer in the wavelength interval of 300–2500 nm and the Fourier transform infrared spectrophotometer in the wavelength of infrared region (2500–25,000 nm). As a result, aluminium and tin phases were detected at the coating surface. The Al₂O₃ films were formed and compacted as a barrier on the Al substrate. The compositions of the oxide film composed of tin (Sn), aluminium (Al) and oxygen (O) elements. With increasing Sn content, the solar absorptance (α_{sol}) gradually increased, but it has little effect on the thermal emittance (ϵ_{therm}). The thermal conductivity of Sn–Al₂O₃ samples decreased with increasing Sn content as a result of the increasing thickness of the Sn layer at the interface leading to obstruct the free electrons and phonon contributions. The present result suggests that the increasing Sn content in the Sn–Al₂O₃ coating can enhance the solar selectivity properties and a good solar absorber material.

Keywords Sn–Al₂O₃ · Solar selective absorber · Anodization · Reflectance · Absorptance · Emittance

Introduction

Solar selective coatings on the solar receiver are selected according to the specific characteristics that achieve high solar absorptance (α_{sol}) in the visible region and low thermal emittance (ϵ_{therm}) in the infrared region [1]. There are many techniques for selective coating preparation such as evaporation, sputtering, electro-chemical deposition (anodization), chemical vapour deposition, spray pyrolysis, sol–gel/dip-coating, electro plating, painting and other methods [2]. Anodization is a common technique used to protect the aluminium (Al) from corrosion by creating a thin oxide film on the Al surface. The solar selectivity of the solar

absorber materials can be optimized by varying the metal and ceramic constituent elements, thickness, concentration, shape, size, and orientation [1]. Several metal pigments can be used to deposit into the pores of the film as a solar selective absorber. The thickness of Al₂O₃ based cermet coatings was considered in previous reports [3–5], which correlated with spectral selective properties. In addition, variation of the content of pigment or composite coating on the surface has an influence on the spectral selectivity (α_{sol} and ϵ_{therm}) of the solar selective absorbers [2, 3]. To improve the spectral selectivity of the solar selective absorber and high corrosion resistance, several pigments deposited in the Al₂O₃ film have been studied with different techniques, e.g. coatings of black Cu–Ni, black Ni–Co by electro-deposition [6, 7], Co–Al₂O₃ by anodization [8], Cu–CuAl₂O₄ hybrids deposited in anodic aluminium oxide (AAO) by electrochemical processes [9], carbon nano-particles embedded in SiO₂, ZnO and NiO matrices by a sol–gel technique [10], W–Al₂O₃ cermet, Mo–Al₂O₃, Pt–Al₂O₃, Ag–Al₂O₃ nanocermet, and CrN_xO_y/SiO₂ coated with a sputtering technique [11–14]. Tin (Sn) has been considered a good candidate pigment embedded into the pores of Al₂O₃ film on Al substrate which

✉ Tawat Surlwong
twats@nu.ac.th

¹ School of Renewable Energy Technology, Naresuan University, Phitsanulok 65000, Thailand

² Department of Materials and Production Technology Engineering, Faculty of Engineering, King Mongkut's University of Technology North Bangkok, Bangkok, Thailand

has been successfully prepared by the anodization process as Sn–Al₂O₃ [15, 16]. The corrosion resistance of Sn–Al₂O₃ is higher than that of the Ni–Al₂O₃ [16]. Presently, there are a few prior researches on the influence of Sn content on phase, morphology, thermal conductivity, and solar selectivity of Al₂O₃-based cermet coatings.

Therefore, the purposes of the present study are preparation of the Sn–Al₂O₃ based solar selective absorber by anodic anodization with three different contents of Sn pigment. Phase, morphology and chemical distributions of the Sn–Al₂O₃ coatings were characterized. The influence of Sn contents on the α_{sol} , ϵ_{therm} and thermal conductivity of the coatings were also investigated, including the discussion of solar radiation and heat transfer mechanism through the Sn–Al₂O₃ coatings.

Experimental section

Preparation of anodized aluminium

Aluminium (Al) sheet of 9 cm wide \times 160 cm long with a thickness of 0.02 cm was used as a substrate. It was followed by the anodization process, under suitable conditions calculated by the surface area of the samples. First, the aluminium sheet was degreased with a commercial cleaning solution, and then etched by NaOH solution, and immersed in 165 g/L sulphuric acid solution. The Al substrate was connected with an anode (+) and a lead plate was used as the cathode (–), and then a direct current of electrical density with 1000 A at the constant potential of 15–17 V at 20 °C was applied for 45 min to achieve the Al₂O₃ film thickness of 9.1–9.5 μm . Subsequently, the formed Al₂O₃ film was directly transferred to the colouring bath containing tin (II) sulphate (SnSO₄). The Sn pigment was deposited into the pores of Al₂O₃ film for 5, 7 and 10 min, which coded as Sn–Al₂O₃-5, Sn–Al₂O₃-7 and Sn–Al₂O₃-10, respectively. Then, the porous Al₂O₃ was sealed in a hot water tank at 50–60 °C for 30 min.

Instrumentation

The phase and morphology of the samples were characterized by X-ray diffraction technique (XRD, PHILIPS X'Pert-MPD) with Cu–K α radiation in the 2 θ range of 20–90°, a low vacuum scanning electron microscope equipped with an energy dispersive X-ray analyser (LV-SEM-EDX, JSM-5910 JEOL). The reflectance (R) was measured using the ultraviolet visible near infrared (UV–Vis–NIR) spectrophotometer (Shimadzu UV-3101PC) in the wavelength of 300–2500 nm, and the Fourier transform infrared spectrophotometer (FTIR, Bruker Tensor 27) in the wavelength of infrared region (2500–25,000 nm). The α_{sol} and the ϵ_{therm}

were calculated from the measured R spectrum by the following equations [2]:

$$\alpha_{\text{sol}} = \frac{\int_{0.3\mu\text{m}}^{2.5\mu\text{m}} I_s(\lambda)(1 - R(\lambda))d\lambda}{\int_{0.3\mu\text{m}}^{2.5\mu\text{m}} I_s(\lambda)d\lambda} \quad (1)$$

$$\epsilon_{\text{therm}} = \frac{\int_{2.5\mu\text{m}}^{25\mu\text{m}} I_b(\lambda)(1 - R(\lambda))d\lambda}{\int_{2.5\mu\text{m}}^{25\mu\text{m}} I_b(\lambda)d\lambda} \quad (2)$$

where $I_s(\lambda)$ is the solar spectral irradiance at AM 1.5, and $R(\lambda)$ is the measured reflectance spectrum of the coating. Furthermore, the thermal diffusivity (κ_p) was measured by laser flash analyser (LFA 447 NanoFlash-A) over the temperature of 25–275 °C according to ASTM 1461-13 standard. The thermal conductivity (k) was then calculated with density (ρ) and specific heat (C_p) as follows:

$$k = \kappa_p \rho C_p \quad (3)$$

Results and discussion

Figure 1 shows the XRD patterns of Sn–Al₂O₃ with various Sn contents, compared with the JCPDS database No. 01-1176, 01-1243 and 01-0926 for Al, Al₂O₃ and Sn phases, respectively. The phase of Al and Sn were indexed for all samples, and the phase intensity of Sn was increased by increasing the Sn contents. The crystallite size was also

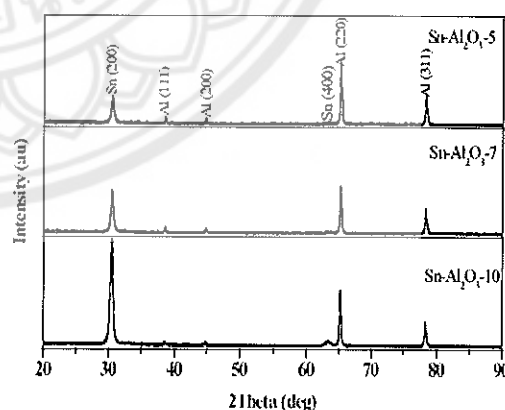


Fig. 1 The XRD patterns of the Sn–Al₂O₃ with different Sn contents

calculated by Scherrer's equation [17] using the Sn (200) peak in the XRD spectrum.

$$D = \frac{K\lambda}{\beta \cos \theta} \quad (4)$$

K is the crystallite shape factor which usually takes a value of 0.9, λ is the X-ray wavelength of Cu- K_{α} radiation (0.15406 nm), β is the full width at half maximum (FWHM) in radians and θ is the Bragg's angle of the (200) peak of Sn. The calculated results for the Sn- Al_2O_3 -5, Sn- Al_2O_3 -7 and Sn- Al_2O_3 -10 were 23.24, 23.24 and 46.48 nm, respectively. It is observed that the crystallite size of the Sn- Al_2O_3 -10 sample is double the size of the others, indicating that the crystal growth of Sn inside the Al_2O_3 pores continuously occurred in the colouring bath beyond 7 min. According to the double intensity for (200) plane of Sn, the crystallinity of the highest content of Sn is also improved due to the sufficient time in the colouring process. However, the Al_2O_3 phase was not found in the XRD patterns because its structure is the amorphous phase, which is consistent with previous studies of W- Al_2O_3 [11], Pt- Al_2O_3 [18] and Mo- Al_2O_3 [13].

Figure 2 presents the SEM images for surface morphology of the Sn- Al_2O_3 coatings prepared by the anodization process. In Fig. 2a-c, the surface of the samples was quite homogeneous similar to the ordinary anodized Al substrate prepared to be a solar absorber black coatings [3, 19, 20]. The shallow marks of the surfaces occurred during the phenomenon of sealing the Al_2O_3 pores. Figure 2d-f indicates

that the Al_2O_3 films were formed with a thickness of 9.1–9.5 μm , with a perpendicular pore structure and compact Al_2O_3 barrier on Al substrate, corresponding with Ni- Al_2O_3 selective absorber [21]. Fundamentally, the elements with higher atomic numbers exhibit the lighter region in that area compared to lower atomic numbers. It is observed that there are different contrast regions on the Sn- Al_2O_3 films, due to the different atomic numbers of the elements. The Al_2O_3 phase exhibit dark grey regions in all the samples. While, Sn has its highest atomic number in the Al_2O_3 phase, the Sn rich reveal a spike shape and light region close to the interface of Al substrate, according to a previous study [16]. The increasing and sharpness of the lighter regions of each sample depend on an increase in the Sn content of the Al_2O_3 pores.

To ascertain the increase of Sn content in the porous Al_2O_3 films, SEM-EDX with line scan analysis techniques were used (as shown in Fig. 3). All the samples consist of detected Al, O and Sn elements, corresponding to the XRD pattern. The Sn content exhibited a high count rate close to the interface of the Al substrate, and the accumulation of Sn according to the incremental deposition time.

In addition, the chemical distribution over a cross section, the surface of the Sn- Al_2O_3 coatings indicated the different chemical distributions in each layer, as presented by the EDX mapping images in Fig. 4. The fundamental elements of these samples were dispersed in different densities in each region. Al displayed the highest density in the Al substrate, while the O revealed the highest density in the Al_2O_3 layer,

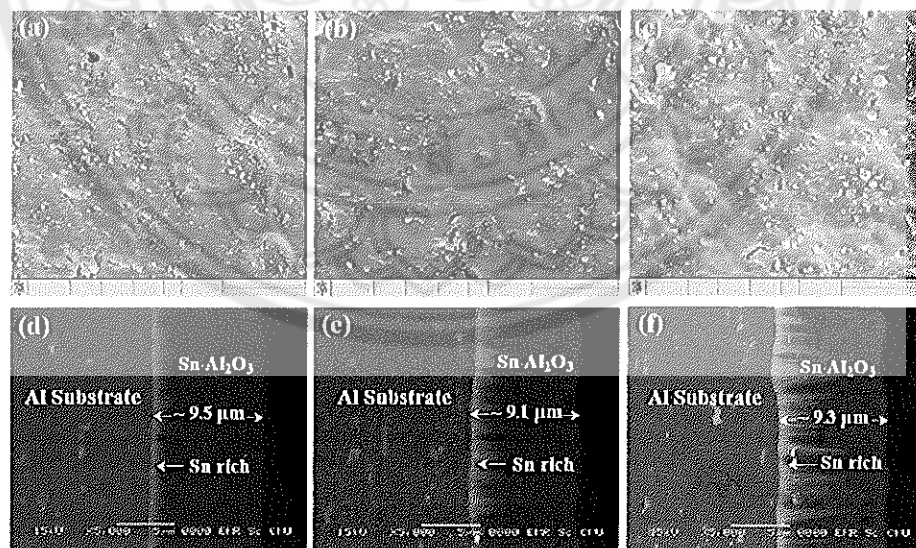


Fig. 2 LV-SEM images of (a-c) surface and (d-f) sectional image of Sn- Al_2O_3 -5, Sn- Al_2O_3 -7 and Sn- Al_2O_3 -10

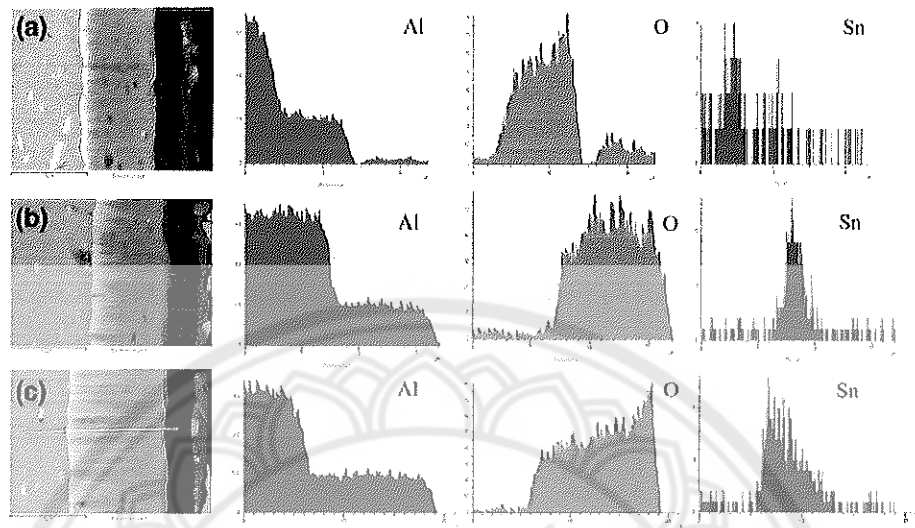


Fig. 3 SEM-EDX line scanning profiles of a Sn-Al₂O₃-5, b Sn-Al₂O₃-7 and c Sn-Al₂O₃-10 coatings

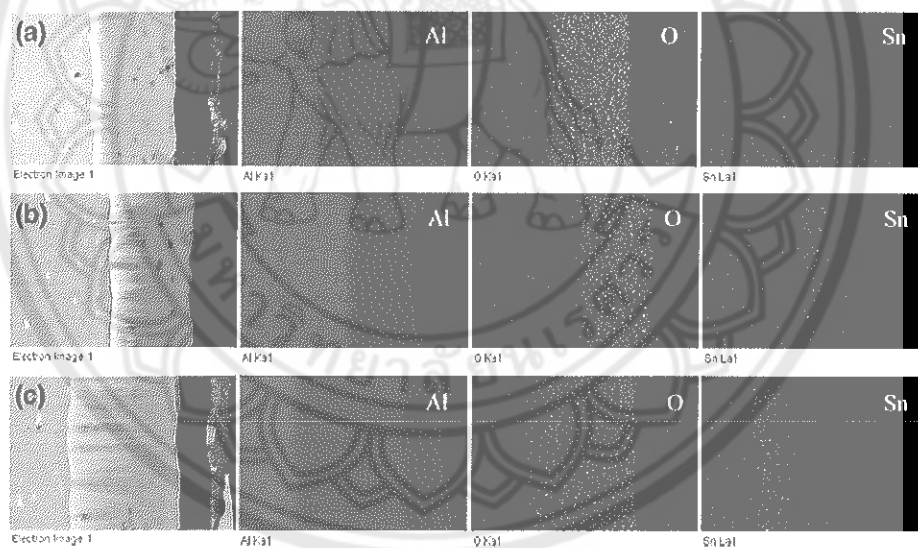


Fig. 4 SEM image and EDX mapping analysis of the a Sn-Al₂O₃-5, b Sn-Al₂O₃-7 and c Sn-Al₂O₃-10 coatings

and the Sn also appeared in the Al₂O₃ layer but the highest density is at the interface of the Al substrate, consistent with the EDX line scanning images (Fig. 3). Furthermore, the highest concentration of Sn in all the samples was found at 1 μ m distance from the interface. The dispersion distance of Sn, from the interface, in Sn-Al₂O₃-5, is 1 μ m, increasing

to 4 μ m and 7 μ m in the Sn-Al₂O₃-7 and the Sn-Al₂O₃-10, respectively.

Figure 5a presents the measured spectral reflectance (*R*) of Sn-Al₂O₃ with different Sn contents in the whole wavelength range of UV-Vis-NIR regions. All the Sn-Al₂O₃ samples exhibit the low *R* in the wavelength range of

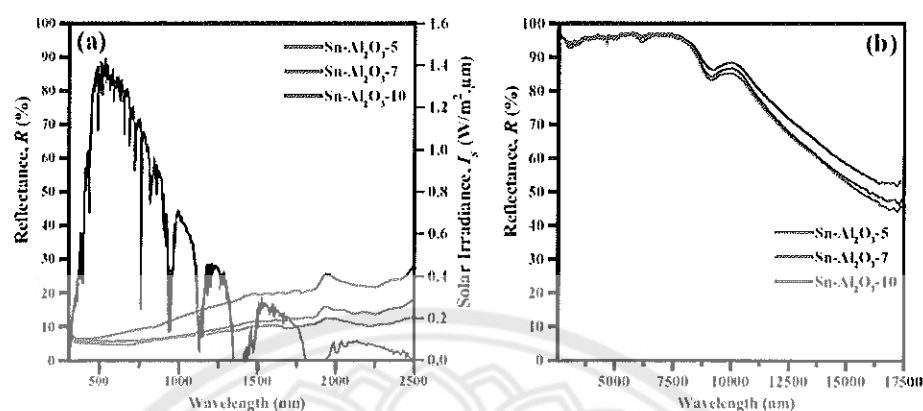


Fig. 5 Spectral reflectance (R) of Sn-Al₂O₃ solar absorber with different Sn contents in the wavelength range of a the UV-Vis-NIR regions compared with the solar spectrum at AM 1.5 and b the IR region

300–2000 nm. However, the R of all samples gradually increased with the increasing wavelength due to the maximum of the scattering and reflectance efficiencies at the high wavelength [11]. With increasing Sn content in the pores of Al₂O₃, the spectral R of the samples relatively decreased in the wavelength range of UV-Vis-NIR regions due to the thickness of Al₂O₃ layer behaved as anti-reflection (AR) layer reducing the reflection between the air and the Sn pigment layer [18, 22]. The α_{sol} of the samples are calculated and summarized in Table 1, together with the previous reports. The α_{sol} of the Sn-Al₂O₃-5, Sn-Al₂O₃-7 and Sn-Al₂O₃-10 were 0.89, 0.93 and 0.94, respectively. All are close to commercial solar absorbers (0.85–0.95) [1], and consistent with solar absorbers with related metal-Al₂O₃ film such as Co-Al₂O₃, W-Al₂O₃, Ag-Al₂O₃, Mo-Al₂O₃, Pt-Al₂O₃ and Ni-Al₂O₃ [8, 11–13, 18, 21]. In addition, α_{sol} of the Sn-Al₂O₃ samples increased according to the increase

of Sn content as a result of the solar radiation trapped inside the Al₂O₃ pores by the light resonant scattering with Sn particles [1, 21]. It corresponds to a previous study which found that the Al₂O₃ layer plays the role of antireflection and the amount of Sn pigment filling in the Al₂O₃ pores affect the α_{sol} [16]. Furthermore, the measured spectral R in the wavelength range of the IR region is presented in Fig. 5b. The spectral R was above 0.95 for all the samples in the wavelengths of 2.5–8.0 μm, and there was no display of the spectral R beyond 17.5 μm due to extreme noise. It is observed that the spectral R has little effect on Sn content in the wavelength range of the IR region. The ϵ_{therm} was calculated by Eq. 2, on the Planck blackbody distribution at 100 °C, as shown in Table 1. The ϵ_{therm} was 0.23, 0.24 and 0.21 for Sn-Al₂O₃-5, Sn-Al₂O₃-7 and Sn-Al₂O₃-10, respectively. It seems that the ϵ_{therm} is insignificantly changed with the increasing Sn content. When considering

Table 1 The solar absorptance (α_{sol}) and thermal emittance (ϵ_{therm}) of the Sn-Al₂O₃ samples with different Sn contents compared with the previous studies

Solar selective absorber	Preparation	Solar absorptance (α_{sol})	Thermal emittance (ϵ_{therm})
In the present study			
Sn-Al ₂ O ₃ -5	Anodization	0.89	0.23 (100 °C)
Sn-Al ₂ O ₃ -7	Anodization	0.93	0.24 (100 °C)
Sn-Al ₂ O ₃ -10	Anodization	0.94	0.21 (100 °C)
Previous studies			
Co-Al ₂ O ₃ [8]	Anodization/electro-deposition	> 0.98	0.03 (100 °C)
W-Al ₂ O ₃ [11]	Sputtering	0.94	0.10 (400 °C)
Ag-Al ₂ O ₃ [12]	Sputtering	0.93	0.04–0.05 (82 °C)
Ni-Al ₂ O ₃ [21]	Anodization	0.92–0.97	0.14–0.23 (70 °C)
Pt-Al ₂ O ₃ [23]	Evaporation	0.98	0.36 (200 °C)
Mo-Al ₂ O ₃ [24]	Sputtering	0.91–0.93	0.19–0.27 (80 °C)

previous studies, the ϵ_{therm} of this study was lower than the Pt–Al₂O₃ coating ($\epsilon_{\text{therm}} = 0.36$) [23] and close to the Ni–Al₂O₃ coatings ($\epsilon_{\text{therm}} = 0.14\text{--}0.23$) [21] and Mo–Al₂O₃ coating ($\epsilon_{\text{therm}} = 0.19\text{--}0.27$) [24]. As the results shown in Fig. 5, all the Sn–Al₂O₃ samples exhibit low R in the wavelength range of 300–2000 nm, and high R in the wavelength range of 2.5–17.5 μm , according to the theoretical property of solar absorber materials for achieving a high solar selectivity. Therefore, increasing Sn content in the pore of Al₂O₃ leads to a significant increase in the α_{sol} , but has little effect on the ϵ_{therm} .

Figure 6 presents the temperature dependences of thermal conductivity for non-anodized Al and Sn–Al₂O₃ solar absorber with various Sn contents to propose the quantity of heat transmitted through a unit thickness of the samples at interval temperatures from 25 to 275 °C. The thermal conductivity of non-anodized Al was the highest related to the thermal conductivity of pure Al which was reported by National Standard Reference Data Series-National Bureau of Standards [25]. While, the thermal conductivity of the Sn–Al₂O₃ samples was lower than that of the non-anodized Al because Al₂O₃ film on the surface presents the same as an insulator and imperfections in the atomic structure as ceramic behavior. It is observed that the thermal conductivity of all the samples slightly decreased with increasing temperature, indicating that the Sn–Al₂O₃ coatings are able to be used in special thermal applications by maintaining the thermal conductivity of materials over the operational temperature range (50–275 °C). Furthermore, the thermal conductivity in each sample decreased with increasing Sn content as a result of the increasing thickness of Sn layer at the interface leading to obstruct free electrons and phonon contributions.

Figure 7 represents a diagram of the heat flow in the sample for thermal conductivity measurement indicating

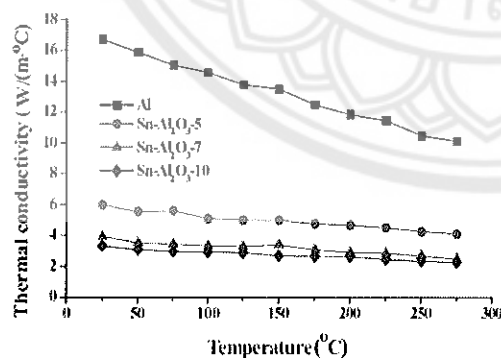


Fig. 6 Temperature dependences of thermal conductivity of non-anodized Al and Sn–Al₂O₃ with different Sn contents

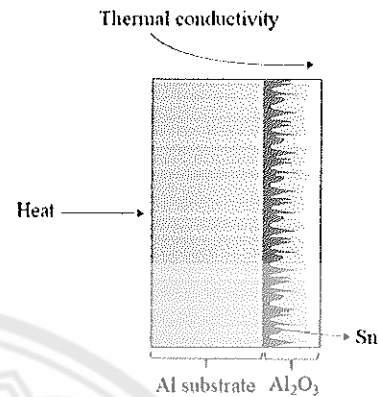
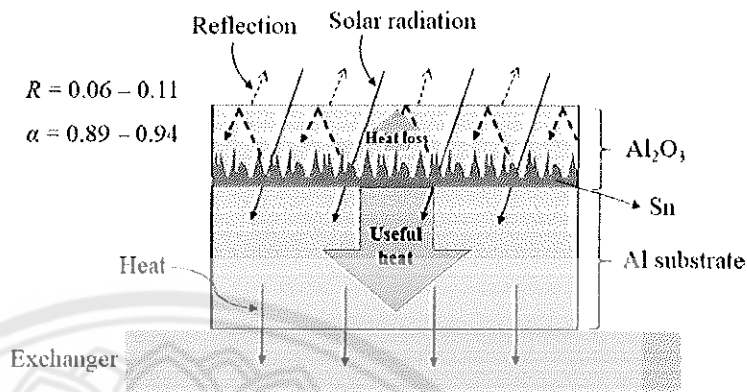


Fig. 7 Heat flow in the thermal conductivity measurement on the Sn–Al₂O₃ specimen

the thermal direction from Al substrate to the Al₂O₃ layer. In the Sn–Al₂O₃ samples, thermal conduction in the Al substrate occurs from free electrons, where heat is transferred through kinetic energy in the elements but is easily scattered [26]. The heat transferred through the Al₂O₃ layer by lattice vibration (phonons), which is directly transmitted from high to low temperature regions. It is well known that free electrons are predominant in the thermal conductivity of metals and non-anodized Al, causing high thermal conductivity. However, the thermal conductivity of all Sn–Al₂O₃ samples was higher than commercial hard anodic coatings (0.7 W/m K) and also greater than previous studies with Al anodic coatings using several electrolytes (no more than 1.33 W/m K) [27]. The solar spectrum is converted to thermal energy at the Sn–Al₂O₃ solar absorber, then, useful heat is easily transferred through the Al substrate to the exchanger. It implies that the heat loss from the Sn–Al₂O₃ solar absorber to its surroundings is blocked and reduced by the Al₂O₃ layer, as illustrated in Fig. 8. Therefore, the low thermal conductivity of the Sn–Al₂O₃ solar absorber (Al₂O₃ layer) has advantages in solar thermal applications. However, the melting point of Sn is not too high (232 °C), compared to the melting point of other pigments (Ni, W, Mo, Ag, Co, Pt and Ti). Based on the operational temperature ranges, solar absorber materials for solar thermal applications can be classified as: (1) low temperature ($T < 100$ °C), (2) mid-temperature (100 °C $< T < 400$ °C) and (3) high temperature ($T > 400$ °C) [1]. In the previous studies, metal–Al₂O₃ solar absorbers are stable in a mid-temperature range between 250 and 350 °C of solar thermal applications [1, 28, 29]. Therefore, the Sn–Al₂O₃ solar absorber is considered to be thermally stable for solar collectors operated at low and mid-temperatures such as flat plate collectors and evacuated tube solar collectors, which are generally applied for water

Fig. 8 Solar radiation and heat transfer through the Sn–Al₂O₃ specimen



heating systems ($T < 150$ °C). In the present study, the thermal stability of the Sn–Al₂O₃ solar absorber is still unknown and further experiments need to be conducted, including a long-term (e.g. year) thermal stability test in a practical solar collector.

Conclusions

The Sn-pigment on aluminium oxide (Sn–Al₂O₃) with selective absorber successfully prepared by anodization using dilute sulphuric acid followed by electrolysis in SnSO₄ solution (coloration) for various three contents of Sn in the Al₂O₃ film. The Sn–Al₂O₃ samples were composed of Al and Sn phases while the Al₂O₃ phase was not detected due to the amorphous phase. The Sn rich was a spike shape expanding into the oxide film layer and had a high concentration at the interface of the Al substrate. The R of the Sn–Al₂O₃ solar absorbers decreased as the Sn contents increased over the whole solar spectrum region (300–2500 nm) and the Al₂O₃ layer plays the role of anti-reflection. The α_{sol} increased according to the increase of Sn contents (0.89–0.94). While the ϵ_{therm} changes were insignificant when compared to the increase of Sn content. The thermal conductivity of anodized Al samples was relatively lower than non-anodized Al, especially with Sn filling in the pores leading to the decrease in heat loss from the Al substrate in the surroundings. It can be concluded that the increased Sn contents in Sn–Al₂O₃ is able to enhance the solar selective properties and hence considered to be a candidate for good solar absorber materials for solar collectors operated at low and mid-temperature.

Acknowledgements The authors gratefully acknowledge Thailand's Office of the Higher Education Commission (Contract no. 026/2556) and the National Research Council of Thailand (NRCT) through Naresuan University (R2561B107), Phitsanulok, Thailand, for financial support, including School of Renewable Energy and Technology,

Naresuan University, for general funding. Thanks also to the NULC Writing Clinic for editing this paper.

Open Access This article is distributed under the terms of the Creative Commons Attribution 4.0 International License (<http://creativecommons.org/licenses/by/4.0/>), which permits unrestricted use, distribution, and reproduction in any medium, provided you give appropriate credit to the original author(s) and the source, provide a link to the Creative Commons license, and indicate if changes were made.

References

- Kennedy, C.E.: Review of Mid-to High-Temperature Solar Selective Absorber Materials. Colorado, National Renewable Energy Laboratory (NREL) (2002)
- Tesfamichael, T.: Characterization of Selective Solar Absorbers. Dissertation for the Degree of Doctor of Philosophy in Solid State Physics, Ph.D., Uppsala University, Uppsala, Sweden (2000)
- Belghith, M., Arrault, L., Bes, R.S.: Selective absorber obtained by nickel-pigmented anodized 6060 aluminium surface. *Arab. J. Sci. Eng.* **38**, 751–757 (2013)
- Sella, C., Maaiza, M., Pardo, B., Dunsteter, F., Martin, J.C., Sainte Catherine, M.C.: Microstructure and growth mechanism of Pt–Al₂O₃ co-sputtered nanocermet films studied by SAXS, TEM and AFM. *Phys. A* **241**, 192–198 (1997)
- Maaiza, M., Nemraoui, O., Sella, C., Lafait, J., Gibaud, A., Baruch-Barak, B., Beye, A.C.: Thickness induced transversal percolation in Pt–Al₂O₃ nano-composites. *Solid State Commun.* **137**, 166–170 (2006)
- Shashikala, A.R., Sharma, A.K., Bhandari, D.R.: Solar selective black nickel–cobalt coatings on aluminum alloys. *Sol. Energy Mater. Sol. Cells* **91**, 629–635 (2007)
- Tharamani, C.N., Mayanna, S.M.: Low-cost black Cu–Ni alloy coatings for solar selective applications. *Sol. Energy Mater. Sol. Cells* **91**, 664–669 (2007)
- Karoro, A., Nuru, Z.Y., Kotsedi, L., Bouziane, K., Mothudi, B.M., Maaiza, M.: Selective solar absorbers' properties of laser treated electrodeposited tubular Co–Al₂O₃ nanocomposites. *Mater. Today's* **2**, 4028–4037 (2015)
- Ding, D., Cai, W., Long, M., Wu, H., Wu, Y.: Optical, structural and thermal characteristics of Cu–CuAl₂O₄ hybrids deposited in

- anodic aluminum oxide as selective solar absorber. *Sol. Energy Mater. Sol. Cells* **94**, 1578–1581 (2010)
10. Katumba, G., Makiwa, G., Baisitse, T.R., Olumekor, L., Forbes, A., Wäckelgård, E.: Solar selective absorber functionality of carbon nanoparticles embedded in SiO₂, ZnO and NiO matrices. *Phys. Status Solidi C* **5**, 549–551 (2008)
 11. Antoniaia, A., Castaldo, A., Addonizio, M.L., Esposito, S.: Stability of W-Al₂O₃ cermet based solar coating for receiver tube operating at high temperature. *Sol. Energy Mater. Sol. Cells* **94**, 1604–1611 (2010)
 12. Barshilia, H.C., Kumar, P., Rajani, K.S., Biswas, A.: Structure and optical properties of Ag–Al₂O₃ nanocermet solar selective coatings prepared using unbalanced magnetron sputtering. *Sol. Energy Mater. Sol. Cells* **95**, 1707–1715 (2011)
 13. Cheng, J., Wang, C., Wang, W., Du, X., Liu, Y., Xue, Y., Wang, T., Chen, B.: Improvement of thermal stability in the solar selective absorbing Mo–Al₂O₃ coating. *Sol. Energy Mater. Sol. Cells* **109**, 204–208 (2013)
 14. Wu, L., Gao, J., Liu, Z., Liang, L., Xia, F., Cao, H.: Thermal aging characteristics of CrN_xO_y solar selective absorber coating for flat plate solar thermal collector applications. *Sol. Energy Mater. Sol. Cells* **114**, 186–191 (2013)
 15. Shafiei, M.F., Khattab, N., Awad, A.M., Hussein, H.S.: Characterization of black Ni and Sn as optically selective absorber coatings in thermal solar collectors mainly (part I). *Res. J. Pharm. Biol. Chem. Sci.* **5**, 173–182 (2014)
 16. Chorchoeng, T., Suriwong, T., Sukchai, S., Threerujirapong, T.: Characterization and spectral selectivity of Sn–Al₂O₃ solar absorber. *Key Eng. Mater.* **675–676**, 467–472 (2015)
 17. Suriwong, T., Thongtem, S., Thongtem, T.: Solid-state synthesis of cubic ZnTe nanocrystals using a microwave plasma. *Mater. Lett.* **63**, 2103–2106 (2009)
 18. Nuru, Z.Y., Arendse, C.J., Nemetudi, R., Nemraoui, O., Maaza, M.: Pt–Al₂O₃ nanocoatings for high temperature concentrated solar thermal power applications. *Phys. B Condens. Matter.* **407**, 1634–1637 (2012)
 18. M.: Pt–Al₂O₃ nanocoatings for high temperature concentrated solar thermal power applications. *Phys. B Condens. Matter.* **407**, 1634–1637 (2012)
 19. Zemanová, M., Chovanová, M., Gálíková, Z., Krivošík, P.: Nickel electrolytic colouring of anodic alumina for selective solar absorbing films. *Renew. Energy* **33**, 2303–2310 (2008)
 20. Aggerbeck, M., Canulescu, S., Dirscherl, K., Johansen, V.E., Engberg, S., Schou, J., Ambat, R.: Appearance of anodised aluminium: effect of alloy composition and prior surface finish. *Surf. Coat. Technol.* **254**, 28–41 (2014)
 21. Wazwaz, A., Salmi, J., Bes, R.: The effects of nickel-pigmented aluminium oxide selective coating over aluminium alloy on the optical properties and thermal efficiency of the selective absorber prepared by alternate and reverse periodic plating technique. *Energy Convers. Manag.* **51**, 1679–1683 (2010)
 22. Xue, Y., Wang, C., Wang, W., Liu, Y., Wu, Y., Ning, Y., Sun, Y.: Spectral properties and thermal stability of solar selective absorbing AlNi–Al₂O₃ cermet coating. *Sol. Energy* **96**, 113–118 (2013)
 23. Craighead, H.G., Howard, R.E., Sweeney, J.E., Buhman, R.A.: Graded-index Pt–Al₂O₃ composite solar absorbers. *Appl. Phys. Lett.* **39**, 29–31 (1981)
 24. Xinkang, D., Cong, W., Tianmin, W., Long, Z., Buliang, C., Ning, R.: Microstructure and spectral selectivity of Mo–Al₂O₃ solar selective absorbing coatings after annealing. *Thin Solid Films* **516**, 3971–3977 (2008)
 25. Powall, R.W., Ho, C.Y., Liley, P.E.: *Thermal Conductivity of Selected Materials*. In: National Standard Reference Data Series—National Bureau of Standard-8, United States Department of Commerce, Washington D.C. (1966)
 26. Vincent, C., Silvain, J.F., Heintz, J.M., Chandra, N.: Effect of porosity on the thermal conductivity of copper processed by powder metallurgy. *J. Phys. Chem. Solids* **73**, 499–504 (2012)
 27. Ogden, T.R.: *Thermal Conductivity of Hard Anodized Coatings on Aluminium*. AIAA/SAE/ASME/ASSEE 23rd Joint Propulsion Conference, Naval Ocean Systems Center, California, USA (June 29–July 2, 1987)
 28. Wäckelgård, E., Bartali, R., Gerosa, R., Laidani, N., Mattsson, A., Micheli, V., et al.: New cermet coatings for mid-temperature applications for solar concentrated combine heat and power system. *Energy Procedia* **48**, 242–249 (2014)
 29. Cao, F., McEnaney, K., Chen, G., Ren, Z.: A review of cermet-based spectrally selective solar absorbers. *Energy Environ. Sci.* **7**, 1615–1627 (2014)
 29. based spectrally selective solar absorbers. *Energy Environ. Sci.* **7**, 1615–1627 (2014)

Publisher's Note Springer Nature remains neutral with regard to jurisdictional claims in published maps and institutional affiliations.



tawats@nu.ac.th

Ms. Ref. No.: S5-O2 (from MRS Thailand 2017)

Title: **Thermal Efficiency of a New Prototype of Evacuated Tube Collector using Sn-Al₂O₃ as a Selective Solar Absorber**

31-Jan-2018

Dear Dr. T. Suriwong

Thank you for submitting your revised manuscript. I am satisfied with the changes you have made, and it is therefore a pleasure to accept your manuscript entitled “**Thermal Efficiency of a New Prototype of Evacuated Tube Collector using Sn-Al₂O₃ as a Selective Solar Absorber**” in its current form for publication in **Walailak Journal of Science and Technology**

Thank you again for your submission to the First MRS Thailand International Conference 2017.

With best wishes,

รติกรณ์ ยิ้มศิริ

Assoc. Prof. Dr. Rattikorn Yinnirun

Chairman of Academic Committee, MRS-Thailand 2017

Thermal Efficiency of a New Prototype of Evacuated Tube Collector using Sn-Al₂O₃ as a Selective Solar Absorber

W. Wamae^a, T. Suriwong^{a,*}, T. Threrujirapong^b

^a*School of Renewable Energy Technology, Naresuan University, Phitsanulok, 65000, Thailand*

^b*Department of Materials and Production Technology Engineering, Faculty of Engineering, King Mongkut's University of Technology North Bangkok, Bangkok, Thailand*

(Corresponding Author's E-mail: tawats@nu.ac.th)

Abstract

Three tin pigmented aluminium oxide (Sn-Al₂O₃) films were prepared with different tin content using an anodization process, which is applied as a selective solar absorber in a new prototype of evacuated tube collector (ETC). The morphology and distribution of elements on the coatings were characterized using a Scanning electron microscope (SEM) equipped with an Energy dispersive X-ray (EDX) analyzer. The spectrally selective properties, defined as the ratio of solar absorptance ($\alpha_{s,01}$) to thermal emittance ($\epsilon_{th,020}$) were examined. In order to investigate the thermal performance of ETC using Sn-Al₂O₃ on an Al fin as a solar receiver, thermal efficiency (η) of the ETC was collected under steady-state conditions, as prescribed by ISO 9806-1 standard. The results, of the Sn-Al₂O₃ coatings reached a darker black colour with an increase in the colouring time. The samples were composed of different contents of Sn in the Al₂O₃ layer. The solar selectivity ($\alpha_{s,01}/\epsilon_{th,020}$) significantly increased with the increases in Sn content. The maximum thermal efficiency (η_{max}) of the ETC under the nearly constant heat loss coefficient (U_L), was obviously increased with the increasing Sn content. Therefore, the Sn-Al₂O₃ with different Sn contents is a good candidate for selective solar absorbers in a new prototype of ETC.

Keywords: Evacuated tube collector, Selective solar absorber, Anodization, Absorptance, Thermal emittance

Introduction

The normal selective solar absorber coating, is coated on the surface of the inner glass tube as in Figure 1 (a, b), which is applied using high technology and a complicated process, which causes high production costs. During the applications, it was found that it is inclined to crack or splits which means that it needs to be replaced, thus causing extra dissipation costs. A changing of solar absorber coating on an aluminium (Al) fin and inserting it into a transparent evacuated tube were developed as a new prototype of ETC (see Figure 1 (c, d)). The thermal efficiency and potential for energy production are similar to commercially available ETC's [1].



October 31 - November 3, 2017 at Convention Center, The Empress Hotel, Chiang Mai, THAILAND
<http://www.mrs-thailand2017.science.cmu.ac.th>

6 October 2017

Dear Miss Warisa Wannae

On behalf of the MRS Thailand 2017 organizing committee, we are pleased to cordially confirm your registration as **Conference Participant** at The First Materials Research Society of Thailand International Conference (MRS-Thailand 2017), which will be held during October 31 - November 3, 2017 at **Convention Center, The Empress Hotel, Chiang Mai, THAILAND**. We are expecting that there will be about 800 participants including about 300 participants from overseas. The details of MRS-Thailand 2017 can be found from the conference website: <http://www.mrs-thailand2017.science.cmu.ac.th>.

If you have further inquiries, please contact us at email: 1mrsthailand2017@gmail.com

We are looking forward to meeting you in Chiang Mai, Thailand.

Best regards,

A handwritten signature in black ink, appearing to read "Santi Maensiri".

Prof. Dr. Santi Maensiri
President, Materials Research Society of Thailand
& Chairman for MRS-Thailand 2017 Organizing Committee